UNIVERSITY OF CALIFORNIA, SAN DIEGO

Neurotransmission defines functional chemosensory neural circuits to regulate behavior

A dissertation submitted in partial satisfaction of the requirements for the degree Doctor of Philosophy

in

Neurosciences

by

Sarah Goldberg Leinwand

Committee in charge:

Professor Sreekanth Chalasani, Chair
Professor Yishi Jin, Co-Chair
Professor Edward Callaway
Professor Timothy Gentner
Professor Jing Wang

2015

The Dissertation of Sarah Goldberg Leinwand is approved, and it is acceptable in quality and form for publication on microfilm and electronically:

_____

_____

_____

_____
Co-Chair

_____
Chair

University of California, San Diego

2015

TABLE OF CONTENTS

LIST OF FIGURES

LIST OF TABLES

ACKNOWLEDGEMENTS

First and foremost, I would like to thank my thesis advisor Sreekanth Chalasani. This work would not have been possible without his incredible guidance and mentorship. His enduring creativity, optimism and enthusiasm for science and for discoveries, both big and small, inspired me. I am a better scientist for his challenges to examine every question and piece of data from multiple different angles and his reminders to consider the big picture motivation for every experiment.

I would also like to acknowledge my thesis committee: Drs. Yishi Jin, Ed Callaway, Jing Wang and Tim Gentner. Their input and guidance throughout my graduate career have been invaluable, and I also thank them for their extra support as I transition to the next phase of my career.

I would also like to thank all the past and present members of the Chalasani lab—their thoughtful ideas, perspectives on science and life, technical advice and all the shared laughs made every day in lab so much more enjoyable. In particular, I want to acknowledge Claire Yang for all of her experimental contributions to the aging project and much more; Adam Calhoun for challenging me to think from a different (almost computational) perspective; Laura Hale for her thoughtful advice on all kinds of topics; Ada Tong for all her help and for expertly keeping the lab running smoothly; Eunice Lau for more helpful conversations than I can count; Kathleen Quach, Zack Cecere, Chen-Min Yeh and Zheng Liu for the camaraderie and the many valuable conversations. I would also like to thank everyone in the Waitt Biophotonics core for their help and patience on several challenging imaging projects.

Finally, I thank my family, friends and classmates, and Michael for their endless kindness, encouragement, humor and everything else that made my time in graduate school so enjoyable. It is impossible to imagine how I could have done any of this without you.

Chapter 1 includes a partial reprint of material in Leinwand, S.G. and Chalasani, S.H. (2011). Olfactory networks: from sensation to perception. Curr Opin Genet Dev, 21 and is included with permission from the journal and all authors. The dissertation author was the primary author of this paper.

Chapter 2 is a reprint of the material as it appears in Leinwand, S.G. and Chalasani, S.H. (2013). Neuropeptide signaling remodels chemosensory circuit composition in *Caenorhabditis elegans.* Nat Neurosci 16, 1461-7 and is included all authors' permission. The dissertation author was the primary author of this paper.

Chapter 3 is a reprint of the material as it appears in Leinwand, S.G. and Chalasani, S.H. (2014). From genes to circuits and behaviors: neuropeptides expand the coding potential of the nervous system. Worm, 3 and is included with permission from all authors. The dissertation author was the primary author of this paper.

Chapter 4 is a reprint of the material as it appears in Leinwand, S.G., Yang, C.J., Bazopoulou, D., Srinivasan, J., Chronis, N., and Chalasani, S.H. (2015). Neural mechanisms regulating aging-associated behavioral decline in *Caenorhabditis elegans* (in preparation) and is included with permission from all authors. The dissertation author was the primary author of this paper.

VITA

2015 Doctor of Philosophy, Neurosciences, University of California, San Diego

2008 Bachelor of Arts, Biological Basis of Behavior, University of Pennsylvania

PUBLICATIONS

Leinwand, S.G., Yang, C.J., Bazopoulou, D., Srinivasan, J., Chronis, N., and Chalasani, S.H. (2015). Neural mechanisms regulating aging-associated behavioral decline in *Caenorhabditis elegans*. *In preparation*.

Leinwand, S.G., and Chalasani, S.H. (2014). From genes to circuits and behaviors: neuropeptides expand the coding potential of the nervous system. Worm 3.

Leinwand, S.G., and Chalasani, S.H. (2013). Neuropeptide signaling remodels chemosensory circuit composition in Caenorhabditis elegans. Nat Neurosci 16, 1461-1467.

Leinwand, S.G., and Chalasani, S.H. (2011). Olfactory networks: from sensation to perception. Curr Opin Genet Dev 21, 806-811.

Xu, H., Leinwand, S.G., Dell, A.L., Fried-Cassorla, E., and Raper, J.A. (2010). The calmodulin-stimulated adenylate cyclase ADCY8 sets the sensitivity of zebrafish retinal axons to midline repellents and is required for normal midline crossing. J Neurosci 30, 7423-7433.

ABSTRACT OF THE DISSERTATION

Neurotransmission defines functional chemosensory neural circuits to regulate behavior

by

Sarah Goldberg Leinwand

Doctor of Philosophy in Neurosciences

University of California, San Diego, 2015

Professor Sreekanth Chalasani, Chair
Professor Yishi Jin, Co-Chair

Neural circuits detect and process environmental changes to drive appropriate food-seeking or toxin-avoiding behaviors. However, we lack a complete understanding of the cellular and molecular mechanisms that represent chemosensory cues and generate appropriate behaviors. Furthermore, these vital sensory abilities deteriorate with age in humans and most animals, but it is unknown how aging impairs the underlying neural circuits to cause sensory behavioral declines. With powerful genetic tools, a complete connectome and robust chemosensory behaviors, the nematode *Caenorhabditis elegans* is ideally suited for a circuit-level analysis of these behaviors in young and aged animals. The aim of this dissertation is to identify neural signaling and circuit principles for flexibly encoding chemosensory stimuli and generating behavioral plasticity in *C. elegans*, which may be broadly conserved.

In Chapters 2 and 3, I define a novel, sensory context-dependent and neuropeptide-regulated switch in the composition of a *C. elegans* salt sensory circuit. The ASE primary salt sensory neurons cleave and release insulin-like peptides in response to large but not small changes in external salt stimuli. Insulin signaling functionally switches the AWC olfactory sensory neuron into an interneuron in the high salt circuit, potentiating behavioral responses. Thus, sensory context and neuropeptide signaling act together to shape the flow of information in active neural circuits, suggesting a general mechanism for generating dynamic behavioral outputs.

In Chapter 4, I identify an aging-associated decline in *C. elegans* olfactory behavior and map a novel underlying circuit motif. Two primary olfactory sensory neuron pairs, AWC and AWA, directly detect benzaldehyde and release insulin peptides and acetylcholine to activate two secondary neuron pairs, ASE and AWB, and drive behavioral plasticity. Interestingly, odor-evoked activity in the secondary, but not primary, neurons degrades with age. Experimental manipulations to increase primary neuron transmitter release rescue these aging-associated neuronal deficits. Furthermore, aged animals' olfactory abilities are correlated with lifespan, suggesting that olfaction may be indicative of overall health and physiology. These results show how chemosensory stimuli are encoded by a population code composed of primary and secondary neurons and suggest reduced neurotransmission as a novel mechanism driving aging-associated sensory neural activity and behavioral declines. In sum, this dissertation establishes the crucial role of peptidergic and classical neurotransmission in defining the active neural circuit configurations that regulate chemosensory behaviors.

CHAPTER 1.

Introduction

Chemosensation and conserved principles of neural circuit function

Animals, including people, must navigate through a complex world made up of diverse smells, tastes, sights, sounds and textures. Survival depends on the use of this sensory information to find food and avoid toxins or other dangers in the environment. The sensory systems function to transduce these environmental signals into neural representations. However, the sensory systems do not passively represent the environment; instead, they have the difficult task of actively extracting features of the world and combining them to generate meaningful sensory representations that can guide behavior (Ache and Young, 2005).

Most species have exquisitely sensitive chemosensory systems that are essential for their successful navigation of the world. Specifically, the olfactory system is important for recognizing volatile cues from possible food-sources at long-ranges. The gustatory system detects water-soluble chemicals at short-range, serving as the final check for accepting or rejecting prospective foods that are nutritious or toxic (Scott, 2005). Together, the chemosensory systems also contribute to mating, rearing of offspring and predator-prey interactions (Ache and Young, 2005). From the simplest forms of life like bacteria and slime molds, to worms, insects, rodents and humans,

chemical sensitivity is fundamental for life and health (Ache and Young, 2005). Chemosensation is therefore a very ancient sense. The basic organization of the chemosensory system has been highly conserved throughout evolution such that common genes, structures and circuits are observed across phyla (Ache and Young, 2005; Bargmann, 2006). However, many unknowns remain about chemosensory system function.

A key challenge in neuroscience is to understand how signals in the environment are translated into behavior. Here, this dissertation focuses on the ancient and conserved chemosensory system with the aim of gaining insight into the general functional principles of the nervous system. Specifically, the question that drives this dissertation, and a fundamentally important question in neuroscience, is *how is chemosensory information represented and processed by the nervous system to generate appropriate behavioral outputs?* In the chemosensory system, the inputs (chemical cues) and the outputs (behavior) can be observed and quantified. However, how precise sensory neural circuit dynamics and signaling shape motor outputs or generate behavioral plasticity remain open questions. Fully answering these questions requires identifying, functionally characterizing and manipulating all of the relevant neurons, neurotransmitters and neural circuits. While studies in mammals and insects have made progress towards this goal, the simpler nervous system of the nematode *C. elegans* (the model organism employed for this dissertation research) permits the study of genes, neurons and circuits in whole, behaving animals. In this way, the doctoral research presented here will provide a more complete understanding of neural circuit function.

To begin to unravel circuit function and, in particular, how chemosensory information is represented and processed by the nervous system to generate appropriate behavior, this introduction chapter reviews key findings from the literature and identifies the limits of this knowledge base. The ***organization*** and anatomy of the mammalian, insect and nematode chemosensory systems are discussed first. Next, this chapter highlights several overarching principles of chemosensory system ***function***. The evidence from studies in different species supporting two alternative models of sensory encoding (the population coding and labeled line models) is discussed. Then, ***modulation*** of chemosensory circuits and behaviors by neuropeptides and other neuromodulators is explored. Finally, ***aging***-associated declines in chemosensory function are considered.

Chemosensory system organization: mammals

In mammals and in other animals, chemicals in the environment are detected and processed by sensory neurons, which relay the chemosensory information to higher order brain regions. Olfactory and gustatory sensory neurons in peripheral sensory organs may have specialized ciliary endings to detect chemicals. These sensory neurons express receptors, usually of the G protein-coupled receptor (GPCR) family (Godfrey et al., 2004; Malnic et al., 2004; Sengupta et al., 1996). When odorants or tastants in the environment bind to these receptors, a signal transduction cascade is initiated and then information about the chemicals in the environment is relayed, in multiple steps, to higher order chemosensory processing regions of the brain (Ache and Young, 2005). In the case of the mammalian olfactory system, olfactory sensory neurons project from the olfactory epithelium in the nose to target structures called glomeruli in the olfactory bulb (**Figure**

1.1) (Price and Powell, 1970). The olfactory sensory neurons synapse with mitral cells, which, in turn, carry olfactory information to piriform cortex, entorhinal cortex, the anterior olfactory cortex and the amygdala (Ghosh et al., 2011; Miyamichi et al., 2011; Sosulski et al., 2011). A vast inhibitory network also shapes the flow of olfactory information through the brain (Stokes and Isaacson, 2010). Taste information like sweet, salty, bitter and sour is relayed from taste cells clustered in taste buds on the tongue to the nucleus of the solitary tract, the thalamus and then gustatory cortex (Liman et al., 2014). Additional information about other sensory cues in the environment, internal physiological state, or experience may also be integrated at different stages in this processing, transforming the neural representations of chemosensory cues (as discussed in more detail in the chemosensory modulation section below) (Maier et al., 2012; Root et al., 2011). Ultimately, these chemosensory neural circuits provide crucial information to drive nearly all of an animal's behavioral choices.

Chemosensory system organization: insect

The numerically simpler insect chemosensory system has been studied extensively and has yielded many conserved chemosensory organization principles. In *Drosophila melanogaster*, the most widely studied insect, olfactory sensory neurons are located in the antennae and maxillary palps where they express one or occasionally two specific olfactory receptors, along with a ubiquitous receptor, Or83b (Larsson et al., 2004; Vosshall et al., 1999). The sensory neurons expressing the same receptor converge on the same glomerulus in the antennal lobe, the second order olfactory processing region (**Figure 1.1**) (Vassar et al., 1994). Projection neurons then carry this olfactory

information to third order olfactory brain regions such as the lateral horn and mushroom body (Masse et al., 2009). In this way, insect olfaction parallels mammalian olfaction. The number of synaptic relays and the roles of inhibition in the olfactory pathway are similar across species (Olsen and Wilson, 2008). Furthermore, convergence of functionally similar inputs at the glomerular level is conserved throughout animal evolution, suggesting that it is important for odor processing. Taste information follows a different path in *Drosophila,* from gustatory sensory neurons located primarily in the proboscis to the subesophageal ganglion and then the brain; this pathway also shows striking conservation with the mammalian taste system (Scott, 2005). However, how does the conserved organization of the chemosensory system give rise to smell and taste perception and related behaviors?

Chemosensory function: mammalian and insect chemosensory population coding

Chemosensory functions have been inferred based on anatomy and systematically investigated. In both the peripheral sensory organs and in central sensory processing regions of the mammalian and insect brain, there is overwhelming evidence that chemosensory cues are encoded by distinctive patterns of activity across groups of neurons (Honegger et al., 2011; Oka et al., 2006; Stettler and Axel, 2009; Wang et al., 2003). For example, individual odor molecules may activate multiple olfactory sensory neurons (Malnic et al., 1999). Conversely, individual olfactory sensory neurons may be (strongly or weakly) activated by the binding of numerous different odorants (Malnic et al., 1999). Furthermore, small changes in the concentration or the chemical structure of an odorant can alter which neurons are activated (Malnic et al., 1999; Stettler and Axel,

2009). There is a chemotropic organization to the active neurons in the sensory periphery (Vassar et al., 1994; Vosshall et al., 2000). However, fascinatingly, this chemotropic organization is lost in the higher order piriform cortex in rodents and mushroom bodies in insects, and no other organizing principle or stereotypy is apparent in these odor responsive neuronal populations (Honegger et al., 2011; Miyamichi et al., 2011; Sosulski et al., 2011; Stettler and Axel, 2009). In this way, chemosensory information must be encoded by the combined activity of a spatially distributed population of neurons, rather than specialized activity in single neurons. This coding strategy is alternately referred to as a combinatorial or distributive model or simply population coding (Galizia, 2014; Liman et al., 2014; Malnic et al., 1999). It is important to note that only a small percentage of neurons in a given brain region are activated by a particular odor stimulus, indicating that olfactory population codes are sparse (Honegger et al., 2011; Poo and Isaacson, 2009; Stettler and Axel, 2009). Gustatory information can also be encoded by sparse population activity; however, the organization is somewhat different than in olfactory circuits (as discussed below) (Katz et al., 2001; Maier and Katz, 2013).

Population coding of chemosensory information has several interesting properties. First, natural cues like food and predator signals are complex and composed of numerous monomolecular chemicals (Thomas-Danguin et al., 2014). Population codes can simultaneous represent these diverse chemical inputs, which co-occur in nature. These neural representations can be distinct from the sum of the components, suggesting that the natural stimulus has a unique significance for the animal (Stettler and Axel, 2009). Conversely, the circuits that encode different, complex sensory stimuli are likely composed of partially overlapping sets of neurons (Poo and Isaacson, 2009; Stettler and

Axel, 2009). Interestingly, individual or, more likely, subsets of these multiplexed neurons could be wired such that they each have the capacity to drive a distinct behavioral module (Choi et al., 2011). Therefore, a particular stimulus could lead to a portion of the many possible behavioral modules being combined and executed. Moreover, neural circuits that integrate multisensory cues may permit animals to generate behaviors that are appropriate for the global environment rather than unitary environmental features, which may be beneficial for survival. This coding strategy may also prevent against sensory encoding failures since there may be multiple ways for sensory stimulation to reliably activate neurons that trigger the execution of a relevant behavior.

An alternative model for sensory encoding also exists. The labeled line model of coding posits that each cell represents a distinct odor or taste cue and faithfully conveys this information to higher order sensory processing regions of the brain. Evidence for the labeled line model is found in both mammals and flies (Semmelhack and Wang, 2009; Suh et al., 2004; Zhao et al., 2003). This form of sensory coding is genetically hardwired and appears to predominate for particular stimuli that have an innate valence such as apple cider vinegar and amines (Dewan et al., 2013; Semmelhack and Wang, 2009; Suh et al., 2004; Zhao et al., 2003). In the gustatory system, tastes that promote feeding typically activate one set of gustatory sensory neurons, while tastes that lead to rejection behaviors may activate a different, common set of gustatory neurons (Liman et al., 2014). This labeled line coding requires dedicated neural space (i.e. specialized neurons and pathways), so it is more “resource-intensive” than population coding. A reasonable hypothesis is that labeled line coding is used only for detecting chemicals for which

recognition offers a strong survival or reproductive benefit. Consequently, labeled line and population coding strategies for chemosensory encoding are not mutually exclusive. Taken together, the data described above suggest that labeled line and population coding strategies co-exist to permit insects and mammals to have hardwired responses to innately attractive or aversive cues and flexibility to respond to dynamic, multisensory environments, respectively. Nevertheless, the precise sensory encoding and circuit mechanisms that give rise to appropriate chemosensory behaviors remain to be elucidated.

Chemosensory system organization and function: identified sensory neurons in *C. elegans* drive chemosensory behaviors

One approach to understanding how sensory stimuli drive behavior is to trace the paths of information flow between all of the neurons in the corresponding neural circuits and then analyze the effects of perturbing this neural activity. This task is challenging in humans, other mammals and even in insects because of the sheer number of neurons in the brain and because information could be routed through dense networks of hundreds, thousands or even millions of anatomically connected neurons in multiple ways (Baldridge et al., 1998; Weimann and Marder, 1994). In contrast, the small, free-living nematode worm *Caenorhabditis elegans* is advantageous for such studies. Accordingly, the small nervous system of *C. elegans* has been studied extensively to increase our understanding of the neural basis of sensory behaviors, with the aim of uncovering conserved principles.

Several factors make *C. elegans* a useful model organism for probing the cellular, molecular and neural circuit-level basis of chemosensory behavior. First, many genes are conserved between *C. elegans* and mammals, and they use many of the same neurotransmitter systems (Hobert, 2013). Second, the *C. elegans* model offers a relatively simple nervous system composed of just 302 neurons (in the mature hermaphrodite animal) (White et al., 1986). The morphology, chemical synapses and gap junction connections of all *C. elegans* neurons were mapped by serial section electron microscopy (White et al., 1986). As a result of these efforts, *C. elegans* is the only animal that possesses a complete map of the nervous system. This connectome cannot simply be read to predict how behaviors are generated, but it does illustrate the many possible connections, whose roles can be tested in diverse contexts (Bargmann, 2012). Additionally, there are many powerful genetic tools available to probe the *C. elegans* nervous system at the cellular and molecular levels (Praitis and Maduro, 2011; Wang and Sherwood, 2011). New tools for the optical measurement of neural activity, including GCaMP family calcium indicators, take advantage of the transparency of *C. elegans* to offer unprecedented ability to analyze circuit function *in vivo* and with single-cell resolution (Nakai et al., 2001).

C. elegans has a highly developed chemosensory system, which it uses to find bacterial food, avoid predators and other dangers, and aid in mating (Bargmann, 2006). Its robust chemosensory behaviors are readily probed in the lab and quantified (Ward, 1973). In particular, chemotaxis behavior directed towards an attractive or repulsive chemical has been well studied (Bargmann et al., 1993; Bargmann and Horvitz, 1991; Iino and Yoshida, 2009; Pierce-Shimomura et al., 1999; Ward, 1973). *C. elegans* uses a

biased random walk strategy to chemotax in which it suppresses its reorientations while moving up an attractive salt or odor gradient and increases its reorientations while going down such a gradient (Pierce-Shimomura et al., 1999). In this way, animal movement is non-directional; however, overall locomotion is biased because forward movement toward the higher attractant concentration is less likely to be interrupted than movement in the opposite direction. A contrasting weathervane chemotaxis strategy has also been proposed (Iino and Yoshida, 2009). The weathervane approach consists of animals gradually steering or curving their path of forward locomotion towards higher concentrations of an attractive chemical (Iino and Yoshida, 2009). These two strategies are not exclusive; *C. elegans* may navigate steep and shallow chemical gradients in these different ways. Numerous studies have taken advantage of the small nervous system and powerful genetic tools in *C. elegans* to dissect the neural basis of this chemosensory behavior. Anatomical and functional studies have implicated neurons located in the amphid ganglia in the head of the animal in chemotaxis behavior and in chemosensation more broadly (Bargmann, 2006; Chalasani et al., 2007; Perkins et al., 1986). There are 12 pairs of sensory neurons in the amphid ganglia, which all have dendrites that extend to the nose of animal, where they terminate with specialized sensory cilia structures that are directly or indirectly exposed to the environment (Perkins et al., 1986). The axons of the amphid sensory neurons form synapses in the nerve ring with other sensory neurons and interneurons (White et al., 1986). On average, no more than three synapses are required to connect these sensory neurons with the motor neurons that control body muscles for initiating locomotion toward or away from chemical cues (Gray et al., 2005; White et al., 1986).

Previous research has suggested a hardwired labeled line model of chemosensation in *C. elegans* in which individual cells encode particular sensory cues and specify the behavioral output (Liman et al., 2014; Troemel et al., 1997). Studies using a laser to ablate individual neurons revealed that the ASE neurons are necessary for attraction to salt (Bargmann and Horvitz, 1991). The paired ASE neurons can be genetically and functionally separated; the ASEL (left) neurons preferentially detect sodium ions, while the ASER (right) neurons may be specialized for chloride detection (Pierce-Shimomura et al., 2001). Further analysis by functional calcium imaging revealed that the ASEL neurons are specifically activated by an increase in (sodium chloride) salt concentration, while the ASER neurons are activated by a decrease in salt concentration (Suzuki et al., 2008). The functional asymmetries between the two ASE neurons were proposed to be essential for normal chemotaxis to salt, and perhaps an important motif for all navigation guided by the sense of taste (Suzuki et al., 2008).

Similarly, previous studies found that volatile odor cues (including ketones, alcohols and aldehydes) are detected by a small number of *C. elegans* amphid sensory neurons. It was suggested that these olfactory sensory neurons are hardwired to drive either attractive or repulsive behavioral programs (Bargmann et al., 1993; Troemel et al., 1997). For example, cell ablation experiments revealed that the AWC and AWA sensory neurons are specifically required for behavior towards attractive odorants (Bargmann et al., 1993). Calcium imaging and behavior experiments suggest that their response properties are complex. The paired AWC neurons (which can be genetically and functionally separated, much like the ASE neurons) detect multiple attractive odors including benzaldehyde, isoamyl alcohol and trimethylthiazole at a wide range of

concentrations (Bargmann et al., 1993; Chalasani et al., 2007; Wes and Bargmann, 2001). The AWA neurons detect a partially overlapping set of attractive odors including trimethylthiazole and diacetyl and initiate a similar attractive behavioral program (Bargmann et al., 1993). In contrast, the AWB neurons appeared to be specialized for detecting repulsive odorants such as 2-nonanone (Troemel et al., 1997). This data suggests that the identity of the neuron that binds a particular odorant could determine whether that odor is attractive or repulsive to the animal. In support of this hypothesis, mis-expression of the ODR-10 receptor, for the normally attractive odor diacetyl, in the AWB neuron is sufficient to induce behavioral avoidance of diacetyl (Troemel et al., 1997). Therefore, the identity and connectivity of the active olfactory sensory neuron may determine which signaling pathways and downstream neural circuitry are recruited to generate attractive or repulsive chemotaxis behavior. Many of the amphid sensory neurons synapse onto common set of interneurons (AIA, AIY and others); however, the precise interneuron to motor neuron circuitry remain to be elucidated (White et al., 1986). Taken together, these studies suggest that *C. elegans* sensory encoding follows a labeled line model whereby individual neurons drive hardwired behaviors to specific, unimodal olfactory or gustatory cues. This is in contrast to the distributed, population coding strategies used in other species with larger brains to represent many dynamic and complex (multi)sensory stimuli. I will present data challenging this fixed view of *C. elegans* sensory neural circuits in Chapters 2-4.

Chemosensory modulation: neuropeptide signaling modulates chemosensory neural activity in mammals and insects

Depending on the context, a single chemosensory input is frequently able to trigger more than one behavioral output. A major question in neuroscience is how this behavioral plasticity is achieved. Several studies suggest that neuromodulatory signaling could be the key mediator of the differential behavioral responses. Specifically, neuropeptides and other modulatory signaling may impart sensory neural circuits with an additional layer of flexibility so that animals may fine-tune their behavior to match their external environment and their internal physiological needs. By depressing or facilitating the activity of sensory neurons, neuropeptides may increase the ability of sensory neurons to transmit information about wide ranges of chemosensory stimuli (Ignell et al., 2009; Nassel et al., 2008; Ni et al., 2008; Root et al., 2011). This fine regulation may aid animals in accurately localizing a desirable food source or comparing the different sensory cues present in the environment. For example, interneurons in the *Drosophila* antennal lobe release neuropeptide signals to reduce olfactory sensory neuron activity. Tackykinin-related peptides bind a GPCR, DTKR, expressed by olfactory sensory neurons to inhibit their function (**Figure 1.1**) (Ignell et al., 2009). This reduction in sensory neuron function can dampen the animal's attraction to high odorant concentrations (Ignell et al., 2009). This peptide-mediated inhibition scales proportionally with the strength of the sensory stimulus, providing a robust mechanism for encoding diverse stimuli.

Genetic analyses in *Drosophila* have also identified peptides that facilitate sensory neuron activity. Short neuropeptide F, a homolog of neuropeptide Y, is released by olfactory sensory neurons and increases the activity of other sensory neurons that project to the same glomerulus (Nassel et al., 2008; Root et al., 2011). Increased activity

of a glomerulus could make the representations of the specific odors that it processes more salient in higher order sensory processing centers. Interestingly, sensory neurons only express the receptor for short neuropeptide F, sNPFR1, upon starvation (Root et al., 2011). This observation indicates that peptide signaling integrates behavioral state information (like hunger status) with odorant information directly in the sensory neurons. Similar mechanisms could also exist in rodents (**Figure 1.1**). For example, an FMRFamide peptide increases the magnitude of delayed-rectifier potassium currents in the mouse olfactory bulb, as measured by whole cell patch-clamp recordings (Ni et al., 2008). The action of such neuropeptides may modulate the excitability of olfactory sensory neurons. Furthermore, insulin peptidergic signaling has also been shown to modulate the signal to noise ratio of mammalian olfactory sensory neuron activity over long timescales (Savigner et al., 2009). One hypothesis is that this insulin signaling matches an animal's olfactory abilities to its satiety status. However, the behavioral relevance of these mammalian forms of neuropeptide modulation remains to be established.

Taken together, antagonist neuropeptide signals may act as gain controls for sensory encoding, shaping the patterns of neuronal activity that give rise to innate and learned behaviors. Presynaptic inhibition increases the ability of the neurons to respond to high stimulus concentrations, while facilitation may increase neuronal sensitivity to lower stimulus concentrations. The relatively slow time course of these forms of neuropeptide signaling could also extend the time that a sensory neuron remains active. Effectively, this would stabilize the stimulus representation over the second to minute timescales that are relevant for the execution of sensory-guided behaviors. These results

suggest that neuropeptide signaling is essential for animals' responses to constantly changing environments and physiological drives.

Chemosensory modulation: neuropeptide and monoamine signaling shape chemosensory activity and behavior in *C. elegans*

Despite the apparent one sensory neuron-to-one behavioral output mechanism in *C. elegans,* neuromodulatory signaling provides the worm's nervous system a crucial mechanism for generating flexible outputs, much like in insects and mammals. There are several *C. elegans* studies demonstrating a role for both neuropeptide and monoamine signaling in altering sensory neuron or interneuron dynamics and modulating behavior. In one instance, the AWC sensory neurons release the neuropeptide NLP-1. NLP-1 peptides bind to an interneuron expressed GPCR, NPR-11 (**Figure 1.1**) (Chalasani et al., 2010). These interneurons in turn release their own peptide signals, the insulin-like peptide INS-1, which suppress odor-evoked responses in AWC sensory neurons (**Figure 1.1**) (Chalasani et al., 2010). This forms a neuropeptide feedback loop. Ultimately, this neuropeptide feedback modulates olfactory adaptation behavior (Chalasani et al., 2010). In another example, a feed-forward neuropeptide pathway regulates a learned aversive olfactory behavior to pathogenic food sources (Chen et al., 2013). The insulin-like peptide INS-6 is released from ASI sensory neurons to promote the aversive learning (Chen et al., 2013). Interestingly, INS-6 inhibits the transcription of another insulin-like peptide, INS-7, in the URX sensory neurons (Chen et al., 2013). This peptide-peptide antagonism regulates the activity of a downstream interneuron, RIA, which is critical for the learned behavioral output (Chen et al., 2013). Neuropeptide-to-neuropeptide

pathways and loops were first observed in *C. elegans,* where the genetic tools made such studies feasible; however, it is reasonable to hypothesize that they are a general mechanism for generating a large repertoire of adaptive behaviors in other animal species.

Neuropeptide-mediated flexibility in the architecture of neural circuits, not just the dynamics of neural activity, may also exist to modulate behavior. For example, internal physiological states like starvation may trigger a particular complement of neuropeptides or monoamines to be released to change neural circuits and modify the behavioral outputs (Chao et al., 2004). *C. elegans* avoidance of the odorant octanol is reduced upon starvation (Chao et al., 2004). This starvation-induced behavioral plasticity depends on both serotonin and octopamine, which may switch the composition of the octanol circuit (Chao et al., 2004; Mills et al., 2012). Specifically, fed animals predominately rely on the ASH nociceptive neurons to detect octanol and drive avoidance behavior, but starved animals recruit two other neurons (AWB and ADL) in addition to ASH neurons to detect octanol (Chao et al., 2004). Food and lack thereof are powerful signals that modulate many other circuits and behaviors, often through the actions of monoamines and neuropeptides (Chang et al., 2006). Nevertheless, further analysis is still required to fully understand the precise mechanisms that modulate these neural circuits to produce behavioral plasticity.

Thus, from worms to insects and rodents, animals employ neuropeptide signaling to alter their neural activity and fine-tune their behavior based on the sensory environment, internal physiological needs and experience. In Chapter 2, I will describe a novel form of insulin neuropeptide-regulated and context-dependent plasticity in a

distributed *C. elegans* gustatory neural circuit, which does not simply follow the labeled line model. This chapter demonstrates that neuropeptides can regulate neural circuit composition, allowing animals to behave appropriately when they encounter sensory stimuli of different strengths. In Chapter 3, I will discuss the broader implications of these findings. In Chapter 4, I will show that similar principles govern flexible olfactory circuits and behaviors, in both young and aged animals.

Aging-associated declines in sensory system functions

Progressive declines in vital sensory abilities are nearly ubiquitous in aged people and other animals (Schumm et al., 2009). Specifically, aging is associated with reductions in the ability to detect and correctly identify sounds, sights, smells, tastes and fine tactile stimuli (Schumm et al., 2009). Therefore, another important question in neuroscience is *how does aging alter neural circuits to degrade sensory behavioral outputs?* Here, I will focus on aging's deleterious effects on the olfactory system. Age-related loss of olfactory function (termed presbyosmia) can be quantified in people using simple scratch and sniff tests (Doty and Kamath, 2014). These tests reveal that more than 50% of people aged 65-80 years exhibit significant olfactory dysfunction, and the frequency rises to more than 75% of people over 80 years old (Doty and Kamath, 2014). In the elderly, the threshold for detecting odors decreases more strongly than odor identification or discrimination, although all three classes of olfactory abilities exhibit significant age-related declines (Hummel et al., 2007). Additionally, reduced olfactory function may predict the onset and progression of neurodegenerative diseases such as mild cognitive impairment, Alzheimer's and Parkinson's disease (Wilson et al., 2008; Wilson et al., 2009).

Furthermore, olfactory function strongly predicts mortality in people (Pinto et al., 2014). Hyposmic and anosmic individuals who have moderate or complete olfactory dysfunction, respectively, have proportionately higher 5-year mortality rates, even when other health indicators are controlled for (Pinto et al., 2014). Even in the absence of death or disease, olfactory declines greatly impair quality of life, threaten overall safety and increase the risk of nutritional deficits (Doty and Kamath, 2014). While these studies suggest a strong link between olfaction and health, the results only show a correlation, not that declines in olfaction cause disease.

Since the precise causes of aging-associated declines in olfactory functions are not well understood, prevention or treatment has not been feasible. Head trauma, inflammatory disease and cumulative exposure to environmental toxins are among the many factors proposed to underlie olfactory declines in mammals (Murphy et al., 2002); however, causation has been impossible to demonstrate. Reductions in the number of olfactory neurons (due to cell death or reduced regenerative capacity) and changes in the distribution of their synapses have been also observed in aged animals (Chihara et al., 2014; Murphy et al., 2002; Richard et al., 2010). Still, the functional consequences of such cellular changes remain to be determined. Additionally, a genetic association was found between olfactory declines in the elderly and a single nucleotide polymorphism in the BDNF gene (Hedner et al., 2010). However, to causally establish the mechanisms driving aging-associated olfactory impairment, a new model that allows genes, cells and circuit function to be analyzed and perturbed throughout life is needed.

C. elegans is amenable to *in vivo* analysis of the functional outputs of many genetic pathways (with single cell resolution) throughout the entirety of the animal's

short lifespan. This model has already provided many insights into the genetic and cellular basis of longevity and aging (Kenyon, 2010; Liu et al., 2013; Wolff and Dillin, 2006). Conserved signaling pathways such as insulin, mitochondrial and autophagy signaling regulate *C. elegans* lifespan, as mutations that reduce insulin signaling, reduce mitochondrial respiration, reduce TOR signaling or increase autophagy promote longevity (Hansen et al., 2008; Wolff and Dillin, 2006). At the level of the nervous system, aging is associated with aberrant neuronal morphology, reductions in the monoamine transmitter levels and progressive deterioration of neuromuscular junction functioning (Liu et al., 2013; Toth et al., 2012; Yin et al., 2014). These cellular changes impair animals' locomotion abilities, mating behaviors and food-induced slowing behavior (Liu et al., 2013; Yin et al., 2014). Furthermore, several studies have linked the function of *C. elegans* sensory neurons to lifespan, suggesting that perception of environmental stimuli and food signals modulates survival across species (Alcedo and Kenyon, 2004). In Chapter 4, I will describe a new *C. elegans* model of aging-associated sensory behavioral decline and I will present evidence for a novel neural circuit mechanism that drives this behavioral decline whereby impaired neurotransmitter release in aged animals may reduce neural activity in a defined olfactory circuit.

Summary

In this dissertation, I will describe my research into the molecular and neural circuit basis of behavior. Using the *C. elegans* model, I identify novel, flexible circuit motifs, which function in the gustatory and olfactory systems of young and aged animals to drive chemosensory behaviors. In Chapter 2, I will describe an insulin neuropeptide-

regulated and sensory context-dependent switch in the composition of a salt sensory neural circuit that drives behavioral plasticity. In Chapter 3, I will further discuss the context and implications of the results described in Chapter 2. Specifically, in the context of genes, circuits and behaviors, I will discuss the diverse modes of neuropeptide processing and signaling, which expand the coding potential of the nervous system. In Chapter 4, I will functionally characterize a distributed neural circuit composed of primary and secondary olfactory neurons that generates olfactory behavioral plasticity. I will also describe specific impairments in neural activity in this circuit in aged animals, which underlie aging-associated behavioral declines. Finally, in Chapter 5, I will highlight the conclusions that may be drawn from this body of research, discuss new insights into key principles of nervous system function and describe several future directions worthy of additional study in *C. elegans* and other species.

Acknowledgments

This chapter includes a partial reprint of material in Leinwand, S.G. and Chalasani, S.H. (2011). Olfactory networks: from sensation to perception. Curr Opin Genet Dev, 21 and is included with permission from the journal and all authors. The dissertation author was the primary author of this paper.

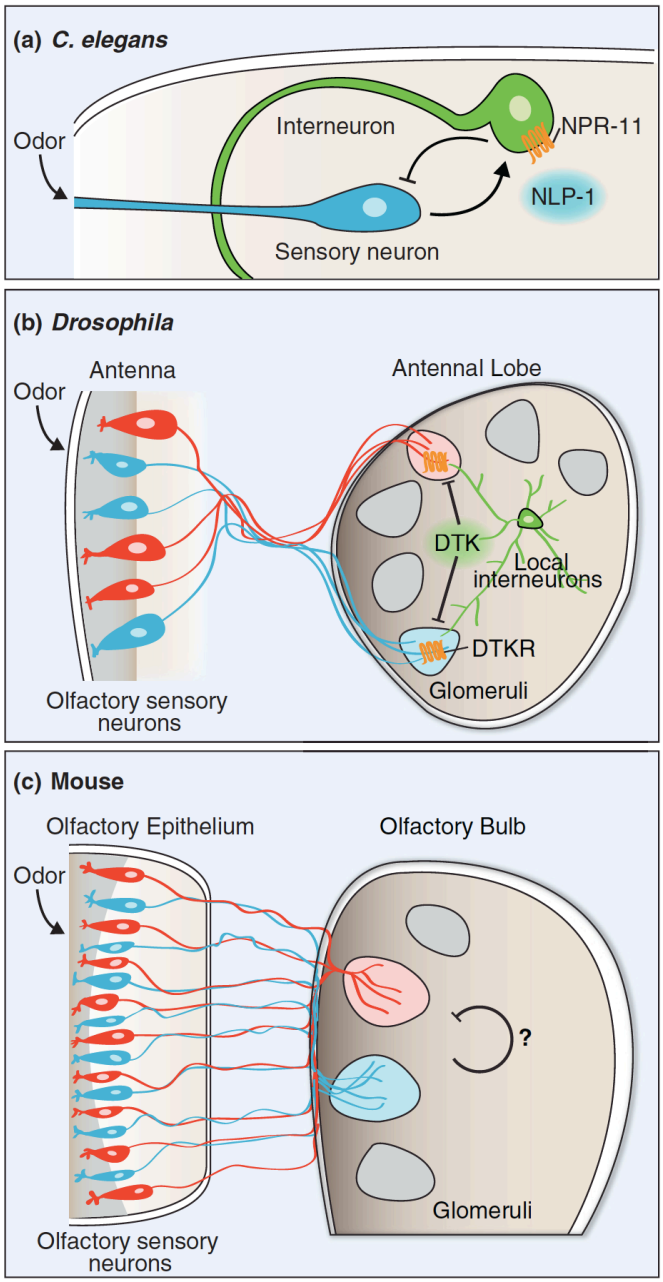

Figure 1.1: Neuropeptide modulation of olfactory sensory neurons. (a) A *C. elegans* chemosensory neuron releases a neuropeptide, NLP-1, which binds an interneuron-expressed receptor, NPR-11, and in turn suppresses the odor-evoked responses of the sensory neuron. (b) *Drosophila* olfactory sensory neurons expressing the same receptor project to target cells in a glomerulus. Local interneurons in the antennal lobe release a tackykinin-related peptide, DTK, which binds its receptor, DTKR, on olfactory sensory neuron axons and suppresses neurotransmitter release from them. (c) In mice, a similar mechanism is postulated.

References

Ache, B.W., and Young, J.M. (2005). Olfaction: diverse species, conserved principles. Neuron 48, 417-430.

Alcedo, J., and Kenyon, C. (2004). Regulation of C. elegans longevity by specific gustatory and olfactory neurons. Neuron 41, 45-55.

Baldridge, W.H., Vaney, D.I., and Weiler, R. (1998). The modulation of intercellular coupling in the retina. Semin Cell Dev Biol 9, 311-318.

Bargmann, C.I. (2006). Chemosensation in C. elegans. WormBook, 1-29.

Bargmann, C.I. (2012). Beyond the connectome: how neuromodulators shape neural circuits. Bioessays 34, 458-465.

Bargmann, C.I., Hartwieg, E., and Horvitz, H.R. (1993). Odorant-selective genes and neurons mediate olfaction in C. elegans. Cell 74, 515-527.

Bargmann, C.I., and Horvitz, H.R. (1991). Chemosensory neurons with overlapping functions direct chemotaxis to multiple chemicals in C. elegans. Neuron 7, 729-742.

Chalasani, S.H., Chronis, N., Tsunozaki, M., Gray, J.M., Ramot, D., Goodman, M.B., and Bargmann, C.I. (2007). Dissecting a circuit for olfactory behaviour in Caenorhabditis elegans. Nature 450, 63-70.

Chalasani, S.H., Kato, S., Albrecht, D.R., Nakagawa, T., Abbott, L.F., and Bargmann, C.I. (2010). Neuropeptide feedback modifies odor-evoked dynamics in Caenorhabditis elegans olfactory neurons. Nat Neurosci 13, 615-621.

Chang, A.J., Chronis, N., Karow, D.S., Marletta, M.A., and Bargmann, C.I. (2006). A distributed chemosensory circuit for oxygen preference in C. elegans. PLoS Biol 4, e274.

Chao, M.Y., Komatsu, H., Fukuto, H.S., Dionne, H.M., and Hart, A.C. (2004). Feeding status and serotonin rapidly and reversibly modulate a Caenorhabditis elegans chemosensory circuit. Proc Natl Acad Sci U S A 101, 15512-15517.

Chen, Z., Hendricks, M., Cornils, A., Maier, W., Alcedo, J., and Zhang, Y. (2013). Two insulin-like peptides antagonistically regulate aversive olfactory learning in C. elegans. Neuron 77, 572-585.

Chihara, T., Kitabayashi, A., Morimoto, M., Takeuchi, K., Masuyama, K., Tonoki, A., Davis, R.L., Wang, J.W., and Miura, M. (2014). Caspase inhibition in select olfactory neurons restores innate attraction behavior in aged Drosophila. PLoS Genet 10, e1004437.

Choi, G.B., Stettler, D.D., Kallman, B.R., Bhaskar, S.T., Fleischmann, A., and Axel, R. (2011). Driving opposing behaviors with ensembles of piriform neurons. Cell 146, 1004-1015.

Dewan, A., Pacifico, R., Zhan, R., Rinberg, D., and Bozza, T. (2013). Non-redundant coding of aversive odours in the main olfactory pathway. Nature 497, 486-489.

Doty, R.L., and Kamath, V. (2014). The influences of age on olfaction: a review. Frontiers in psychology 5, 20.

Galizia, C.G. (2014). Olfactory coding in the insect brain: data and conjectures. Eur J Neurosci 39, 1784-1795.

Ghosh, S., Larson, S.D., Hefzi, H., Marnoy, Z., Cutforth, T., Dokka, K., and Baldwin, K.K. (2011). Sensory maps in the olfactory cortex defined by long-range viral tracing of single neurons. Nature 472, 217-220.

Godfrey, P.A., Malnic, B., and Buck, L.B. (2004). The mouse olfactory receptor gene family. Proc Natl Acad Sci U S A 101, 2156-2161.

Gray, J.M., Hill, J.J., and Bargmann, C.I. (2005). A circuit for navigation in Caenorhabditis elegans. Proc Natl Acad Sci U S A 102, 3184-3191.

Hansen, M., Chandra, A., Mitic, L.L., Onken, B., Driscoll, M., and Kenyon, C. (2008). A role for autophagy in the extension of lifespan by dietary restriction in C. elegans. PLoS Genet 4, e24.

Hedner, M., Nilsson, L.G., Olofsson, J.K., Bergman, O., Eriksson, E., Nyberg, L., and Larsson, M. (2010). Age-Related Olfactory Decline is Associated with the BDNF Val66met Polymorphism: Evidence from a Population-Based Study. Front Aging Neurosci 2, 24.

Hobert, O. (2013). The neuronal genome of Caenorhabditis elegans. WormBook, 1-106.

Honegger, K.S., Campbell, R.A., and Turner, G.C. (2011). Cellular-resolution population imaging reveals robust sparse coding in the Drosophila mushroom body. J Neurosci 31, 11772-11785.

Hummel, T., Kobal, G., Gudziol, H., and Mackay-Sim, A. (2007). Normative data for the "Sniffin' Sticks" including tests of odor identification, odor discrimination, and olfactory thresholds: an upgrade based on a group of more than 3,000 subjects. European archives of oto-rhino-laryngology : official journal of the European Federation of Oto-Rhino-Laryngological Societies 264, 237-243.

Ignell, R., Root, C.M., Birse, R.T., Wang, J.W., Nassel, D.R., and Winther, A.M. (2009). Presynaptic peptidergic modulation of olfactory receptor neurons in Drosophila. Proc Natl Acad Sci U S A 106, 13070-13075.

Iino, Y., and Yoshida, K. (2009). Parallel use of two behavioral mechanisms for chemotaxis in Caenorhabditis elegans. J Neurosci 29, 5370-5380.

Katz, D.B., Simon, S.A., and Nicolelis, M.A. (2001). Dynamic and multimodal responses of gustatory cortical neurons in awake rats. J Neurosci 21, 4478-4489.

Kenyon, C.J. (2010). The genetics of ageing. Nature 464, 504-512.

Larsson, M.C., Domingos, A.I., Jones, W.D., Chiappe, M.E., Amrein, H., and Vosshall, L.B. (2004). Or83b encodes a broadly expressed odorant receptor essential for Drosophila olfaction. Neuron 43, 703-714.

Liman, E.R., Zhang, Y.V., and Montell, C. (2014). Peripheral coding of taste. Neuron 81, 984-1000.

Liu, J., Zhang, B., Lei, H., Feng, Z., Liu, J., Hsu, A.L., and Xu, X.Z. (2013). Functional aging in the nervous system contributes to age-dependent motor activity decline in C. elegans. Cell Metab 18, 392-402.

Maier, J.X., and Katz, D.B. (2013). Neural dynamics in response to binary taste mixtures. J Neurophysiol 109, 2108-2117.

Maier, J.X., Wachowiak, M., and Katz, D.B. (2012). Chemosensory convergence on primary olfactory cortex. J Neurosci 32, 17037-17047.

Malnic, B., Godfrey, P.A., and Buck, L.B. (2004). The human olfactory receptor gene family. Proc Natl Acad Sci U S A 101, 2584-2589.

Malnic, B., Hirono, J., Sato, T., and Buck, L.B. (1999). Combinatorial receptor codes for odors. Cell 96, 713-723.

Masse, N.Y., Turner, G.C., and Jefferis, G.S. (2009). Olfactory information processing in Drosophila. Current biology : CB 19, R700-713.

Mills, H., Wragg, R., Hapiak, V., Castelletto, M., Zahratka, J., Harris, G., Summers, P., Korchnak, A., Law, W., Bamber, B., and Komuniecki, R. (2012). Monoamines and neuropeptides interact to inhibit aversive behaviour in Caenorhabditis elegans. EMBO J 31, 667-678.

Miyamichi, K., Amat, F., Moussavi, F., Wang, C., Wickersham, I., Wall, N.R., Taniguchi, H., Tasic, B., Huang, Z.J., He, Z., *et al*. (2011). Cortical representations of olfactory input by trans-synaptic tracing. Nature 472, 191-196.

Murphy, C., Schubert, C.R., Cruickshanks, K.J., Klein, B.E., Klein, R., and Nondahl, D.M. (2002). Prevalence of olfactory impairment in older adults. JAMA 288, 2307-2312.

Nakai, J., Ohkura, M., and Imoto, K. (2001). A high signal-to-noise Ca(2+) probe composed of a single green fluorescent protein. Nat Biotechnol 19, 137-141.

Nassel, D.R., Enell, L.E., Santos, J.G., Wegener, C., and Johard, H.A. (2008). A large population of diverse neurons in the Drosophila central nervous system expresses short neuropeptide F, suggesting multiple distributed peptide functions. BMC Neurosci 9, 90.

Ni, M.M., Luo, Y., Liu, J., Liao, D.Q., and Tang, Y.D. (2008). FMRFamide modulates outward potassium currents in mouse olfactory sensory neurons. Clinical and experimental pharmacology & physiology 35, 563-567.

Oka, Y., Katada, S., Omura, M., Suwa, M., Yoshihara, Y., and Touhara, K. (2006). Odorant receptor map in the mouse olfactory bulb: in vivo sensitivity and specificity of receptor-defined glomeruli. Neuron 52, 857-869.

Olsen, S.R., and Wilson, R.I. (2008). Lateral presynaptic inhibition mediates gain control in an olfactory circuit. Nature 452, 956-960.

Perkins, L.A., Hedgecock, E.M., Thomson, J.N., and Culotti, J.G. (1986). Mutant sensory cilia in the nematode Caenorhabditis elegans. Dev Biol 117, 456-487.

Pierce-Shimomura, J.T., Faumont, S., Gaston, M.R., Pearson, B.J., and Lockery, S.R. (2001). The homeobox gene lim-6 is required for distinct chemosensory representations in C. elegans. Nature 410, 694-698.

Pierce-Shimomura, J.T., Morse, T.M., and Lockery, S.R. (1999). The fundamental role of pirouettes in Caenorhabditis elegans chemotaxis. J Neurosci 19, 9557-9569.

Pinto, J.M., Wroblewski, K.E., Kern, D.W., Schumm, L.P., and McClintock, M.K. (2014). Olfactory dysfunction predicts 5-year mortality in older adults. PLoS One 9, e107541.

Poo, C., and Isaacson, J.S. (2009). Odor representations in olfactory cortex: "sparse" coding, global inhibition, and oscillations. Neuron 62, 850-861.

Praitis, V., and Maduro, M.F. (2011). Transgenesis in C. elegans. Methods Cell Biol 106, 161-185.

Price, J.L., and Powell, T.P. (1970). The mitral and short axon cells of the olfactory bulb. Journal of cell science 7, 631-651.

Richard, M.B., Taylor, S.R., and Greer, C.A. (2010). Age-induced disruption of selective olfactory bulb synaptic circuits. Proc Natl Acad Sci U S A 107, 15613-15618.

Root, C.M., Ko, K.I., Jafari, A., and Wang, J.W. (2011). Presynaptic facilitation by neuropeptide signaling mediates odor-driven food search. Cell 145, 133-144.

Savigner, A., Duchamp-Viret, P., Grosmaitre, X., Chaput, M., Garcia, S., Ma, M., and Palouzier-Paulignan, B. (2009). Modulation of spontaneous and odorant-evoked activity of rat olfactory sensory neurons by two anorectic peptides, insulin and leptin. J Neurophysiol 101, 2898-2906.

Schumm, L.P., McClintock, M., Williams, S., Leitsch, S., Lundstrom, J., Hummel, T., and Lindau, S.T. (2009). Assessment of sensory function in the National Social Life, Health, and Aging Project. The journals of gerontology Series B, Psychological sciences and social sciences 64 Suppl 1, i76-85.

Scott, K. (2005). Taste recognition: food for thought. Neuron 48, 455-464.

Semmelhack, J.L., and Wang, J.W. (2009). Select Drosophila glomeruli mediate innate olfactory attraction and aversion. Nature 459, 218-223.

Sengupta, P., Chou, J.C., and Bargmann, C.I. (1996). *odr-10* encodes a seven transmembrane domain olfactory receptor required for responses to the odorant diacetyl. Cell 84, 899-909.

Sosulski, D.L., Bloom, M.L., Cutforth, T., Axel, R., and Datta, S.R. (2011). Distinct representations of olfactory information in different cortical centres. Nature 472, 213-216.

Stettler, D.D., and Axel, R. (2009). Representations of odor in the piriform cortex. Neuron 63, 854-864.

Stokes, C.C., and Isaacson, J.S. (2010). From dendrite to soma: dynamic routing of inhibition by complementary interneuron microcircuits in olfactory cortex. Neuron 67, 452-465.

Suh, G.S., Wong, A.M., Hergarden, A.C., Wang, J.W., Simon, A.F., Benzer, S., Axel, R., and Anderson, D.J. (2004). A single population of olfactory sensory neurons mediates an innate avoidance behaviour in Drosophila. Nature 431, 854-859.

Suzuki, H., Thiele, T.R., Faumont, S., Ezcurra, M., Lockery, S.R., and Schafer, W.R. (2008). Functional asymmetry in Caenorhabditis elegans taste neurons and its computational role in chemotaxis. Nature 454, 114-117.

Thomas-Danguin, T., Sinding, C., Romagny, S., El Mountassir, F., Atanasova, B., Le Berre, E., Le Bon, A.M., and Coureaud, G. (2014). The perception of odor objects in everyday life: a review on the processing of odor mixtures. Frontiers in psychology 5, 504.

Toth, M.L., Melentijevic, I., Shah, L., Bhatia, A., Lu, K., Talwar, A., Naji, H., Ibanez-Ventoso, C., Ghose, P., Jevince, A., *et al*. (2012). Neurite sprouting and synapse

deterioration in the aging Caenorhabditis elegans nervous system. J Neurosci 32, 8778-8790.

Troemel, E.R., Kimmel, B.E., and Bargmann, C.I. (1997). Reprogramming chemotaxis responses: sensory neurons define olfactory preferences in C. elegans. Cell 91, 161-169.

Vassar, R., Chao, S.K., Sitcheran, R., Nunez, J.M., Vosshall, L.B., and Axel, R. (1994). Topographic organization of sensory projections to the olfactory bulb. Cell 79, 981-992.

Vosshall, L.B., Amrein, H., Morozov, P.S., Rzhetsky, A., and Axel, R. (1999). A spatial map of olfactory receptor expression in the Drosophila antenna. Cell 96, 725-736.

Vosshall, L.B., Wong, A.M., and Axel, R. (2000). An olfactory sensory map in the fly brain. Cell 102, 147-159.

Wang, J.W., Wong, A.M., Flores, J., Vosshall, L.B., and Axel, R. (2003). Two-photon calcium imaging reveals an odor-evoked map of activity in the fly brain. Cell 112, 271-282.

Wang, Z., and Sherwood, D.R. (2011). Dissection of genetic pathways in C. elegans. Methods Cell Biol 106, 113-157.

Ward, S. (1973). Chemotaxis by the nematode Caenorhabditis elegans: identification of attractants and analysis of the response by use of mutants. Proc Natl Acad Sci U S A 70, 817-821.

Weimann, J.M., and Marder, E. (1994). Switching neurons are integral members of multiple oscillatory networks. Curr Biol 4, 896-902.

Wes, P.D., and Bargmann, C.I. (2001). C. elegans odour discrimination requires asymmetric diversity in olfactory neurons. Nature 410, 698-701.

White, J.G., Southgate, E., Thomson, J.N., and Brenner, S. (1986). The structure of the nervous system of the nematode Caenorhabditis elegans. Philos Trans R Soc Lond B Biol Sci 314, 1-340.

Wilson, R.S., Arnold, S.E., Buchman, A.S., Tang, Y., and Bennett, D.A. (2008). Odor identification and progression of parkinsonian signs in older persons. Exp Aging Res 34, 173-187.

Wilson, R.S., Arnold, S.E., Schneider, J.A., Boyle, P.A., Buchman, A.S., and Bennett, D.A. (2009). Olfactory impairment in presymptomatic Alzheimer's disease. Ann N Y Acad Sci 1170, 730-735.

Wolff, S., and Dillin, A. (2006). The trifecta of aging in Caenorhabditis elegans. Exp Gerontol 41, 894-903.

Yin, J.A., Liu, X.J., Yuan, J., Jiang, J., and Cai, S.Q. (2014). Longevity manipulations differentially affect serotonin/dopamine level and behavioral deterioration in aging Caenorhabditis elegans. J Neurosci 34, 3947-3958.

Zhao, G.Q., Zhang, Y., Hoon, M.A., Chandrashekar, J., Erlenbach, I., Ryba, N.J., and Zuker, C.S. (2003). The receptors for mammalian sweet and umami taste. Cell 115, 255-266.

CHAPTER 2.

Neuropeptide signaling remodels chemosensory circuit composition in *Caenorhabditis elegans*

Abstract

Neural circuits detect environmental changes and drive behavior. The routes of information flow through dense neural networks are dynamic; however, the mechanisms underlying this circuit flexibility are poorly understood. Here, we define a novel, sensory context-dependent and neuropeptide-regulated switch in the composition of a *C. elegans* salt sensory circuit. The primary salt detectors, ASE sensory neurons, use BLI-4 endoprotease-dependent cleavage to release the insulin-like peptide INS-6 in response to large but not small changes in external salt stimuli. Insulins, signaling through the insulin receptor DAF-2, functionally switch the AWC olfactory sensory neuron into an interneuron in the salt circuit. Animals with disrupted insulin signaling have deficits in salt attraction, suggesting that peptidergic signaling potentiates responses to high salt stimuli, which may promote ion homeostasis. Our results show that sensory context and neuropeptide signaling modify neural networks and suggest general mechanisms for generating flexible behavioral outputs by modulating neural circuit composition.

Introduction

All sensory circuits use specialized sensory neurons to detect environmental changes and downstream interneurons to transform that information, generating flexible behaviors. In particular, chemosensory neural circuits have an additional challenge of representing not only commonly encountered cues, but also a potentially limitless set of novel smell and taste stimuli (Touhara and Vosshall, 2009). One approach to understanding how chemical cues drive behavior is to trace the paths of information flow in the corresponding neural circuits. Remarkably, the active route through networks of anatomically connected sensory, inter- and motor neurons can also switch based on context, as observed in circuits processing nutrients (Weimann and Marder, 1994) and light (Baldridge et al., 1998). However, the underlying molecular mechanisms that configure active neural circuits are poorly understood. The *C. elegans* nervous system, with just 302 neurons connected by identified synapses (White et al., 1986), is ideally suited for a circuit-level analysis of how chemosensory stimuli are represented and transformed into behavioral outputs (de Bono and Maricq, 2005).

Cell ablation experiments in *C. elegans* identified individual sensory neurons critical for directed locomotion towards chemical stimuli. In particular, the ASE sensory neurons are necessary to drive attraction to salts, while the AWC sensory neurons drive attraction to odors (**Figure 2.5a**) (Bargmann and Horvitz, 1991). The neural circuitry acting downstream of these neurons to drive behavior has not been fully mapped; however, neuroanatomical studies identify a set of common interneuron targets, including AIA (**Figure 2.1a**) (White et al., 1986). Interestingly, the pair of bilateral ASE neurons are functionally distinct: ASELeft (ASEL) detects an increase in sodium chloride (NaCl)

and ASERight (ASER) responds to a decrease in NaCl (Suzuki et al., 2008). Similarly, the two AWC neurons, AWC^{ON} and AWC^{OFF}, collectively respond to the odorant benzaldehyde and uniquely respond to other odorants (Wes and Bargmann, 2001). Here, we combine genetic manipulations, *in vivo* calcium imaging and behavioral analysis to investigate how the functional ASE-driven salt circuit represents specific changes in salt to drive dynamic behavioral responses. *C. elegans*, much like mammals, prefer a concentration of salt that maintains ion homeostasis, providing a physiological correlate for salt attraction behavior (Bargmann, 2006; Chandrashekar et al., 2010). We find that insulin neuropeptide signaling transiently remodels the composition of the salt neural circuit and modulates behavior in response to high, but not low, salt stimuli by switching the AWC^{ON} olfactory sensory neuron into an interneuron.

Results

A distributed neural network encodes salt concentration

To characterize the functional neural circuit representing salt stimuli, we recorded neural activity from the anteriorly localized amphid sensory neurons using genetically expressed calcium indicators of the GCaMP family. Calcium signals in *C. elegans* neurons have been shown to strongly correlate with neuronal depolarization (Clark et al., 2006; Ramot et al., 2008). Previous studies have shown that ASEL neurons are activated by the addition of NaCl stimuli greater than or equal to 10 mM (Suzuki et al., 2008) (**Figures 2.1b, 2.5b** and **2.6a**), while ASER is sensitive to removal of at least 1 mM NaCl (Suzuki et al., 2008) (**Figures 2.6c,e**). Unexpectedly, we found that AWC^{ON} olfactory sensory neurons respond to a +50 mM increase in NaCl, much like ASEL (**Figures 2.1b,**

2.5b and **2.6b**). AWC^{OFF} neurons respond similarly to +50 mM NaCl (**Figure 2.6d**). In contrast, a weaker +10 mM increase in NaCl only activates ASEL, but not AWC^{ON} (**Figures 2.1c, 2.5c** and **2.6b)**, or AWC^{OFF} (**Figure 2.6f**). AWC^{ON} responses to salt are dose-dependent and have a threshold of +20 mM NaCl (**Figure 2.6b**). Furthermore, AWC^{ON} specifically responds to salt and is not a generalized osmolarity sensor (**Figure 2.6g**). Moreover, there is specificity in the salt circuit as other amphid sensory neurons AWA, ASI, ASK, AWB and ASH do not respond to increases in NaCl (**Figures 2.1b** and **2.6h**). These results show that the *increase* in salt concentration is not encoded by the specialized responses of unimodal neurons, as was predicted from earlier cell ablation studies(Bargmann and Horvitz, 1991). Instead, the combined activity of multiple sensory neurons represents external salt concentrations: ASEL together with polymodal AWC^{ON} encode larger than 20 mM increases in salt. Finally, these experiments complement studies showing that a distinct, but similarly distributed circuit encodes the *decrease* in salt concentration (Thiele et al., 2009).

AWC neurons play key role in the salt circuit and behavior

We further investigated the role of AWC sensory neurons in the salt circuit by recording activity from a downstream interneuron, AIA, which receives inputs from both AWC and ASE neurons (White et al., 1986) (**Figure 2.1a**). AIA interneurons respond to an increase of +50 mM NaCl (**Figures 2.1d** and **2.5d**). These responses are greatly reduced in animals with genetically-ablated AWC neurons (Beverly et al., 2011) (**Figures 2.1d** and **2.5d**), suggesting a non-redundant role for AWC in the salt neural circuit. AWC neurons are glutamatergic and peptidergic (Chalasani et al., 2010), so we

first investigated whether AWC signals the presence of high (+50 mM) salt to AIA by releasing glutamate. We knocked down the vesicular glutamate transporter, *eat-4,* which is essential for functional glutamatergic neurotransmission (Lee et al., 1999), specifically in AWC neurons. AWC-specific *eat-4* knockdown has no effect on AIA responses to +50 mM NaCl suggesting that glutamate was not the neurotransmitter (**Figure 2.1d**). We then tested whether AWC signaling to AIA uses neuropeptides. Calcium-dependent secretion activator (CADPS) is an essential component of the release machinery for neuropeptide-containing dense core vesicles (*unc-31* in *C. elegans*) (Richmond, 2005). AWC-specific *unc-31* knockdown or ablating AWC significantly reduces AIA responses to +50 mM NaCl (**Figure 2.1d**). This suggests that peptidergic signaling from AWC is a critical component of the high salt circuit. Neither AWC ablation nor knockdown of AWC peptide release machinery has an effect on AIA responses to +10 mM NaCl (within the 10 s post-stimulus addition period), as predicted from the unresponsiveness of AWC to this weak stimulus (**Figures 2.1e** and **2.5e**). Our results reveal that AWC has different effects on AIA activity based on sensory modality. Previous work showed that, in an odor circuit, AWC-released glutamate inhibits AIA responses (Chalasani et al., 2010), while we show that, in the high salt circuit, AWC-released neuropeptides excite AIA.

To validate the salt circuit configurations characterized by imaging, we performed chemotaxis behavior assays to test whether AWC contributes to salt-driven behavior. In a salt chemotaxis assay, animals migrate towards a point source of NaCl over an hour (Ward, 1973) (**Figure 2.7b**). This behavior requires ASE neurons since *che-1* mutants which lack functional ASE neurons do not chemotax to salt (Uchida et al., 2003) (**Figure 2.1f,** n = 10 for all concentrations). Notably, AWC ablation causes a specific reduction in

chemotaxis to steep, high salt gradients (with point sources of 500 and 750 mM NaCl, n = 10 and 10 respectively; "WT" n = 13 and 12 respectively), but has no effect on shallow, low salt gradient behavior (100 and 250 mM NaCl sources, n = 10 and 11; "WT" n = 10 and 10 respectively) (**Figure 2.1f**). In fact, both the AWC^{ON} and AWC^{OFF} neurons contribute non-redundantly to high salt chemotaxis behavior (**Figure 2.7c**). Furthermore, *unc-31*-dependent neuropeptide release from AWC is necessary for chemotaxis to high salt sources, but dispensable for low salt-directed behavior (**Figures 2.1g,h**). These results suggest that AWC signaling may increase the dynamic range of the salt circuit and prevent behavioral responses from saturating at high salt levels. The specific contribution of AWC neurons to high salt concentration behavior supports our imaging findings that AWC specifically responds to high, but not low salt stimuli (**Figures 2.1b,c**).

AWC^{ON} acts as an interneuron in the salt circuit

The results described above suggest a crucial role for AWC neurons in the salt neural circuit and in salt-evoked behaviors. AWC^{ON} could adopt these roles either by intrinsically sensing salt, much like ASE (Suzuki et al., 2008), or by acting as an interneuron in an ASE-driven circuit. To distinguish between these two circuit configurations, we performed genetic manipulations that eliminate the ability of sensory neuron dendrites to contact the environment. We analyzed hypomorphic *osm-6* mutants that lack functional sensory cilia (dendritic endings) and found them to have greatly reduced ASEL salt responses and AWC^{ON} salt and odor responses (Collet et al., 1998) (**Figures 2.2b,c** and **2.8b,c**). OSM-6 acts cell-autonomously (Collet et al., 1998); therefore, we restored OSM-6 function under an ASEL cell-selective promoter and

verified by confocal imaging that this enabled only ASEL, and not AWC^{ON}, to contact the environment (**Figures 2.2a** and **2.8a**). In this ASEL-specific *osm-6* rescued animal, AWC^{ON} responds to +50 mM salt, suggesting that ASEL with functional cilia is sufficient to restore salt responses to AWC^{ON} (**Figures 2.2b,c** and **2.8a,c**). In contrast, rescuing *osm-6* under an AWC-selective promoter does not restore AWC^{ON} responses to salt, implying that AWC^{ON} alone is insufficient to respond to salt (**Figures 2.2b** and **2.8c**). We confirmed that this rescuing array was functional as it fully restored the expected AWC^{ON} responses to the odor benzaldehyde (**Figure 2.2c**). Taken together, these results indicate that AWC^{ON} is not an intrinsic salt sensor. Moreover, in the context of the high salt circuit, AWC acts as an interneuron by responding to a signal from ASEL.

Our work shows that ASEL to AWC^{ON} signaling functions in the adult. However, it is also possible that signaling between ASEL and AWC^{ON} may occur during development to instruct the wiring of the salt circuit. To probe this temporal requirement and eliminate the possibility of developmental contributions to the phenotypes observed in genetic mutants, we photo-ablated the ASEL neuron in the L4 larvae (Qi et al., 2012), and subsequently analyzed those adults. Consistently, AWC^{ON} neurons fail to respond to +50 mM NaCl after larval ASEL ablation, while mock ablation has no effect on salt responses (**Figure 2.2d**). These results suggest that the observed ASEL-AWC^{ON} high salt circuit configuration is required in the adult and is not a consequence of changes in circuitry during early development.

AWC^{ON} salt responses require neuropeptides from ASEL

The results described above suggest that ASEL sensory neurons signal the presence of large increases in NaCl in the environment to the AWC^{ON} neurons, recruiting AWC^{ON} into the salt circuit. To further confirm the role of ASEL in mediating AWC^{ON} responses to salt, we tested the effects of manipulating ASEL neurotransmission. Mutations in *tom-1,* the *C. elegans* homolog of *Tomosyn,* which encodes a syntaxin interacting protein, upregulate all forms of neurotransmission (Gracheva et al., 2007) (for clarifying schematic see **Figure 2.7a**). We generated an ASEL-selective knockdown of *tom-1* to increase ASEL neurotransmitter and neuropeptide release. We hypothesized that enhanced transmission from ASEL would promote AWC^{ON} responses to the previously unresponsive +10 mM NaCl change. We found that AWC^{ON} did indeed respond to this small +10 mM stimulus in the ASEL-specific *tom-1* knockdown animal (**Figure 2.3a**), confirming the crucial role of ASEL neurotransmission in initiating AWC^{ON} responses to salt.

C. elegans neurons including ASEL release amino acid and small molecule neurotransmitters, like glutamate, GABA and acetylcholine, from small, clear synaptic vesicles and neuropeptides from large, dense core vesicles (Richmond, 2005). We tested genetic mutants to identify the nature of the ASEL to AWC^{ON} signal. First, we analyzed mutants in *unc-13*, the *C. elegans* homolog of Munc13, which promotes the open syntaxin conformation needed for the release of small, clear synaptic vesicles (Richmond et al., 1999) (**Figure 2.7a**). Surprisingly, we found that AWC^{ON} neurons continue to respond to +50 mM salt even in the *unc-13* mutants (**Figure 2.3b**), suggesting that ASEL-AWC^{ON} communication does not require glutamate or other small molecule neurotransmitters. Therefore, we tested the salt responses of animals with a null mutation

in the *C. elegans* homolog of Calcium-dependent secretion activator, *unc-31*, in which the release of dense core vesicles containing neuropeptides is defective (Speese et al., 2007) (**Figure 2.7a**). We found that AWC^{ON} responses to 50 mM increases in salt are eliminated in *unc-31* mutants and this gene is specifically required in ASEL (**Figure 2.3c**). In contrast AWC^{OFF} neurons respond normally to +50 mM NaCl in both *unc-13* and *unc-31* mutants, suggesting that this neuron is an intrinsic sensor of large changes in salt (**Figure 2.9a**). Consistent with previous results, ASEL responses to salt are unchanged in *unc-13* and *unc-31* mutants (Suzuki et al., 2008) (**Figure 2.9d**). Taken together, these results suggest that ASEL detects large increases in salt and releases a neuropeptide to recruit AWC^{ON} into the salt circuit.

The *C. elegans* genome includes at least 113 neuropeptide genes (40 insulin-like, 31 FMRFamide-related and 42 other neuropeptide-like) that encode approximately 250 distinct neuropeptides (Li and Kim, 2008). In order to identify the cognate neuropeptide family, we tested mutants in the neuropeptide-processing pathway. Neuropeptides are synthesized as much larger propeptides, then cleaved by specific proprotein convertase enzymes and further modified to generate mature peptides. Four distinct proprotein convertases have been identified in the worm (Li and Kim, 2008). We hypothesized that in one or more proprotein convertase mutant, ASEL would not be able to process, cleave and release the mature peptide(s) necessary for recruiting AWC^{ON} to respond to high salt. Surprisingly, null mutations in *egl-3*, the major neuronal processor of FMRFamide-related peptides and neuropeptide-like proteins (Husson et al., 2006), as well as mutations in the convertases *kpc-1* and *aex-5,* do not alter AWC^{ON} responses to salt (**Figures 2.3d** and **2.9b**). By contrast, a hypomorphic mutation in the proprotein convertase *bli-4*, which

cleaves procollagens in the worm cuticle, but has no known function in the nervous system (Thacker et al., 1995), blocks AWC^{ON} responses to salt (**Figure 2.3d**). Furthermore, BLI-4 is specifically required in ASEL for AWC^{ON} salt responses (**Figure 2.3d**, see also **Figure 2.9b**). We also tested ASEL responses to salt in *bli-4* mutants and found them to be normal (**Figure 2.9e**). These results suggest that ASEL uses a BLI-4 protease cleavage step downstream of salt detection to generate the mature peptide(s) that recruit AWC^{ON} into the salt circuit.

We confirmed a behavioral role for BLI-4 and ASEL-released neuropeptides using a salt chemotaxis assay. We found that animals with AWC-ablated, ASEL-specific knockdown of *unc-31*-dependent neuropeptide release, or ASEL-specific knockdown of *bli-4* (but not mutations in *egl-3*) show specific defects in attraction to a high concentration of salt (750 mM point source, **Figures 2.3e** and **2.7e**), but have no effect on attraction to lower salt (250 mM point source, **Figure 2.7d**). Taken together, these results indicate that ASEL uses BLI-4 cleavage to generate and release neuropeptides that modify the salt neural circuit and salt attraction behavior.

ASEL-released INS-6 recruits AWC^{ON} to the salt circuit

Mass spectrometry experiments show that the proprotein convertase EGL-3 processes many FMRFamide-like peptides and neuropeptide-like proteins, while BLI-4 has no role in processing these peptides (Husson et al., 2006). We hypothesized that BLI-4 might instead cleave the remaining major class of neuropeptides (insulins), which are not detectable in these mass spectrometry studies (Husson et al., 2006). Given that ASEL requires BLI-4 to communicate with AWC^{ON}, we analyzed the gene sequences of the 40

insulin-like peptides (Li and Kim, 2008) and identified numerous genes containing the predicted BLI-4 cleavage sites (Thacker et al., 2006) (**Table 2.2**). We then imaged AWC^{ON} responses to high salt in animals with mutations in these candidate insulins. AWC^{ON} neurons in *ins-6* null mutants have significantly reduced responses to +50 mM NaCl (**Figure 2.4a**). Normal responses are restored when *ins-6* is rescued specifically in ASEL (**Figure 2.4a**, see also **Figure 2.9c**). Importantly, ASEL-specific expression of a mutated *ins-6* gene, in which two serine residues replace the two critical arginine amino acids in the predicted BLI-4 cleavage motif (RARR to RASS) (Thacker et al., 1995), fails to rescue the mutant AWC^{ON} responses to salt (**Figure 2.4a**). We also tested ASEL responses to salt in *ins-6* mutants and found them to be normal (**Figure 2.9d**). These data suggest that BLI-4 is required for the proteolytic processing that generates mature INS-6 peptides in ASEL, which signal to AWC^{ON}. However, the small, residual AWC^{ON} responses to high salt observed in *ins-6* mutants (**Figure 2.4a**) suggest that there are additional neuropeptides relaying information from ASEL to AWC^{ON} neurons.

We hypothesized that INS-6 is also required for behavioral attraction to high concentrations of salt. In a chemotaxis assay, we found that *ins-6* mutants have a significant deficit in attraction to high salt (750 mM, **Figure 2.4b**). ASEL-specific expression of the *ins-6* gene rescues this behavioral deficit; however, the mutant form of *ins-6,* in which the BLI-4 cleavage motif is disrupted, does not rescue the behavioral defect (**Figures 2.4b** and **2.7e**). Furthermore, we found that these mutants behave normally in low salt gradients (**Figure 2.7f**). Together, these results suggest a novel role for BLI-4 cleavage in the production of a mature insulin-like peptide, INS-6, which

recruits AWC^{ON} neurons to the high salt neural circuit and specifically potentiates attraction to high salt.

DAF-2/AGE-1 pathway acts in AWC^{ON} in the high salt circuit

Previous studies showed that INS-6 binds the human insulin receptor and functions as an agonist (Hua et al., 2003). Therefore, to identify the *C. elegans* INS-6 receptor and the downstream signaling machinery that might function in AWC^{ON}, we probed the canonical insulin-signaling cascade. We analyzed animals with hypomorphic mutations in the *C. elegans* homolog of the mammalian insulin/IGF receptor tyrosine kinase, *daf-2* (Kimura et al., 1997). We found that AWC^{ON} responses to +50 mM salt are greatly attenuated in *daf-2* mutants (**Figure 2.4c**). Moreover, restoring function of this receptor to AWC specifically is sufficient to restore normal AWC^{ON} responses to salt (**Figure 2.4c**). We then tested partial loss of function mutants of *age-1*, the *C. elegans* PI3-Kinase homolog, which has been shown to act downstream of the DAF-2 insulin receptor (Dorman et al., 1995). AWC^{ON} NaCl responses are much reduced in *age-1* mutants and normal responses are restored to animals when AGE-1 function is specifically rescued in AWC^{ON} (**Figure 2.4d**). ASEL responses to salt are not affected in *daf-2* or *age-1* mutants, suggesting that insulin signaling functions downstream of the stimulus detection (**Figure 2.9e**). These results indicate that AWC^{ON} neurons may use DAF-2 and AGE-1 to detect the ASEL-released insulin-like peptides and to signal the presence of large changes in salt to the downstream circuit.

In addition, we performed epistasis experiments to determine the genetic relationship between these canonical insulin signaling pathway components and the

ASEL neuropeptide processing and release machinery. We found that the endoprotease BLI-4 acts upstream of the DAF-2 insulin receptor and AGE-1. Knocking down *bli-4* in ASEL completely blocks DAF-2- and AGE-1-dependent AWC^{ON} responses to salt. (**Figure 2.4e**, compared to **Figure 2.4c,d**). We also tested whether the weak AWC^{ON} responses to +10 mM NaCl observed in the *tom-1* knockdown (shown in **Figure 2.3a**) were regulated by the same insulin signaling pathway. Consistently, we found that these AWC^{ON} responses are lost in the *ins-6*, *daf-2* or *age-1* mutants (**Figure 2.4f**). This suggests that an effect of ASEL-specific *tom-1* knockdown may be to increase INS-6 release, and this peptide is necessary for the weak AWC^{ON} responses to +10 mM NaCl. Additionally, these results indicate that neuropeptide processing in ASEL and transmitter release from ASEL function upstream of the insulin receptor and PI3-Kinase in the pathway that recruits AWC^{ON} to the high salt circuit.

Discussion

Our results show that *C. elegans* chemosensory neural circuits are flexible and their neuronal composition can be modified by sensory context and insulin neuropeptide signals. Previous studies and our results show that ASEL responds to an increase in NaCl in the environment (Suzuki et al., 2008). Notably, we show that the circuit downstream of ASEL exists in two different configurations: at small changes in NaCl (< 20 mM), we find that ASEL neurons signal directly to downstream, classically-defined interneurons (**Figure 2.10a**). However, at larger changes in NaCl (> 20 mM), ASEL neurons release INS-6 and other neuropeptides to functionally transform the AWC^{ON} sensory neuron into an interneuron and recruit it into the salt circuit (**Figure 2.10b**). These results show that

sensory context and peptide signals switch the response profile of AWC^{ON} neurons and modulate the information that is relayed to downstream circuitry. Consistent with these results, AWC plays a crucial role in transmitting information to the downstream AIA interneurons and in mediating salt behaviors. Our behavioral analyses indicate that this novel ASEL–AWC^{ON} neuropeptide signaling is likely to potentiate attraction to high, but not low concentrations of salt. The unique insulin-regulated high salt circuit configuration may be critical in reinforcing salt appetite, perhaps to maintain ion homeostasis that is needed for organ system functioning (Aburto et al., 2013). Similarly, investigations of mammalian salt circuits show that distinct sets of taste sensory neurons detect high and low salt, with particular neuronal populations contributing to appetitive behaviors (Chandrashekar et al., 2010).

Insulin signaling is highly conserved between mammals and *C. elegans*, with well-characterized roles in the regulation of food intake, glucose metabolism and aging (Taguchi and White, 2008; Tissenbaum, 2012). In the mammalian brain, insulin signals modulate the firing of hypothalamic neurons (Klockener et al., 2011) and olfactory sensory neurons (Savigner et al., 2009). In *C. elegans*, neuronal insulin signaling regulates chemotaxis (Tomioka et al., 2006), thermotaxis (Murakami et al., 2005) and learning (Kauffman et al., 2010). However, less is known about the relevant machinery for processing and releasing insulins. Our results demonstrate that insulin signals may be released from dense core vesicles in a Calcium-dependent secretion activator (UNC-31)-dependent manner, and this action remodels sensory circuits. Furthermore, our data suggests that the insulin-like peptide, INS-6, is processed at a dibasic motif by a proprotein convertase, BLI-4. Insulin-like peptides may in fact be cleaved through

diverse mechanisms at different developmental stages and in different cell types. A recent study showed that pan-neuronally expressed INS-6 can be processed by the proprotein convertase EGL-3 (Hung et al., 2013). In this instance, the mature INS-6 peptide functions as a long-range signal to instruct the development of the neuromuscular junction (Hung et al., 2013). In contrast, our results show that BLI-4 in ASEL generates mature INS-6 peptides that act locally to rapidly recruit AWC^{ON} into the adult salt circuit. Additionally, INS-6 released from ASI neurons has been shown to influence the transcription of another insulin (INS-7) and modify aversive olfactory learning (Chen et al., 2013). These results show that the protein processing machinery regulates the activity of mature peptides both spatially and temporally to modulate both the developing and adult nervous systems. Moreover, these multi-functional roles of INS-6 in development and circuit plasticity are consistent with previous studies showing distinct roles for the same insulin ligand (Chalasani et al., 2010; Tomioka et al., 2006).

Our epistasis experiments demonstrate that BLI-4-dependent insulin processing in ASEL occurs upstream of the insulin peptides binding to the insulin receptor tyrosine kinase, DAF-2, and signaling via the PI3-Kinase, AGE-1 (**Figure 2.10b**). Salt-evoked calcium responses in AWC^{ON} occur downstream of PI3-Kinase activation suggesting a link between intracellular signaling and AWC^{ON} neuronal activation. Moreover, our results suggest that ASEL neurons may release other insulin-like peptides along with INS-6 that likely also signal through this canonical insulin pathway to activate AWC^{ON}.

There is increasing evidence in a number of species that sensory signaling is modulated by neuromodulators and external milieu. In *Drosophila*, variable levels of metabotropic $GABA_B$ receptor expression expand the dynamic range of the olfactory

system to drive flexible and ecologically appropriate behavioral outputs (Root et al., 2008). Non-synaptic, lateral signaling between olfactory receptor neurons also modifies the sensory information relayed to the downstream circuit in certain complex olfactory contexts (Su et al., 2012). However, the underlying molecular machinery is largely unknown. Collectively, these studies and ours provide additional detail about how neuropeptides and other modulatory signals fine-tune sensory encoding to generate flexible behaviors.

We show that sensory context (in our case the concentration of salt) causes a rapid switch in the neural circuit and a novel ASEL-AWC^{ON} insulin neuropeptide signaling cascade mediates this switch. Neuropeptides have been previously shown to play crucial roles in switching neural circuits, particularly in the stomatogastric ganglion of the crab (Dickinson et al., 1990). Neuromodulators can switch individual neurons, such as VD motor neurons, from a sub-circuit that drives a fast pyloric rhythm to a slower gastric rhythm circuit and vice versa (Hooper and Moulins, 1989; Weimann et al., 1991). Interestingly, sensory context can also drive a switch in the vertebrate retinal circuitry. At low light levels, inputs from cone and rod photoreceptors converge onto cone bipolar cells. However, as light intensity increases or in presence of neuromodulators like dopamine and nitric oxide, inputs from rod photoreceptors are turned off. Uncoupling the amacrine AII cells prevents rod cell signals from being relayed to cone bipolar cells to accomplish this circuit modification (Baldridge et al., 1998; Xia and Mills, 2004). Nevertheless, the precise mechanisms for releasing and detecting the modulatory cues that switch these crustacean and mammalian circuits remain to be elucidated. Therefore, while there is precedence for neuropeptides remodeling neural networks, we find that the

ASEL-AWC^{ON}-AIA circuit is unique in its context-dependent and insulin-mediated functional transformation of the AWC^{ON} sensory neuron into an interneuron.

Finally, our results suggest that neural circuits are highly flexible and neuroanatomy is only an important first step towards analyzing brain function. The complete *C. elegans* wiring diagram was mapped from electron microscope reconstructions (White et al., 1986). However, this information is not sufficient to explain the intricate functioning of neural circuits in complex environments. We suggest one explanation for this discrepancy: information can be relayed through numerous alternative neural paths, including flowing through sensory neurons that transiently act like interneurons, depending on environmental context and modulatory states. We speculate that the highly interconnected nature of vertebrate brains (Markov et al., 2012) represents alternate paths for information processing and propose that neuropeptide signaling selects active routes based on context. These flexible neural circuit configurations may be critical for responding to novel and dynamic sensory environments.

Methods

C. elegans strains (**Table 2.1**) were grown and maintained under standard conditions, at 20 degrees C (Brenner, 1974).

Molecular biology and transgenesis

cDNA corresponding to the entire coding sequences of *osm-6*, *tom-1, unc-31, eat-4, daf-2*, and *age-1* was amplified by PCR and expressed under cell-selective promoters.

ins-6 genomic DNA was amplified by PCR and two point mutations (AC to TA) were generated to change the basic arginine residues in the predicted BLI-4 cleavage site(Thacker et al., 1995) to serines (using the Agilent QuikChange II Site-Directed Mutagenesis Kit, primers 5'–CAATGCCACGAGCAAG**TA**GTGTTCCAGCACCAG and 5'– CTGGTGCTGGAACAC**TA**CTTGCTCGTGGCATTG). Neuron-selective RNAi transgenes were created as previously described by co-injection of equal concentrations of sense and antisense oriented gene fragments driven by cell-specific promoters (Esposito et al., 2007). For *bli-4* knockdowns, a fragment matching exons 2–10, containing the protease domain, was synthesized (GenScript) and subcloned in both orientations. For light-inducible ASEL cell ablations and mock ablations, miniSOG was targeted to the mitochondrial outer membrane (tomm-20(N'55AA)::miniSOG) and expressed under an ASEL cell-specific promoter(Qi et al., 2012). Cell-specific expression was achieved using the following promoters: *gcy-7* for ASEL, *gcy-5* for ASER, *odr-3* or *ceh-36* for AWC, *str-2* for AWC^{ON}, *srsx-3* for AWC^{OFF}, *ins-1* for AIA, *gpa-4* for AWA and ASI, *str-3* for ASI, *str-1* for AWB, *sra-6* for ASH and *sra-9* for ASK. For all experiments, a splice leader (SL2) fused to a *mCherry* transgene was used to confirm cell-specific expression of the gene of interest.

Germline transformations were performed by microinjection of plasmids at concentrations between 25 and 100 ng/µl with 10 ng/µl of *unc-122::rfp*, *unc-122::gfp* or *elt-2::gfp* as a co-injection marker. For rescue experiments, DNA was injected into mutant *C. elegans* carrying GCaMP arrays. For cell-specific RNAi knockdown experiments, sense and antisense DNA was injected into wild-type or mutant worms.

Calcium imaging

Transgenic worms with GCaMP expressed under a cell-specific promoter were trapped in a custom designed PDMS microfluidic device (Chronis et al., 2007) and exposed to salt stimuli. Fluorescence from the neuronal cell body was captured using a Zeiss inverted compound microscope for 3 minutes. We first captured 10 s of baseline activity in chemotaxis assay buffer (5 mM potassium phosphate (pH 6), 1 mM $CaCl_2$, 1 mM $MgSO_4$, and 50 mM NaCl), then 2 min of exposure to a higher NaCl concentration chemotaxis buffer stimulus, and lastly 50 s of buffer only.

We used Metamorph and an EMCCD camera (Photometrics) to capture images at a rate of 10 frames per s. For all sensory neurons, the average fluorescence in a 3 s window (t = 1–4 s) was set as F_0. For the AIA interneuron imaging, baseline fluorescence was more variable; therefore, a 10 s window (t = 0–10 s) was set as F_0. A Matlab script was used to analyze the average fluorescence for the cell body region of interest and to plot the percent change in fluorescence for the region of interest relative to F_0, as previously described (Chalasani et al., 2007). For all figures, average and standard errors at each time point were generated and plotted in Matlab. For statistical analysis, the average fluorescence and standard error were calculated for each animal over the 10 s period following the addition of the salt stimulus (t = 10–20 s). For the bar graph in the benzaldehyde odor experiment (**Figure 2.2c**), the average fluorescence and standard error were calculated over the 10 s period after odor removal (t = 130–140 s), with the 3 s window from t = 121–124 s set as F_0. Two-tailed unpaired *t*-tests were used to compare the responses of different genotypes, and the Bonferroni correction was used to adjust for multiple comparisons. No statistical methods were used to pre-determine sample sizes;

however, our sample sizes are similar to those reported in previous publications (Chalasani et al., 2007; Suzuki et al., 2008). Data distribution was assumed to be normal, but this was not formally tested. Wild-type controls, mutants, and rescue strains for each figure were imaged in alternation, in the same session. A single neuron was imaged in each animal, and each animal was imaged only once. No data points were excluded. Data collection and analysis were not performed blind to the conditions of the experiments.

Chemotaxis assays

Chemotaxis assays to sodium chloride were performed as previously described (Ward, 1973). Assays were performed on 2% agar plates (10 cm) containing 5 mM potassium phosphate (pH 6), 1 mM $CaCl_2$ and 1 mM $MgSO_4$. Concentration gradients of NaCl were established by placing a 5 mm agar plug from a 100, 250, 500 or 750 mM NaCl agar plate near the edge of the plate and a control 0 mM NaCl agar plug at the opposite end of the plate. Plugs were removed after 18–20 hours and 1 μl of 1 M sodium azide solution was spotted in the locations previously occupied by the plugs. Animals were washed once in M9 and three times in chemotaxis buffer (5 mM potassium phosphate (pH 6), 1 mM $CaCl_2$ and 1 mM $MgSO_4$). Worms were placed on the plate and allowed to move freely for one hour. The chemotaxis index was computed as the number of worms in the region near the high salt minus the worms in the region near the control divided by the total number of worms that moved beyond the origin. Experiments were performed over 4 or more days; average chemotaxis indices of 9–15 assay plates are presented. Our sample sizes are similar to those reported in previous publications

(Chalasani et al., 2007; Tomioka et al., 2006; Ward, 1973; Wes and Bargmann, 2001). Data distribution was assumed to be normal, but this was not formally tested. Two-tailed unpaired *t*-tests were used to compare the responses of different genotypes, and the Bonferroni correction was used to adjust for multiple comparisons. Data collection and analysis were not performed blind to the conditions of the experiments.

Confocal cilia imaging

Anesthetized young adult worms were imaged on a 2% agarose pad. Images were captured on a Zeiss LSM780 confocal microscope using a 40X objective and maximum intensity projections were generated using Zeiss Zen software. Dendritic cilia were imaged in 4–7 individual animals of each genotype, and the cilia morphology was found to be nearly identical in all animals of the same condition.

miniSOG light-inducible cell ablation

ASEL neurons were ablated or mock ablated in larval (L4) stage transgenic worms with miniSOG specifically targeted to the outer mitochondrial membrane of ASEL. Ablation was performed, using a Zeiss inverted compound microscope equipped with an X-Cite 120Q series fluorescence illumination lamp with the objective removed, by exposing freely moving animals to 90 minutes of pulsed (0.5 s on, 1.5 s off) 488 nm, blue light, as previously described (Qi et al., 2012). Animals appeared to move normally and remain healthy after this illumination. Successful neuronal ablation was confirmed by the absence of ASEL mCherry fluorescence 16 to 24 hours later (prior to calcium imaging). A different wavelength (510 nm, green) light was similarly pulsed for mock

ablation experiments (Qi et al., 2012) and it was confirmed that this did not alter ASEL mCherry fluorescence.

Acknowledgments

This chapter is a reprint of the material as it appears in Leinwand, S.G. and Chalasani, S.H. (2013). Neuropeptide signaling remodels chemosensory circuit composition in *Caenorhabditis elegans.* Nat Neurosci 16, 1461-7 and is included with permission from all authors. The dissertation author was the primary author of this paper.

Additionally, the following centers and people deserve thanks for their contribution to this work: *Caenorhabditis* Genetics Center, the National Brain Research Project, Japan, C. Bargmann, P. Sengupta, P. Sternberg and A. Zaslaver for strains, M. Ailion for *unc-31* cDNA, Y. Jin, C. Stevens, T. Sejnowski, E.J. Chichilnisky and H. Karten for helpful discussions. I also acknowledge J. Fitzpatrick and J. Kasuboski of the Waitt Advanced Biophotonics Center for providing the resources and training to perform confocal imaging and J. Simon for help with the illustrations. And, I am grateful to A. Tong, C. Yang and other members of the Chalasani laboratory for critical help, advice and insights. This work was funded by grants from The Searle Scholars Program, March of Dimes, Whitehall Foundation, Rita Allen Foundation and the NIH R01MH096881-01A1 (S.H.C.) and a graduate research fellowship from the NSF (S.G.L.)

Figure 2.1: A distributed neural network encodes salt concentration. (a) Synapses and synaptic weights (Chen et al., 2006) between ASEL, ASER and AWC sensory neurons and onto AIA interneurons in the head of *C. elegans*. (b) Average GCaMP fluorescence change in wild-type sensory neurons in response to +50 mM NaCl. (c) Fluorescence change in wild-type ASEL (10 s averaged $\Delta F/F$ after salt addition is 31.74 ± 5.76 (s.e.m), n = 13) and AWC^{ON} (–6.97 ± 0.81, n = 13) sensory neurons in response to +10 mM NaCl. (d,e) AIA interneuron responses of wild-type, AWC-ablated, AWC-specific knockdown of *unc-31* (the *C. elegans* homolog of Calcium-dependent secretion activator) and AWC-specific knockdown of *eat-4* (the *C. elegans* vesicular glutamate transporter) worms to +50 mM NaCl (d) and +10 mM NaCl (e). *Significantly different from wild-type ($P < 0.05$, two-tailed *t*-test with Bonferroni correction). (b–e) Dark and light gray shading indicates 2 minute +50 mM or +10 mM NaCl stimulus, respectively, beginning at t = 10 s. Numbers on bars indicate number of neurons imaged. Yellow box indicates the 10 s after stimulus addition, for which the fluorescence change is averaged in the bar graphs. The light color shading around curves and the error bars on bar graphs indicate s.e.m. (f) Salt chemotaxis of wild-type, AWC-ablated, and *che-1* (no ASE) mutant worms to a range of salt concentrations. (g,h) Chemotaxis of wild-type, AWC-specific *unc-31* knockdown, and AWC-specific *eat-4* knockdown to a low 250 mM NaCl point source (g) or a high 750 mM NaCl point source (h). Numbers on bars indicate number of assay plates. (f–h) Error bars indicate s.e.m. *Significantly different from wild-type, as indicated ($P < 0.05$, two-tailed *t*-test with Bonferroni correction).

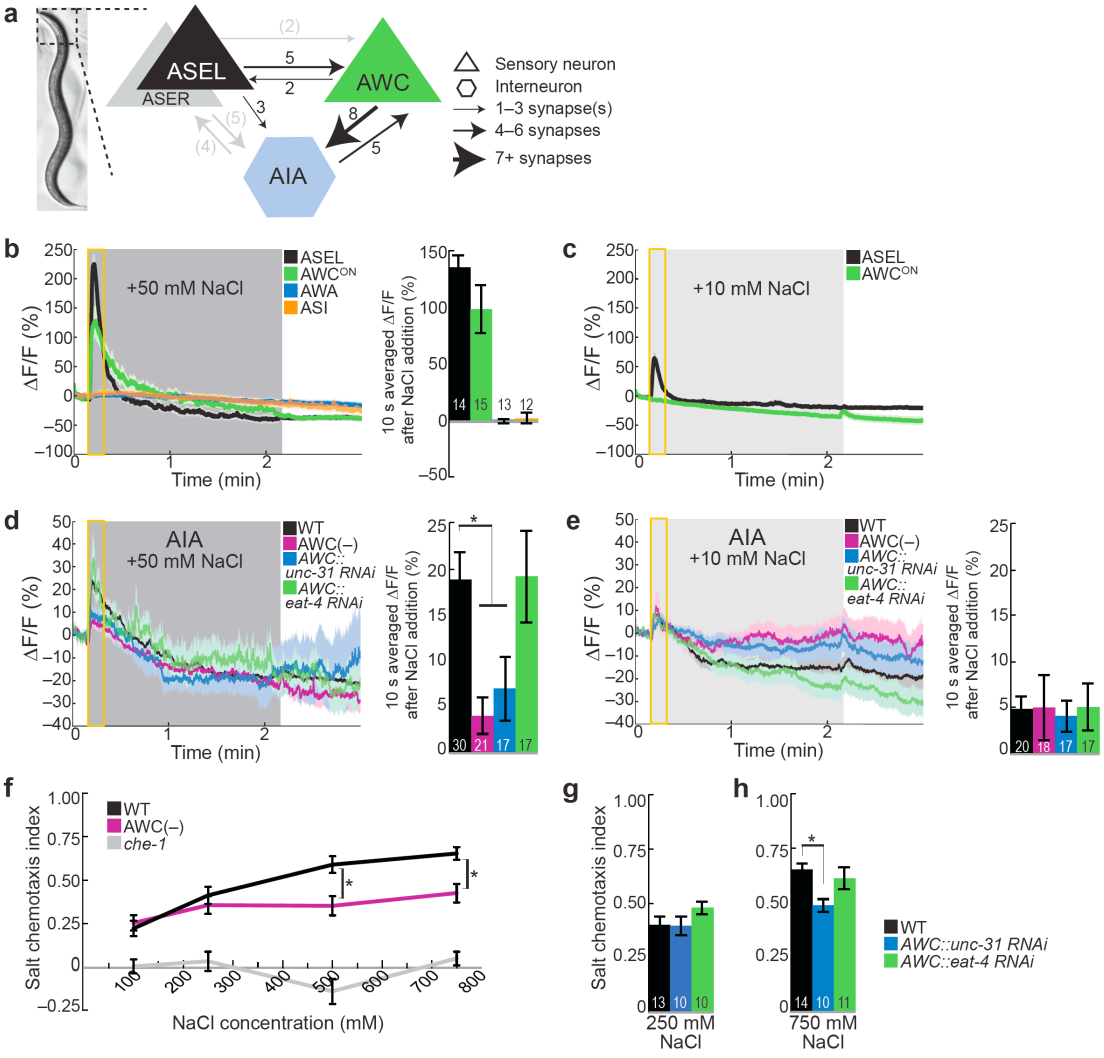
a
ASEL
ASER
AWC
AIA
(2)
5
2
3
(5)
(4)
8
5
Sensory neuron
Interneuron
1–3 synapse(s)
4–6 synapses
7+ synapses
b
+50 mM NaCl
ASEL
AWCON
AWA
ASI
ΔF/F (%)
Time (min)
10 s averaged ΔF/F after NaCl addition (%)
14 15 13 12
c
+10 mM NaCl
ASEL
AWCON
ΔF/F (%)
Time (min)
d
AIA
+50 mM NaCl
WT
AWC(–)
AWC::unc-31 RNAi
AWC::eat-4 RNAi
ΔF/F (%)
Time (min)
10 s averaged ΔF/F after NaCl addition (%)
30 21 17 17
e
AIA
+10 mM NaCl
WT
AWC(–)
AWC::unc-31 RNAi
AWC::eat-4 RNAi
ΔF/F (%)
Time (min)
10 s averaged ΔF/F after NaCl addition (%)
20 18 17 17
f
WT
AWC(–)
che-1
Salt chemotaxis index
NaCl concentration (mM)
g
Salt chemotaxis index
13 10 10
250 mM NaCl
h
14 10 11
750 mM NaCl
WT
AWC::unc-31 RNAi
AWC::eat-4 RNAi

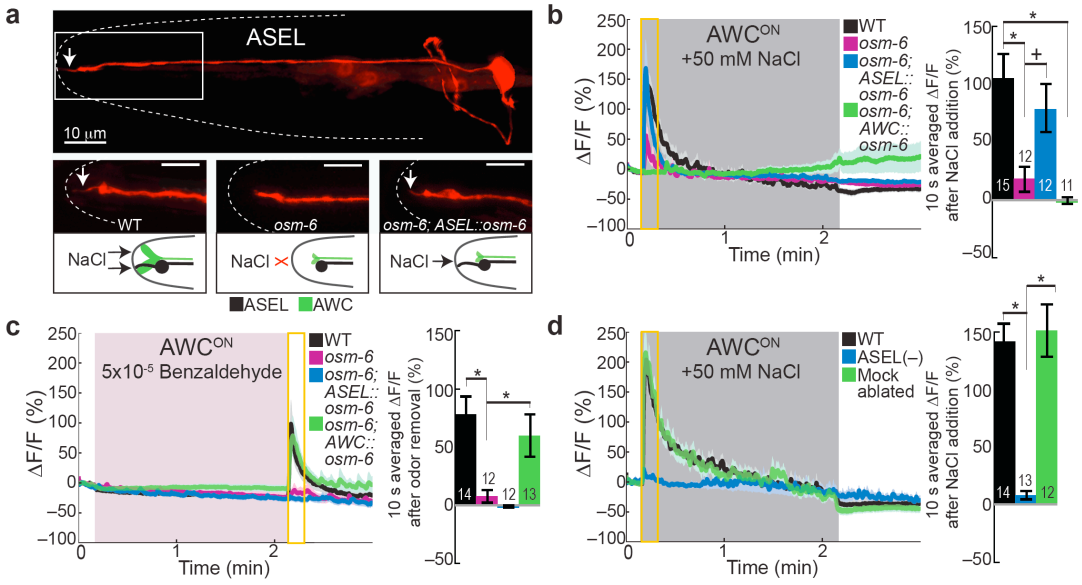

Figure 2.2: AWC^{ON} sensory neurons act as interneurons in the salt circuit. (a) Confocal images and diagrams of the ASEL neuron (i) and cilia morphology (ii–iv) in wild-type (i,ii), *osm-6* mutant (iii), and *osm-6*; *ASEL::osm-6* cell-specific rescue (iv). White arrow indicates elaborated cilia structure in wild-type and *osm-6*; ASEL::osm-6 cell-specific rescue. Scale bar 10 µm. (b,c) AWC^{ON} wild-type, *osm-6* mutant, *osm-6*; *ASEL::osm-6* and *osm-6*; *AWC::osm-6* responses to +50 mM NaCl (b) and a 5x10^{-5} dilution of benzaldehyde odor (c). (d) AWC^{ON} responses to +50 mM NaCl in wild-type and in transgenic worms in which ASEL neurons were photo-ablated or mock ablated in larvae. (b–d) Numbers on bars indicate number of neurons imaged. Yellow box indicates the 10 s time period for which the fluorescence change is averaged in the bar graphs. Light color shading around curves and bar graph error bars indicate s.e.m. *Significantly different from wild-type or mutant, as indicated ($P < 0.05$, two-tailed *t*-test with Bonferroni correction). +($P < 0.1$, two-tailed *t*-test with Bonferroni correction).

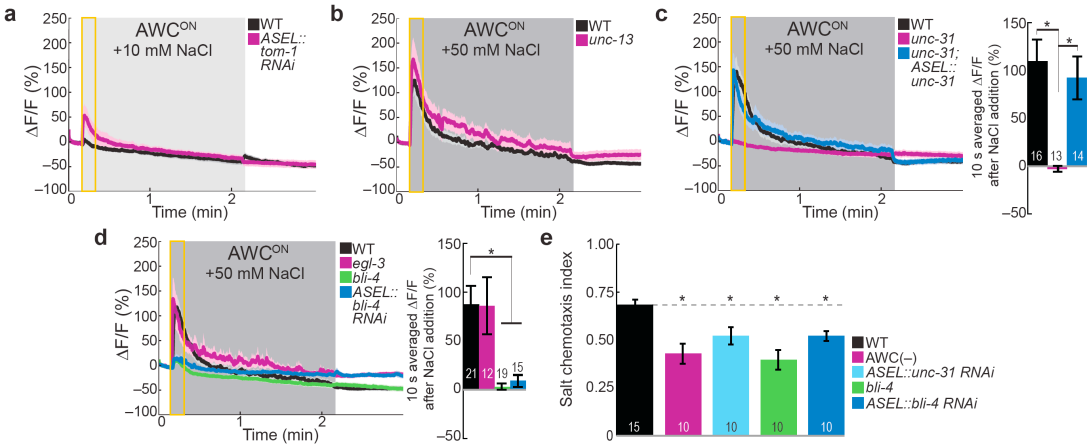

Figure 2.3: AWC^{ON} salt responses require peptidergic neurotransmission from ASEL. (a) AWC^{ON} average calcium responses to +10 mM NaCl in wild-type (averaged ΔF/F after salt addition is –6.15 ± 1.32, n = 21) and ASEL-specific *tom-1* (Tomosyn homolog) knockdown (32.13 ± 18.56, $P < 0.05$ compared to WT, n = 12). (b) AWC^{ON} responses to +50 mM NaCl in wild-type (94.26 ± 22.26, n = 15) and *unc-13* mutants (102.38 ± 30.70, n = 12). (a,b) Numbers in parentheses are mean ± s.e.m. (c,d) AWC^{ON} responses to +50 mM NaCl in *unc-31* mutants and *unc-31; ASEL::unc-31* cell-specific rescue (c), and *egl-3, bli-4*, and ASEL-specific *bli-4* knockdown (d). Numbers on bars indicate number of neurons imaged. *Significantly different from wild-type or mutant, as indicated ($P < 0.05$, two-tailed *t*-test with Bonferroni correction). (a–d) Light color shading around curves and bar graph error bars indicate s.e.m. (e) High salt (750 mM point source) chemotaxis of wild-type, AWC-ablated, ASEL-specific *unc-31 RNAi*, *bli-4,* and ASEL-specific *bli-4 RNAi* worms. Numbers on bars indicate number of assay plates. Error bars indicate s.e.m. *Significantly different from wild-type ($P < 0.05$, two-tailed *t*-test with Bonferroni correction).

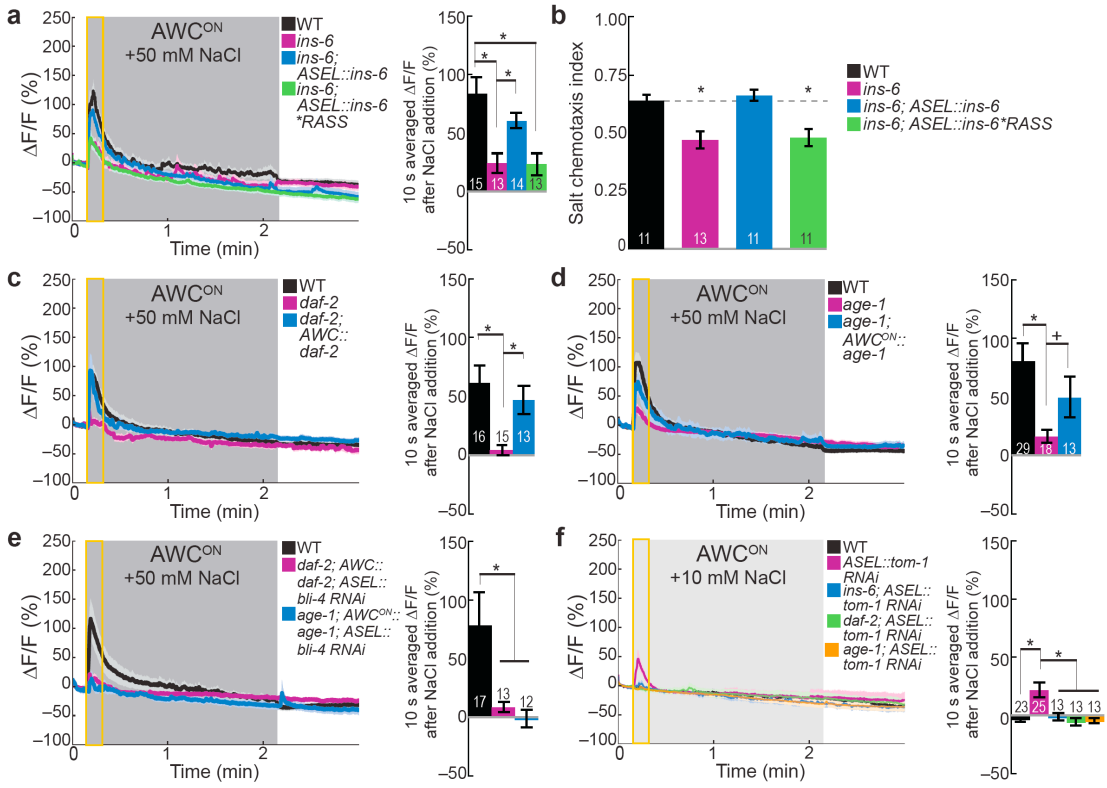

Figure 2.4: INS-6 signals through DAF-2 and AGE-1 to remodel the ASEL-AWC^{ON} salt circuit. (a) AWC^{ON} calcium responses to +50 mM NaCl in wild-type, insulin-like peptide *ins-6* mutants, and *ASEL::ins-6* rescue with or without mutations that replace the two critical arginine amino acids in the predicted BLI-4 cleavage motif with two serine residues (*RASS). (b) High salt (750 mM point source) chemotaxis of wild-type, *ins-6* mutant, *ASEL::ins-6* cell-specific rescue, and BLI-4 cleavage motif mutated *ASEL::ins-6*RASS* transgenic worms. Error bars indicate s.e.m. *Significantly different from wild-type ($P < 0.05$, *t*-test with Bonferroni correction). (c,d) Mutant AWC^{ON} responses to +50 mM NaCl. (c) Insulin-like receptor, *daf-2*, mutant and *AWC::daf-2* rescue. (d) PI3-Kinase, *age-1*, mutant and *AWC^{ON}::age-1* rescue. (e) AWC^{ON} responses to +50 mM NaCl in wild-type and in transgenic animals with ASEL-specific knockdown of the peptide processing enzyme *bli-4* in a *daf-2* mutant background with AWC-specific *daf-2* rescue or in an *age-1* background with AWC^{ON}-specific *age-1* rescue. (f) AWC^{ON} responses to +10 mM NaCl in wild-type and in ASEL-specific *tom-1* (*Tomosyn*) knockdown in a wild-type background or in an *ins-6*, *daf-2* or *age-1* mutant background. (a,c–f) Light color shading around curves and bar graph error bars indicate s.e.m. *Significantly different from wild-type or mutant, as indicated ($P < 0.05$, two-tailed *t*-test with Bonferroni correction). +($P < 0.1$, two-tailed *t*-test with Bonferroni correction).

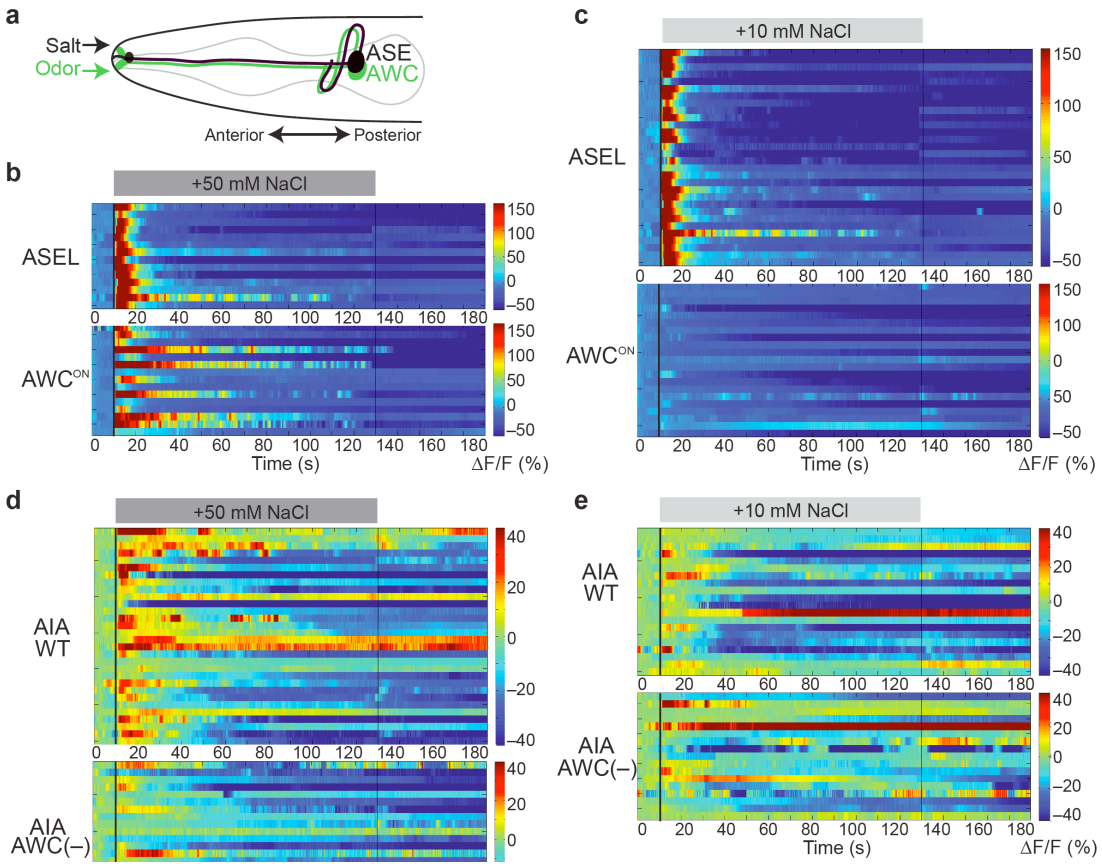

Figure 2.5: Heat maps show individual ASEL and AWC^{ON} sensory neuron and AIA interneuron responses to salt. (a) ASE and AWC chemosensory neurons in the head of *C. elegans*. (b) Heat maps of ratio change in fluorescence to total fluorescence for ASEL and AWC^{ON} responses to +50 mM NaCl show consistent calcium transients in response to onset of salt stimulus. (c) Heat maps of ASEL and AWC^{ON} responses to +10 mM NaCl show consistent calcium transients from ASEL and no responses from AWC^{ON}. (d) Heat maps of ratio change in fluorescence to total fluorescence for AIA responses to +50 mM NaCl in wild-type and AWC-ablated animals. Wild-type responses to the onset of +50 mM NaCl are reliably larger than AWC-ablated responses. (e) Heat maps of wild-type and AWC-ablated AIA responses to +10 mM NaCl show similar small responses to the increase in salt. (b–e) One row in heat map corresponds to one neuron. Dark or light gray shading and black lines at 10 and 130 s indicate the duration of a +50 mM or +10 mM NaCl stimulus.

Figure 2.6: Sensory neuron responses to sodium chloride. (a) ASEL wild-type calcium responses to increasing concentrations of NaCl (+10, 20, 30 and 50 mM) increase in magnitude. (b) AWC^{ON} wild-type neurons switch from a nonresponsive state when stimulated with +10 mM NaCl to responding with increasing magnitude calcium transients to +20, 30 and 50 mM NaCl stimuli. (c) ASE right (ASER) neurons do not respond to the addition of a +50 mM NaCl stimulus; however, they display large calcium transients upon stimulus removal, which is effectively a 50 mM decrease in salt concentration. (d) AWC^{OFF} neurons show large calcium transients in response to a 50 mM increase in NaCl, similar to AWC^{ON} (shown in Figure 2.1c). (e) ASER neurons respond do not respond to the addition of a +10 mM NaCl stimulus; however, they display small calcium transients upon stimulus removal. (f) AWC^{OFF} neurons do not respond to +10 mM NaCl. (g) AWC^{ON} does not respond to +100 mM sucrose. AWC^{ON} is not a generalized osmolarity sensor since 100 mM sucrose is an equivalent osmolarity change to 50 mM NaCl. (h) The amphid sensory neurons ASK, AWB and ASH do not respond to +50 mM NaCl. AWB neurons show small increases in fluorescence upon the removal of the salt stimulus. (a–h) Numbers on bars indicate number of neurons imaged. Dark and light gray shading indicates 2 min +50 mM or +10 mM NaCl stimulus, respectively, beginning at t = 10 s. Yellow box indicates the 10 s after stimulus addition, for which the fluorescence is averaged in the bar graphs. Light color shading around curves and bar graph error bars indicate s.e.m.

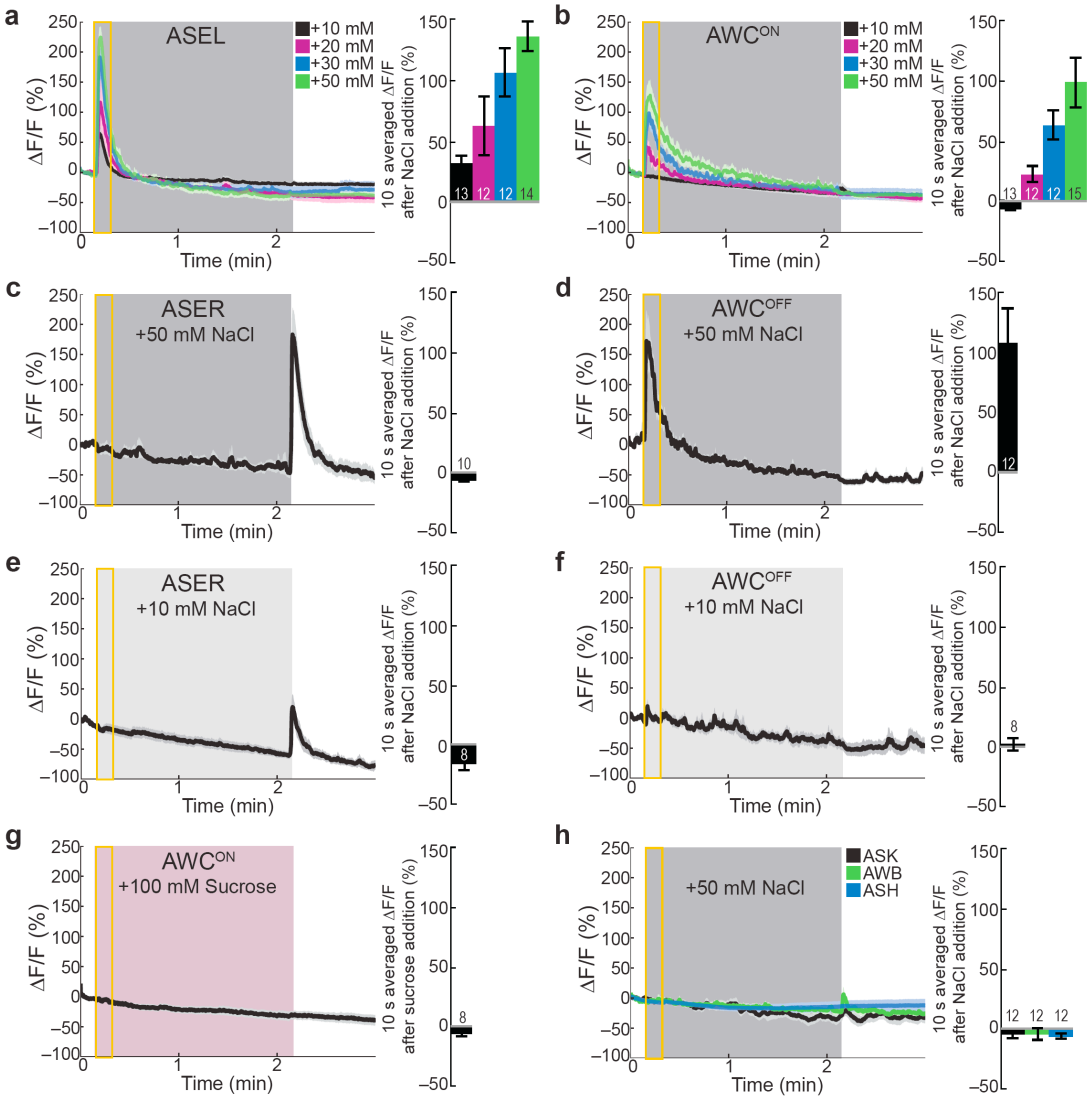
a
ASEL
+10 mM
+20 mM
+30 mM
+50 mM
ΔF/F (%)
Time (min)
10 s averaged ΔF/F after NaCl addition (%)
13 12 12 14
b
AWCON
+10 mM
+20 mM
+30 mM
+50 mM
ΔF/F (%)
Time (min)
10 s averaged ΔF/F after NaCl addition (%)
13 12 12 15
c
ASER
+50 mM NaCl
ΔF/F (%)
Time (min)
10 s averaged ΔF/F after NaCl addition (%)
10
d
AWCOFF
+50 mM NaCl
ΔF/F (%)
Time (min)
10 s averaged ΔF/F after NaCl addition (%)
12
e
ASER
+10 mM NaCl
ΔF/F (%)
Time (min)
10 s averaged ΔF/F after NaCl addition (%)
8
f
AWCOFF
+10 mM NaCl
ΔF/F (%)
Time (min)
10 s averaged ΔF/F after NaCl addition (%)
8
g
AWCON
+100 mM Sucrose
ΔF/F (%)
Time (min)
10 s averaged ΔF/F after sucrose addition (%)
8
h
+50 mM NaCl
ASK
AWB
ASH
ΔF/F (%)
Time (min)
10 s averaged ΔF/F after NaCl addition (%)
12 12 12

Figure 2.7: AWC plays a specific role in high salt chemotaxis. (a) Schematic showing genetic regulators of peptidergic (CADPS homolog/UNC-31) and amino acid or small molecule (Munc13 homolog/UNC-13) synaptic neurotransmission from ASEL. BLI-4 and EGL-3 are proprotein convertase enzymes that proteolytically process neuropeptides to generate mature peptides. (b) Schematic diagram of salt chemotaxis assay. (c) Low 250 mM NaCl point source salt chemotaxis does not differ between wild-type and the AWC cell fate mutants *nsy-1* (which has two AWC^{ON} neurons and no AWC^{OFF} neurons) and *nsy-5* (which has two AWC^{OFF} neurons and no AWC^{ON} neurons) (i). High 750 mM NaCl point source chemotaxis is defective in both *nsy-1* and *nsy-5* mutants, suggesting non-redundant roles for both AWC^{ON} and AWC^{OFF} neurons in high salt behavior (ii). (d) Low salt (250 mM NaCl point source) chemotaxis does not differ between wild-type and the neurotransmission defective *ASEL::unc-31 RNAi, bli-4, ASEL::bli-4 RNAi,* AWC^{ON}*::bli-4 RNAi*, and *egl-3* worms. These results support the specific recruitment of AWC under high but not low salt conditions and indicate that these mutants are capable of normal salt chemotaxis under conditions when AWC is not recruited. (e) High salt (750 mM NaCl point source) chemotaxis of wild-type worms compared to AWC^{ON}*::bli-4 RNAi, egl-3*, and *ins-6*; ASI-specific *ins-6* rescue. ASI-specific expression of *ins-6* is not sufficient to rescue the high salt chemotaxis deficit of this mutant. (f) Low salt (250 mM NaCl point source) chemotaxis does not differ between wild-type, *ins-6* mutants, ASEL-specific rescue of *ins-6* with or without two arginine to serine point mutations in the BLI-4 cleavage motif (*RASS), and ASI-specific *ins-6* rescue. (c–f) Number in each bar indicates number of assay plates. *Significantly different from wild-type ($P < 0.05$, two-tailed *t*-test with Bonferroni correction).

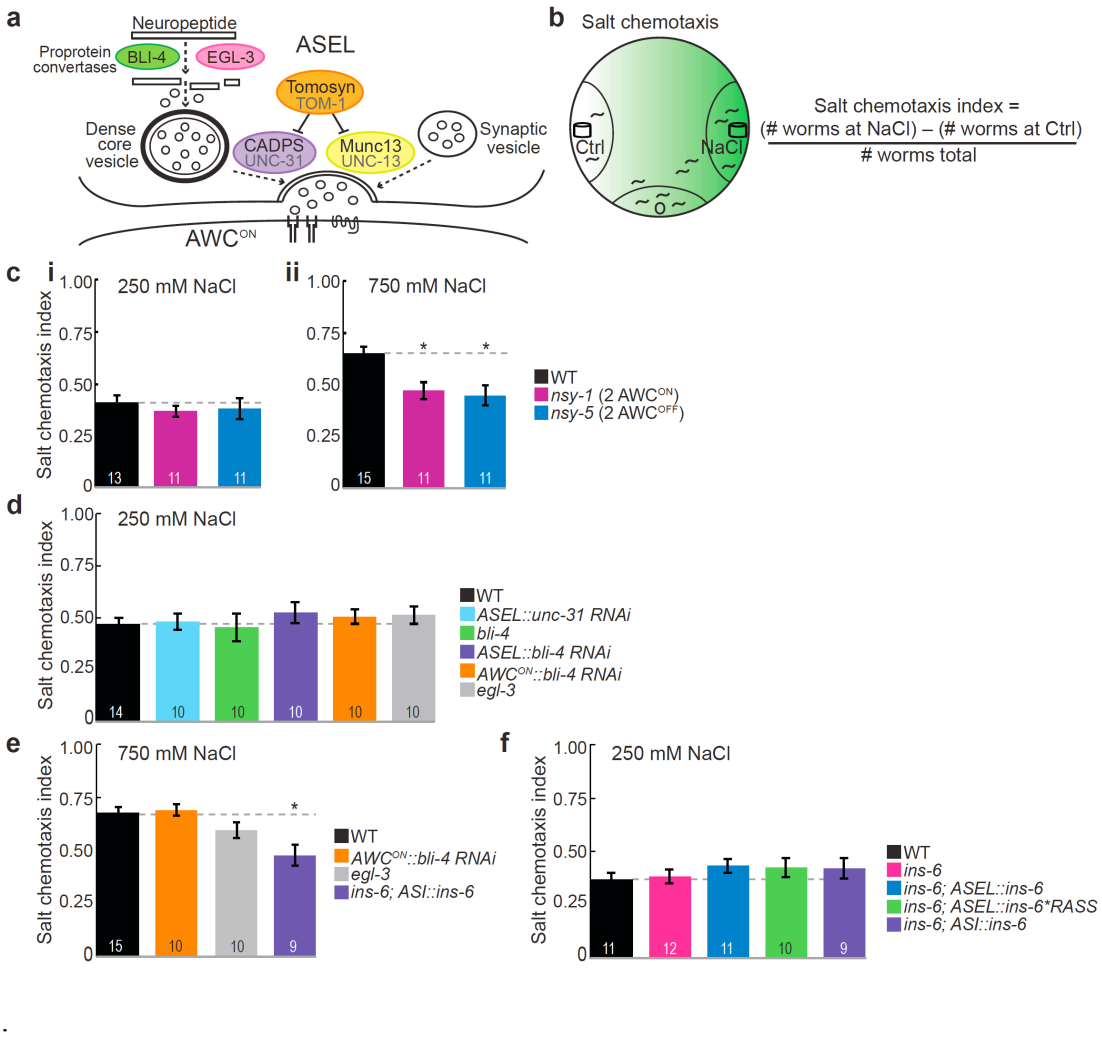
a
Neuropeptide
Proprotein convertases
BLI-4
EGL-3
ASEL
Tomosyn TOM-1
Dense core vesicle
CADPS UNC-31
Munc13 UNC-13
Synaptic vesicle
AWC^ON
b
Salt chemotaxis
Ctrl
NaCl
Salt chemotaxis index = (# worms at NaCl) – (# worms at Ctrl) / # worms total
c
i
250 mM NaCl
ii
750 mM NaCl
Salt chemotaxis index
WT
nsy-1 (2 AWC^ON)
nsy-5 (2 AWC^OFF)
d
250 mM NaCl
WT
ASEL::unc-31 RNAi
bli-4
ASEL::bli-4 RNAi
AWC^ON::bli-4 RNAi
egl-3
e
750 mM NaCl
WT
AWC^ON::bli-4 RNAi
egl-3
ins-6; ASI::ins-6
f
250 mM NaCl
WT
ins-6
ins-6; ASEL::ins-6
ins-6; ASEL::ins-6*RASS
ins-6; ASI::ins-6

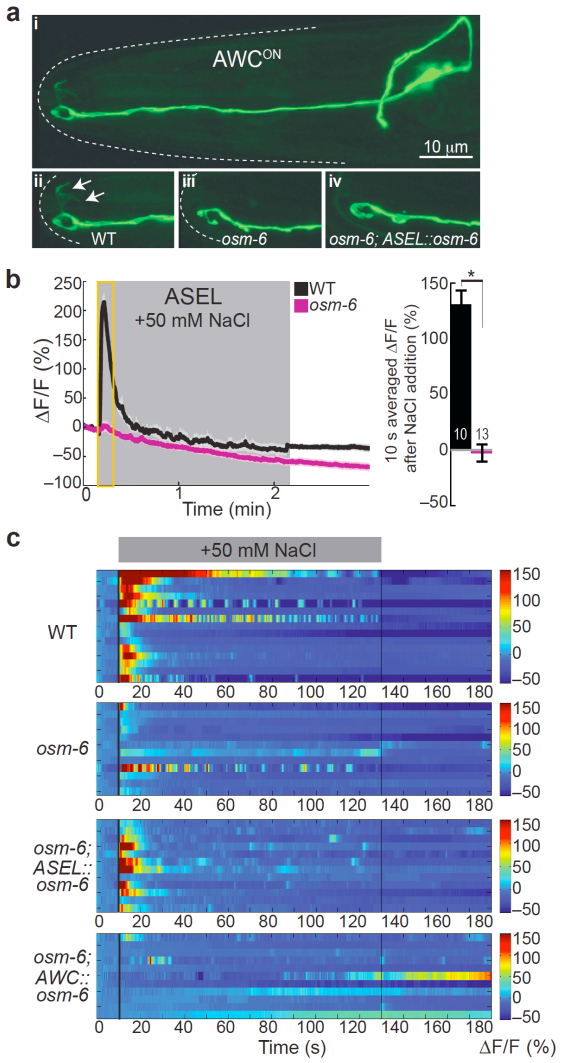

Figure 2.8: *osm-6* cilia control experiments support a role for AWC as an interneuron in the salt circuit. (a) Confocal images of AWC^{ON} neuron (i) and cilia (ii–iv) morphology in wild-type (i,ii), *osm-6* mutants (iii) and *osm-6; ASEL::osm-6* rescue (iv). The elaborate bilateral ciliary structure (indicated by the white arrows) in wild-type AWC^{ON} neurons is lost in *osm-6* mutants (iii) and is not rescued in *osm-6; ASEL::osm-6* (iv). (b) ASEL responses to +50 mM NaCl in wild-type and *osm-6* mutants. ASEL responses to salt are abolished in *osm-6* cilia mutants. Yellow box indicates the 10 s after stimulus addition, for which the fluorescence is averaged in the bar graph. Light color shading around curves and bar graph error bars indicate s.e.m. *Significantly different from wild-type ($P < 0.05$, two-tailed *t*-test). (c) Heat maps of ratio change in fluorescence to total fluorescence for AWC^{ON} responses to +50 mM NaCl in wild-type, *osm-6* mutants, *osm-6; ASEL::osm-6*, and *osm-6; AWC::osm-6*. One row in heat map corresponds to one neuron. Dark gray shading and black lines at 10 and 130 s indicate the duration of the +50 mM NaCl stimulus.

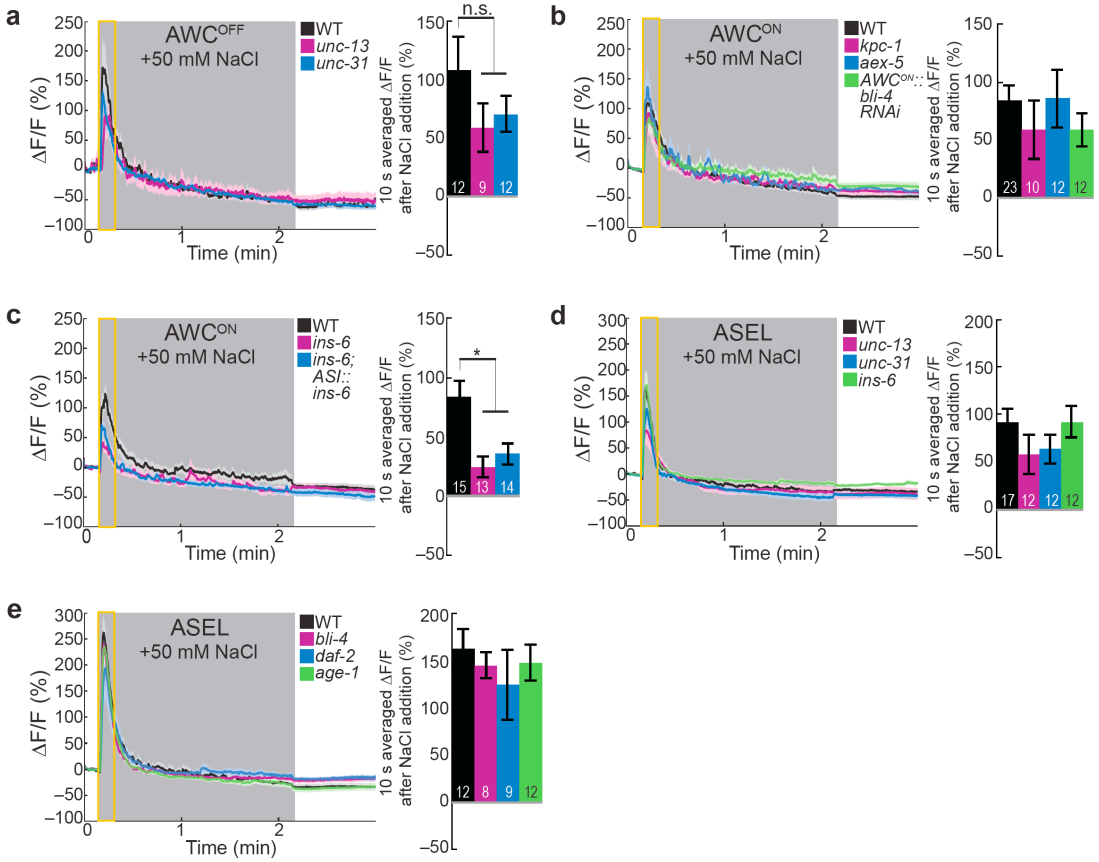

Figure 2.9: Mutant AWC and ASEL calcium responses to +50mM NaCl. (a) AWC^{OFF} neuron responses to +50 mM NaCl are similar in *unc-13* and *unc-31* neurotransmission mutants compared to wild-type, suggesting that this neuron (unlike AWC^{ON}) may be a direct and intrinsic salt detector. (b) AWC^{ON} responses to +50 mM NaCl are unaffected by mutations in the proprotein convertases *kpc-1* and *aex-5*. *AWC^{ON}::bli-4 RNAi* has no effect on AWC^{ON} salt responses, indicating that BLI-4 does not act in this neuron. (c) AWC^{ON} *ins-6* insulin-like peptide mutant responses to +50 mM NaCl are not fully rescued by ASI expression of an *ins-6* genomic DNA construct. (d) ASEL responses to +50 mM NaCl are not significantly different in *unc-13, unc-31* or *ins-6* mutants compared to wild-type. (e) ASEL responses to +50 mM NaCl do not differ significantly in *bli-4, daf-2* or *age-1* mutants compared to wild-type. (a–e) Yellow box indicates the 10 s after stimulus addition, for which the fluorescence is averaged in the bar graphs. Light color shading around curves and bar graph error bars indicate s.e.m. *Significantly different from wild-type ($P < 0.05$, two-tailed *t*-test with Bonferroni correction). n.s., not significant.

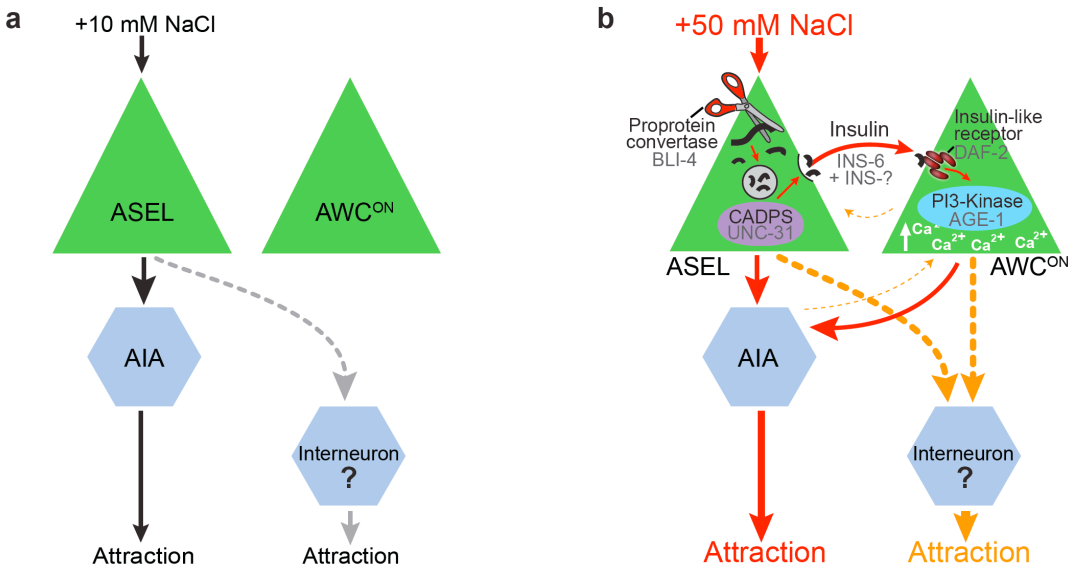

Figure 2.10: Salt neural circuit model. Proposed model for (a) ASEL encoding +10 mM NaCl and (b) AWC^{ON} recruitment to encode +50 mM NaCl by BLI-4, UNC-31, INS-6, DAF-2 and AGE-1 dependent signaling to mediate behavioral attraction.

Table 2.1: Strain list. List of all *C. elegans* strains.

Strain	Genotype	Name
Calcium imaging		
CX10536	*kyEx2595 [str-2::GCaMP2.2b, unc-122::gfp]*	"AWC^{ON}" in Figure 2.1b,c, 2.5b,c and 2.2b,g; "WT" in Figures 2.2b–d, 2.3a–d, 2.4a,c–f, 2.8c and 2.9b,c
PS6253	*pha-1(e2123) III; syEx1238 [srsx-3::GCaMP3, pha-1::pha-1]*	"AWC^{OFF}" in Figure 2.6d,f; "WT" in Figure 2.9a
IV10	*ueEx7 [gcy-7::GCaMP3, unc-122::gfp]*	"ASEL" in Figure 2.1b,c, 2.5b,c and 2.6a; "WT" in Figures 2.8b and 2.9d,e
IV28	*ueEx10 [gcy-5::GCaMP3, unc-122::gfp]*	"ASER" in Figure 2.6c,e
CX10979	*kyEx2865 [sra-6::GCaMP3, unc-122::gfp]*	"ASH" in Figure 2.6h
PY6554	*oyEx[gpa-4p::gcamp2.2b, unc-122::dsRed]*	"AWA" and "ASI" in Figure 2.1b
CX10981	*kyEx2866 [sra-9::GCaMP2.2b, unc-122::gfp]*	"ASK" in Figure 2.6h
CX8446	*kyEx1423 [str-1::GCaMP1.0, unc-122::gfp]*	"AWB" in Figure 2.6h
IV61	*ueEx8 [ins-1::GCaMP3, unc-122::gfp]*	"WT" in Figure 2.1d,e, Figure 2.5d,e
IV237	*ueEx8 [ins-1::GCaMP3, unc-122::gfp]; oyIs [ceh-36del::caspase-3(p12)::nz, ceh-36del::cz::caspase-3(p17), srtx-1::gfp, unc-122::dsRED]*	"AWC(–)" in Figure 2.1d,e and 2.5d,e
IV307	*ueEx8 [ins-1::GCaMP3, unc-122::gfp]; ueEx104 [odr-3::unc-31 sense:sl2mCherry, odr-3::unc-31 antisense:sl2mCherry, unc-122::rfp]*	"*AWC::unc-31 RNAi*" in Figure 2.1d,e
IV304	*ueEx8 [ins-1::GCaMP3, unc-122::gfp]; ueEx4 [odr-3::eat-4 sense, odr-3::eat-4 antisense, elt-2::gfp]*	"*AWC::eat-4 RNAi*" in Figure 2.1d,e
IV75	*osm-6(p811) V; kyEx2595 [str-2::GCaMP2.2b, unc-122::gfp]*	"*osm-6*" in Figure 2.2b,c and 2.8c

Table 2.1: Strain list, continued.

Strain	Genotype	Name
IV92	*osm-6(p811) V; kyEx2595 [str-2::GCaMP2.2b, unc-122::gfp]; ueEx43 [gcy-7::osm-6:sl2mCherry, unc-122::rfp]*	"*osm-6; ASEL::osm-6*" in Figure 2.2b,c and 2.8c
IV126	*osm-6(p811) V; kyEx2595 [str-2::GCaMP2.2b, unc-122::gfp]; ueEx56 [odr-3::osm-6:sl2mCherry, unc-122::rfp]*	"*osm-6; AWC::osm-6*" in Figure 2.2b,c and 2.8c
IV67	*kyEx2595 [str-2::GCaMP2.2b, unc-122::gfp]; ueEx29 [gcy-7::tomm-20(N'55AA):miniSOG:sl2mCherry, unc-122::rfp]*	"ASEL(–)" and "Mock ablated" in Figure 2.2d
IV65	*kyEx2595 [str-2::GCaMP2.2b, unc-122::gfp]; ueEx30 [gcy-7::tom-1 sense:sl2mCherry, gcy-7::tom-1 antisense:sl2mCherry, unc-122::rfp]*	"*ASEL::tom-1 RNAi*" in Figures 2.3a and 2.4f
IV15	*unc-13(e51) I; kyEx2595 [str-2::GCaMP2.2b, unc-122::gfp]*	"*unc-13*" in Figure 2.3b
IV23	*unc-31(e928) IV; kyEx2595 [str-2::GCaMP2.2b, unc-122::gfp]*	"*unc-31*" in Figure 2.3c
IV35	*unc-31(e928) IV; kyEx2595 [str-2::GCaMP2.2b, unc-122::gfp]; ueEx15 [gcy-7::unc-31:sl2mCherry, unc-122::rfp]*	"*unc-31; ASEL::unc-31*" in Figure 2.3c
IV106	*egl-3(tm1377) V; kyEx2595 [str-2::GCaMP2.2b, unc-122::gfp]*	"*egl-3*" in Figure 2.3d
IV143	*bli-4(e937) I; kyEx2595 [str-2::GCaMP2.2b, unc-122::gfp]*	"*bli-4*" in Figure 2.3d
IV251	*kyEx2595 [str-2::GCaMP2.2b, unc-122::gfp]; ueEx158 [gcy-7::bli-4 sense:sl2mCherry, gcy-7::bli-4 antisense:sl2mCherry, unc-122::rfp]*	"*ASEL::bli-4 RNAi*" in Figure 2.3d,e and 2.7d
IV254	*kyEx2595 [str-2::GCaMP2.2b, unc-122::gfp]; ueEx161 [str-2::bli-4 sense:sl2mCherry, str-2::bli-4 antisense:sl2mCherry, unc-122::rfp]*	"*AWC^{ON}::bli-4 RNAi*" in Figures 2.7d,e and 2.9b
IV174	*kpc-1(gk8) I; kyEx2595 [str-2::GCaMP2.2b, unc-122::gfp]*	"*kpc-1*" in Figure 2.9b
IV144	*aex-5(sa23) I; kyEx2595 [str-2::GCaMP2.2b, unc-122::gfp]*	"*aex-5*" in Figure 2.9b
IV302	*ins-6(tm2416) II; kyEx2595 [str-2::GCaMP2.2b, unc-122::gfp]*	"*ins-6*" in Figure 2.4a and 2.9b

Table 2.1: Strain list, continued.

Strain	Genotype	Name
IV320	*ins-6(tm2416) II; kyEx2595 [str-2::GCaMP2.2b, unc-122::gfp] ; ueEx200 [gcy-7::ins-6:sl2:mCherry, unc-122::rfp]*	"*ins-6; ASEL::ins-6*" in Figure 2.4a,b, and 2.7f
IV311	*ins-6(tm2416) II; kyEx2595 [str-2::GCaMP2.2b, unc-122::gfp]; ueEx191 [gcy-7::ins-6*RASS:sl2:mCherry, unc-122::rfp]*	"*ins-6*; *ASEL::ins-6*RASS*" in Figure 2.4a,b, and 2.7f
IV312	*ins-6(tm2416) II; kyEx2595 [str-2::GCaMP2.2b, unc-122::gfp]; ueEx192 [str-3::ins-6:sl2:mCherry, unc-122::rfp]*	"*ins-6; ASI::ins-6*" in Figures 2.7e,f and 2.9c
IV175	*daf-2(e1370) III; kyEx2595 [str-2::GCaMP2.2b, unc-122::gfp]*	"*daf-2*" in Figure 2.4c
IV209	*daf-2(e1370) III; kyEx2595 [str-2::GCaMP2.2b, unc-122::gfp]; ueEx126 [odr-3::daf-2:sl2mCherry, unc-122::rfp]*	"*daf-2; AWC::daf-2*" in Figure 2.4c
IV98	*age-1(hx546) II; kyEx2595 [str-2::GCaMP2.2b, unc-122::gfp]*	"*age-1*" in Figure 2.4d
IV128	*age-1(hx546) II; kyEx2595 [str-2::GCaMP2.2b, unc-122::gfp]; ueEx66 [str-2::age-1:sl2mCherry, unc-122::rfp]*	"*age-1; AWC^{ON}::age-1*" in Figure 2.4d
IV291	*daf-2(e1370) III; kyEx2595 [str-2::GCaMP2.2b, unc-122::gfp]; ueEx126 [odr-3::daf-2:sl2mCherry, unc-122::rfp]; ueEx183 [gcy-7::bli-4 sense:sl2mCherry, gcy-7::bli-4 antisense:sl2mCherry, elt-2::gfp]*	"*daf-2; AWC::daf-2; ASEL::bli-4 RNAi*" in Figure 2.4e
IV281	*age-1(hx546) II; kyEx2595 [str-2::GCaMP2.2b, unc-122::gfp]; ueEx66 [str-2::age-1:sl2mCherry, unc-122::rfp]; ueEx177 [gcy-7::bli-4 sense:sl2mCherry, gcy-7::bli-4 antisense:sl2mCherry, elt-2::gfp]*	"*age-1; AWC^{ON}::age-1; ASEL::bli-4 RNAi*" in Figure 2.4e
IV329	*ins-6(tm2416) II; kyEx2595 [str-2::GCaMP2.2b, unc-122::gfp]; ueEx30 [gcy-7::tom-1 sense:sl2mCherry, gcy-7::tom-1 antisense:sl2mCherry, unc-122::rfp]*	"*ins-6; ASEL::tom-1 RNAi*" in Figure 2.4f

Table 2.1: Strain list, continued.

Strain	Genotype	Name
IV285	*daf-2(e1370) III; kyEx2595 [str-2::GCaMP2.2b, unc-122::gfp]; ueEx30 [gcy-7::tom-1 sense:sl2mCherry, gcy-7::tom-1 antisense:sl2mCherry, unc-122::rfp]*	"*daf-2; ASEL::tom-1 RNAi*" in Figure 2.4f
IV284	*age-1(hx546) II; kyEx2595 [str-2::GCaMP2.2b, unc-122::gfp]; ueEx30 [gcy-7::tom-1 sense:sl2mCherry, gcy-7::tom-1 antisense:sl2mCherry, unc-122::rfp]*	"*age-1; ASEL::tom-1 RNAi*" in Figure 2.4f
IV77	*osm-6(p811) V; ueEx7 [gcy-7::GCaMP3, unc-122::gfp]*	"*osm-6*" in Figure 2.8b
IV141	*unc-13(e51) I; pha-1 (e2123) III; syEx1238 [srsx-3::GCaMP3, pha-1::pha-1]*	"*unc-13*" in Figure 2.9a
IV44	*unc-31(e928) IV; pha-1 (e2123) III; syEx1238 [srsx-3::GCaMP3, pha-1::pha-1]*	"*unc-31*" in Figure 2.9a
IV104	*unc-13(e51) I; ueEx7 [gcy-7::GCaMP3, unc-122::gfp]*	"*unc-13*" in Figure 2.9d
IV22	*unc-31(e928) IV; ueEx7 [gcy-7::GCaMP3, unc-122::gfp]*	"*unc-31*" in Figure 2.9d
IV306	*ins-6(tm2416) II; ueEx7 [gcy-7::GCaMP3, unc-122::gfp]*	"*ins-6*" in Figure 2.9d
IV149	*bli-4(e937) I; ueEx7 [gcy-7::GCaMP3, unc-122::gfp]*	"*bli-4*" in Figure 2.9e
IV172	*daf-2(e1370) III; ueEx7 [gcy-7::GCaMP3, unc-122::gfp]*	"*daf-2*" in Figure 2.9e
IV96	*age-1(hx546) II; ueEx7 [gcy-7::GCaMP3, unc-122::gfp]*	"*age-1*" in Figure 2.9e
Behavior		
N2	Bristol strain	"WT" in all behavior figures
PY7502	*oyIs [ceh-36del::caspase-3(p12)::nz, ceh-36del::cz::caspase-3(p17), srtx-1::gfp, unc-122::dsRED]*	"AWC(–)" in Figures 2.1f and 2.3e
PR672	*che-1(p672) I*	"*che-1*" in Figure 2.1f

Table 2.1: Strain list, continued.

Strain	Genotype	Name
IV183	*ueEx7 [gcy-7::GCaMP3, unc-122::gfp], ueEx104 [odr-3::unc-31 sense:sl2mCherry, odr-3::unc-31 antisense:sl2mCherry, unc-122::rfp]*	"*AWC::unc-31 RNAi*" in Figure 2.1g,h
IV8	*ueEx4 [odr-3::eat-4 sense, odr-3::eat-4 antisense, elt-2::gfp]*	"*AWC::eat-4 RNAi*" in Figure 2.1g,h
IV117	*kyEx2595 [str-2::GCaMP2.2b, unc-122::gfp], ueEx57 [gcy-7::unc-31 sense:sl2mCherry, gcy-7::unc-31 antisense:sl2mCherry, unc-122::rfp]*	"*ASEL::unc-31 RNAi*" in Figure 2.3e and 2.6d
FX1377	*egl-3(tm1377) V*	"*egl-3*" in Figure 2.6d,e
CB937	*bli-4(e937) I*	"*bli-4*" in Figure 2.3e and 2.6d
VC390	*nsy-1(ok593) II*	"*nsy-1*" in Figure 2.6c
CX7442	*nsy-5(tm1896) I*	"*nsy-5*" in Figure 2.6c
FX2416	*ins-6(tm2416) II*	"*ins-6*" in Figure 2.4b and 2.7f
Cilia imaging		
IV101	*ueEx46 [gcy-7::sl2mCherry, unc-122::rfp]*	"WT" in Figure 2.2a
IV102	*osm-6(p811) V; ueEx46 [gcy-7::sl2mCherry, unc-122::rfp]*	"*osm-6*" in Figure 2.2a
IV108	*osm-6(p811) V; kyEx2595 [str-2::GCaMP2.2b, unc-122::gfp]; ueEx43 [gcy-7::osm-6:sl2mCherry, unc-122::rfp]; ueEx46 [gcy-7::sl2mCherry, unc-122::rfp]*	"*osm-6; ASEL::osm-6*" in Figure 2.2a
CX3695	*kyIs140 [str-2::GFP, lin-15(+)] I*	"WT" in Figure 2.8a
IV177	*osm-6(p811) V; kyIs140 [str-2::GFP, lin-15(+)] I; ueEx43 [gcy-7::osm-6:sl2mCherry, unc-122::rfp]*	"*osm-6; ASEL::osm-6*" and non-extrachromosomal array siblings "*osm-6*" in Figure 2.8a

Table 2.2: BLI-4 cleavage sites in insulin-like peptides. The putative BLI-4 cleavage site includes an arginine followed by two other amino acids (the second of which may be an arginine or a lysine) and then another arginine (RXRR, RXKR, or RXXR, where X is any amino acid). We compared the protein sequences of all insulin-like peptides to identify the sites shown.

Insulin	Protein sequence	BLI-4 cleavage sites			Mutant AWC^{ON} +50mM NaCl response deficit?
		RXRR	***RXKR***	RXXR	
ins-1	MYWFRQVYRPSFFFGFLAILLLSSPTP SDASIRLCGSRLTTTLLAVCRNQLCTG LTAFKRSADQSYAPTTRDLFHIHHQQ KRGGIATECCEKRCSFAYLKTFCCNQ DDN	-	-	-	no
ins-2	MNAIIFCLLFTTVTATYEVFGKGIEHR NEHLIINQLDIIPVESTPTPNRASRVQK RLCGRRLILFMLATCGECDTDSSEDLS HICCIKQCDVQDIIRVCCPNSFRK	-	-	yes	
ins-3	MKLSVVLALFIIFQLGAASLMRNWMF DFEKELEHDYDDSEIGFHNIHSLMA***RS RR***GDKVKICGTKVLKMVMVMCGGE CSSTNENIATECCEKMCTMEDITTKC CPSR	yes	-	yes	no
ins-4	MFSFFTYFLLSALLLSASCRQPSMDTS KADRILREIEMETELENQLS***RARR***VP AGEVRACGRRLLLFVWSTCGEPCTPQ EDMDIATVCCTTQCTPSYIKQACCPE K	yes	-	yes	no
ins-5	MHSIVALMLIGTILPIAALHQKHQGFI LSSSDSTGNQPMDAISRADRHTNYRS CALRLIPHVWSVCGDACQPQNGIDVA QKCCSTDCSSDYIKEICCPFD	-	-	yes	
ins-6	MNSVFTIIFVLCALQVAASFRQSFGPS MSEESASMQLLRELQHNMMESAHRP MP***RARR***VPAPGETRACGRKLISLVMA VCGDLCNPQEGKDIATECCGNQCSDD YIRSACCP	yes	-	yes	**yes**
ins-7a	MPPIILVFFLVLIPASQQYPFSLESLND QIINEEVIEYMLENSIRSS***RTRR***VPDEK KIYRCGRRIHSYVFAVCGKACESNTE VNIASKCCREECTDDFIRKQCCP	yes	-	yes	no

Table 2.2: BLI-4 cleavage sites in insulin-like peptides, continued.

Insulin	Protein sequence	BLI-4 cleavage sites			Mutant AWC^{ON} +50mM NaCl response deficit?
		RXRR	***RXKR***	RXXR	
ins-7b	MYKVHYFLINTMPPIILVFFLVLIPASQ QYPFSLESLNDQIINEEVIEYMLENSIR SS***RTRR***VPDEKKIYRCGRRIHSYVFAV CGKACESNTEVNIASKCCREECTDDFI RKQCCP	yes	-	yes	no
ins-8a	MSPIILIFFLVFIPFSQQHTSLEESLNDR IISEEVVEMLSEKEI**I**RPS***RVRR***VPEQK NKLCGKQVLSYVMALCEKACDSNTK VDIATKCCRDACSDEFIRHQCCP	yes	-	yes	
ins-8b	MKTLFNKRDKNIMIIPQNSQFLKVFLD EQNDIFMSPIILIFFLVFIPFSQQHTSLE ESLNDRIISEEVVEMLSEKEIRPS***RVRR*** VPEQKNKLCGKQVLSYVMALCEKAC DSNTKVDIATKCCRDACSDEFIRHQC CP	yes	-	yes	
ins-9	MIVTLIVFLVIGLQMAHLSQVSGNNE NGFLNPFDLSQWSEEILHRQYHHHHH HHHGN***RARR***TLETEKIYRCGRKLYT DVLSACNGPCEPGTEQDLSKLCCGNQ CTFVEIRKACCADKL	yes	-	yes	
ins-10	MSLHFSTIQKTILLISFLLLVTLAPRTS AAFPFQICVKKMEKMCRIINPEQCAQ VNKITEIGALTDCCTGLCSWEEIRISCC SVL	-	-	-	
ins-11	MSSYRQTLFILIILVIILFVNEGQGAPH HDKRHTACVLKIFKALNVMCNHEGD ADVLRRTASDCCRESCSLTEMLASCT LTSSEESTRDI	-	-	-	
ins-12	MQSNITASLFIALLIFGVISAAPSHEKT HKKCSDKLYLAMKSLCSYRGYSEFLR NSATKCCQDNCEISEMMALCVVAPN FDDDLLH	-	-	-	
ins-13	MKLLHIFIIFLLFQSCSNKMCQYSKKK YKICGVALKHMKVYCTRGMTRDYG KLLVTCCSKGCNAIDIQRICL	-	-	-	
ins-14	MLTHLKFLLLVSLFINFAVSSEDIKCD AKFISRITKLCIHGITEDKLVRLLTRCC TSHCSKAHLKMFCTLKPHEEEPHHEI	-	-	-	

Table 2.2: BLI-4 cleavage sites in insulin-like peptides, continued.

Insulin	Protein sequence	BLI-4 cleavage sites			Mutant AWC^{ON} +50mM NaCl response deficit
		RXRR	***RXKR***	RXXR	
ins-15	MKLLPLIVVFALLAVISESYSGNDFQP RDNKHHSYRSCGESLSRRVAFLCNGG AIQTEILRALDCCSTGCTDKQIFSWCD FRKLTRKEKQNYSGLIFRNLNRTQIVS FLLCHVE	-	-	-	
ins-16	MQSLPILACLLTLSVFAPEIHGRELKR CSVKLFDILSVICGTESDAEILQKVAV KCCQEQCGFEEMCQHALKIDKI	-	-	-	
ins-17	MFSTRGVLLLLSLMAAVAAFGLFSRP APITRDTIRPPRAKHGSLKLCPPGGAS FLDAFNLICPM***RRRRR***SVSENYNDGG GSLLGRTMNMCCETGCEFTDIFAICNP FG	yes	-	yes	
ins-18	MVHRLFIVLIAIILVAKSTAISLQQADG RMKMCPPGGSTFTMAWSMSCSMR***R RKR***DVGRYFEKRALIAPSIRQLQTICC QVGCNVEDLLAYCAPI	-	yes	yes	no
ins-19	MIFYLTTYLVTMSPLFLILLLLVSTTYP YIIDSSESYEVLMLFGYKRTCGRRLM NRINRVCVKDIDPADIDPKIKLSEHCC IKGCTDGWIKKHICSEEVLNFGFFEN	-	-	yes	
ins-20	MDKPSYLSSKEAWKMLNELLKEPKH HHHHHRHKGYCGVKAVKKLKQICPD LCSNVDDNLLMEMCSKNLTDDDILQ RCCPE	-	-	-	
ins-21	MKTYSFFVLFIVFIFFISSSKSHSKKHV RFLCATKAVKHIRKVCPDMCLTGEEV EVNEFCKMGYSDSQIKYICCPE	-	-	-	
ins-22	MHTTTILICFFIFLVQVSTMDAHTDKY VRTLCGKTAIRNIANLCPPKPEMKGIC STGEYPSITEYCSMGFSDSQIKFMCCD NQ	-	-	-	no
ins-23	MFVLLIILSIILAQVTDAHSELHVRRV CGTAIIKNIMRLCPGVPACENGEVPSP TEYCSMGYSDSQVKYLCCPTSQ	-	-	-	
ins-24	MRSPTLFLLLLLVPLALCHVFSEPADL ELKSYQALEKSLKEMGLIRANQGPQK ACGRSMMMKVQKLCAGGCTIQNDD LTIKSCSTGYTDAGFISACCPSGFVF	-	-	-	

Table 2.2: BLI-4 cleavage sites in insulin-like peptides, continued.

Insulin	Protein sequence	BLI-4 cleavage sites			Mutant AWC^{ON} +50mM NaCl response deficit
		RXRR	***RXKR***	RXXR	
ins-25	MLFKIIILFFLLLQLSEAKPEAQRRCGRYLIRFLGELCNGPCSGVSSVDIATIACATAVPIEDLKNMCCPNL	-	-	yes	
ins-26	MRALVAILCLMALCHAAMLDELEMQKEVQEFHHMNGMLQEFMNKGLIGNHHHGTKAGLTCGMNIIERVDKLCNGQCTRNYDALVIKSCHRGVSDMEFMVACCPTMKLFIH	-	-	-	
ins-27	MKFFRLILLCALVLTTMAFLAPSTAAKRRCGRLIPYVYSICGGPCENGDIIIEHCFSGTTPTIAEVQKACCPELSEDPTFSS	-	-	yes	
ins-28	MMRSFFVLLALLAIVTSTASPTCGRALLHRIQSVCGLCTIDAHHELIAIACSRGLGDKEIIEMCCPI	-	-	-	
ins-29	MFCKFVFLIFLLISLSVATADFGAQRRCGRHLVNFLEGLCGGPCSEAPTVELASWACSSAVSIQDLEKLCCPSNLA	-	-	yes	
ins-30	MSSHALVLFLLLFLLPVALGHFLSKPAPDPRITFNRKLAETLKELQDMGLIQAPREPVVAAQGAKKTCGRSLLIKIQQLCHGICTVHADDLHETACMKGLTDSQLINSCCPPIPQTPFVF	-	-	-	
ins-31	MKMPLILLLLVAAASAFVHHFDHSMFARPEKTCGGLLIRRVDRICPNLNYTYKIEWELMDNCCEVVCEDQWIKETFCRAPRFNFFGPSFKALERSCGPKLFTRVKTVCGEDINVDNKVKISDHCCTPEGGCTDDWIKENVCKQTRFNFFRQFLDSPQRSCGPQLFKRVNTLCNENINVENNVSVSKSCCESAAGCTDDWIKKNVCTQHKPFVFRPGFY	-	-	yes	
ins-32	MTSILLILLLVITVTGMFQELSDLQNLHRFLEGLQGSSSLAVKS***RSRR***ELICGRRLSKTVTNLCVEMNPQKEEDIATKCCKNKGCSREYIKSIMCPDE	yes	-	yes	no
ins-33	MANTCLILLLLLVIFVTVGFSMPRIFRASENGVNSSDEVSEELSYSPEEAMDLVKQVIKVREQR***RHRR***HRHHGQKHCGTKIVRKLQMLCPKMCTISDDTLLTEMCSHSLFDDEIQLRCCPKEDE	yes	-	yes	

Table 2.2: BLI-4 cleavage sites in insulin-like peptides, continued.

Insulin	Protein sequence	BLI-4 cleavage sites			Mutant AWC^{ON} +50mM NaCl response deficit
		RXRR	***RXKR***	RXXR	
ins-34	MLHHKTLIIALLLTLFISGIDSLPFRKH NNHRHLKNQKAQQLKEEATEAPTPA PTTTKAPSGSATTTTTVKTTAAPLAQ VNPQCLRRLTLLARGVCRQPCQPSDK PKTSAQQLLQLACSARRPTNEQIISYC CPEKSG	-	-	-	
ins-35	MKQIFLVILAACLLAIILASPTGKHHK MDENAFGINNRHCQRALKVYSFAICG AICQNYEKILMEGCGSTVMLTMQRT KLICCPEPVDSDELFN	-	-	-	
ins-36a	MNIGKCSIIFLLFCVFGSILSRAIRKRH PEGKLVIRDCKRYLIMYSRTICKEKCE KFDERNDITFSINLQFIFTDLLVEGCHS NQTLSNERTRELCCPNAGSN	-	-	yes	
ins-36b	MNIGKCSIIFLLFCVFGSILSRAIRKRH PEGKLVIRDCKRYLIMYSRTICKEKCE KFDDLLVEGCHSNQTLSNERTRELCC PNAGSN	-	-	yes	
ins-37	MAAFLPIALSIAMLTVLTNANPIHPVP NAAFLPYRSCGSHLVHRAFEACSGKK DRSSDVDLWKMCCKDECTDLDIKES LCKYASQGYGVKFEEEAEEIDMVSFA AEGFKKSCGHDIVVKTVNVPTKISLK QCARTRGWRR***RPRR***IPDKFNRVQNY ACINCVKIK	yes	-	yes	
ins-38	MNLFLLVCIAFAIITVTSFTPDEKSQRS HVFSYKKHCGRRIVSLVQACDRIDHD LSIDCCTQNCSSEFVKKIMCPSKL	-	-	-	
ins-39	MNTFFFLAVLLVFCSAEQMTAKKFST KTSSPIPELQEVFATVAADEFPFHKAN TQPLAIYLNISTPQDCIHKIFRMTISFCS QVECQNMEAMQKICNTTTPTIKHVGE LCCPEFFEQVKDDFVTLL	-	-	-	
daf-28	MNCKLIAIFAVLVLSVSAHLGAQAAA ANFKAEGPLSRAVRVPGVAVRACGR RLVPYVWSVCGDACEPQEGIDIATQC CTYQCTAEYIQTACCPRLLL	-	-	yes	
		10/40	1/40	20/40	

References

Aburto, N.J., Ziolkovska, A., Hooper, L., Elliott, P., Cappuccio, F.P., and Meerpohl, J.J. (2013). Effect of lower sodium intake on health: systematic review and meta-analyses. BMJ 346, f1326.

Baldridge, W.H., Vaney, D.I., and Weiler, R. (1998). The modulation of intercellular coupling in the retina. Semin Cell Dev Biol 9, 311-318.

Bargmann, C.I. (2006). Chemosensation in C. elegans. WormBook, 1-29.

Bargmann, C.I., and Horvitz, H.R. (1991). Chemosensory neurons with overlapping functions direct chemotaxis to multiple chemicals in C. elegans. Neuron 7, 729-742.

Beverly, M., Anbil, S., and Sengupta, P. (2011). Degeneracy and neuromodulation among thermosensory neurons contribute to robust thermosensory behaviors in Caenorhabditis elegans. J Neurosci 31, 11718-11727.

Brenner, S. (1974). The genetics of Caenorhabditis elegans. Genetics 77, 71-94.

Chalasani, S.H., Chronis, N., Tsunozaki, M., Gray, J.M., Ramot, D., Goodman, M.B., and Bargmann, C.I. (2007). Dissecting a circuit for olfactory behaviour in Caenorhabditis elegans. Nature 450, 63-70.

Chalasani, S.H., Kato, S., Albrecht, D.R., Nakagawa, T., Abbott, L.F., and Bargmann, C.I. (2010). Neuropeptide feedback modifies odor-evoked dynamics in Caenorhabditis elegans olfactory neurons. Nat Neurosci 13, 615-621.

Chandrashekar, J., Kuhn, C., Oka, Y., Yarmolinsky, D.A., Hummler, E., Ryba, N.J., and Zuker, C.S. (2010). The cells and peripheral representation of sodium taste in mice. Nature 464, 297-301.

Chen, B.L., Hall, D.H., and Chklovskii, D.B. (2006). Wiring optimization can relate neuronal structure and function. Proc Natl Acad Sci U S A 103, 4723-4728.

Chen, Z., Hendricks, M., Cornils, A., Maier, W., Alcedo, J., and Zhang, Y. (2013). Two insulin-like peptides antagonistically regulate aversive olfactory learning in C. elegans. Neuron 77, 572-585.

Chronis, N., Zimmer, M., and Bargmann, C.I. (2007). Microfluidics for in vivo imaging of neuronal and behavioral activity in Caenorhabditis elegans. Nat Methods 4, 727-731.

Clark, D.A., Biron, D., Sengupta, P., and Samuel, A.D. (2006). The AFD sensory neurons encode multiple functions underlying thermotactic behavior in Caenorhabditis elegans. J Neurosci 26, 7444-7451.

Collet, J., Spike, C.A., Lundquist, E.A., Shaw, J.E., and Herman, R.K. (1998). Analysis of osm-6, a gene that affects sensory cilium structure and sensory neuron function in Caenorhabditis elegans. Genetics 148, 187-200.

de Bono, M., and Maricq, A.V. (2005). Neuronal substrates of complex behaviors in C. elegans. Annu Rev Neurosci 28, 451-501.

Dickinson, P.S., Mecsas, C., and Marder, E. (1990). Neuropeptide fusion of two motor-pattern generator circuits. Nature 344, 155-158.

Dorman, J.B., Albinder, B., Shroyer, T., and Kenyon, C. (1995). The age-1 and daf-2 genes function in a common pathway to control the lifespan of Caenorhabditis elegans. Genetics 141, 1399-1406.

Esposito, G., Di Schiavi, E., Bergamasco, C., and Bazzicalupo, P. (2007). Efficient and cell specific knock-down of gene function in targeted C. elegans neurons. Gene 395, 170-176.

Gracheva, E.O., Burdina, A.O., Touroutine, D., Berthelot-Grosjean, M., Parekh, H., and Richmond, J.E. (2007). Tomosyn negatively regulates both synaptic transmitter and neuropeptide release at the C. elegans neuromuscular junction. J Physiol 585, 705-709.

Hooper, S.L., and Moulins, M. (1989). Switching of a neuron from one network to another by sensory-induced changes in membrane properties. Science 244, 1587-1589.

Hua, Q.X., Nakagawa, S.H., Wilken, J., Ramos, R.R., Jia, W., Bass, J., and Weiss, M.A. (2003). A divergent INS protein in Caenorhabditis elegans structurally resembles human insulin and activates the human insulin receptor. Genes Dev 17, 826-831.

Hung, W.L., Hwang, C., Gao, S., Liao, E.H., Chitturi, J., Wang, Y., Li, H., Stigloher, C., Bessereau, J.L., and Zhen, M. (2013). Attenuation of insulin signalling contributes to FSN-1-mediated regulation of synapse development. Embo J.

Husson, S.J., Clynen, E., Baggerman, G., Janssen, T., and Schoofs, L. (2006). Defective processing of neuropeptide precursors in Caenorhabditis elegans lacking proprotein convertase 2 (KPC-2/EGL-3): mutant analysis by mass spectrometry. J Neurochem 98, 1999-2012.

Kauffman, A.L., Ashraf, J.M., Corces-Zimmerman, M.R., Landis, J.N., and Murphy, C.T. (2010). Insulin signaling and dietary restriction differentially influence the decline of learning and memory with age. PLoS Biol 8, e1000372.

Kimura, K.D., Tissenbaum, H.A., Liu, Y., and Ruvkun, G. (1997). daf-2, an insulin receptor-like gene that regulates longevity and diapause in Caenorhabditis elegans. Science 277, 942-946.

Klockener, T., Hess, S., Belgardt, B.F., Paeger, L., Verhagen, L.A., Husch, A., Sohn, J.W., Hampel, B., Dhillon, H., Zigman, J.M.*, et al.* (2011). High-fat feeding promotes obesity via insulin receptor/PI3K-dependent inhibition of SF-1 VMH neurons. Nat Neurosci 14, 911-918.

Lee, R.Y., Sawin, E.R., Chalfie, M., Horvitz, H.R., and Avery, L. (1999). EAT-4, a homolog of a mammalian sodium-dependent inorganic phosphate cotransporter, is necessary for glutamatergic neurotransmission in caenorhabditis elegans. J Neurosci 19, 159-167.

Li, C., and Kim, K. (2008). Neuropeptides. WormBook, 1-36.

Markov, N.T., Ercsey-Ravasz, M.M., Ribeiro Gomes, A.R., Lamy, C., Magrou, L., Vezoli, J., Misery, P., Falchier, A., Quilodran, R., Gariel, M.A.*, et al.* (2012). A Weighted and Directed Interareal Connectivity Matrix for Macaque Cerebral Cortex. Cereb Cortex.

Murakami, H., Bessinger, K., Hellmann, J., and Murakami, S. (2005). Aging-dependent and -independent modulation of associative learning behavior by insulin/insulin-like growth factor-1 signal in Caenorhabditis elegans. J Neurosci 25, 10894-10904.

Qi, Y.B., Garren, E.J., Shu, X., Tsien, R.Y., and Jin, Y. (2012). Photo-inducible cell ablation in Caenorhabditis elegans using the genetically encoded singlet oxygen generating protein miniSOG. Proc Natl Acad Sci U S A 109, 7499-7504.

Ramot, D., MacInnis, B.L., and Goodman, M.B. (2008). Bidirectional temperature-sensing by a single thermosensory neuron in C. elegans. Nat Neurosci 11, 908-915.

Richmond, J. (2005). Synaptic function. WormBook, 1-14.

Richmond, J.E., Davis, W.S., and Jorgensen, E.M. (1999). UNC-13 is required for synaptic vesicle fusion in C. elegans. Nat Neurosci 2, 959-964.

Root, C.M., Masuyama, K., Green, D.S., Enell, L.E., Nassel, D.R., Lee, C.H., and Wang, J.W. (2008). A presynaptic gain control mechanism fine-tunes olfactory behavior. Neuron 59, 311-321.

Savigner, A., Duchamp-Viret, P., Grosmaitre, X., Chaput, M., Garcia, S., Ma, M., and Palouzier-Paulignan, B. (2009). Modulation of spontaneous and odorant-evoked activity of rat olfactory sensory neurons by two anorectic peptides, insulin and leptin. J Neurophysiol 101, 2898-2906.

Speese, S., Petrie, M., Schuske, K., Ailion, M., Ann, K., Iwasaki, K., Jorgensen, E.M., and Martin, T.F. (2007). UNC-31 (CAPS) is required for dense-core vesicle but not synaptic vesicle exocytosis in Caenorhabditis elegans. J Neurosci 27, 6150-6162.

Su, C.Y., Menuz, K., Reisert, J., and Carlson, J.R. (2012). Non-synaptic inhibition between grouped neurons in an olfactory circuit. Nature 492, 66-71.

Suzuki, H., Thiele, T.R., Faumont, S., Ezcurra, M., Lockery, S.R., and Schafer, W.R. (2008). Functional asymmetry in Caenorhabditis elegans taste neurons and its computational role in chemotaxis. Nature 454, 114-117.

Taguchi, A., and White, M.F. (2008). Insulin-like signaling, nutrient homeostasis, and life span. Annu Rev Physiol 70, 191-212.

Thacker, C., Peters, K., Srayko, M., and Rose, A.M. (1995). The bli-4 locus of Caenorhabditis elegans encodes structurally distinct kex2/subtilisin-like endoproteases essential for early development and adult morphology. Genes Dev 9, 956-971.

Thacker, C., Sheps, J.A., and Rose, A.M. (2006). Caenorhabditis elegans dpy-5 is a cuticle procollagen processed by a proprotein convertase. Cell Mol Life Sci 63, 1193-1204.

Thiele, T.R., Faumont, S., and Lockery, S.R. (2009). The neural network for chemotaxis to tastants in Caenorhabditis elegans is specialized for temporal differentiation. J Neurosci 29, 11904-11911.

Tissenbaum, H.A. (2012). Genetics, life span, health span, and the aging process in Caenorhabditis elegans. J Gerontol A Biol Sci Med Sci 67, 503-510.

Tomioka, M., Adachi, T., Suzuki, H., Kunitomo, H., Schafer, W.R., and Iino, Y. (2006). The insulin/PI 3-kinase pathway regulates salt chemotaxis learning in Caenorhabditis elegans. Neuron 51, 613-625.

Touhara, K., and Vosshall, L.B. (2009). Sensing odorants and pheromones with chemosensory receptors. Annu Rev Physiol 71, 307-332.

Uchida, O., Nakano, H., Koga, M., and Ohshima, Y. (2003). The C. elegans che-1 gene encodes a zinc finger transcription factor required for specification of the ASE chemosensory neurons. Development 130, 1215-1224.

Ward, S. (1973). Chemotaxis by the nematode Caenorhabditis elegans: identification of attractants and analysis of the response by use of mutants. Proc Natl Acad Sci U S A 70, 817-821.

Weimann, J.M., and Marder, E. (1994). Switching neurons are integral members of multiple oscillatory networks. Curr Biol 4, 896-902.

Weimann, J.M., Meyrand, P., and Marder, E. (1991). Neurons that form multiple pattern generators: identification and multiple activity patterns of gastric/pyloric neurons in the crab stomatogastric system. J Neurophysiol 65, 111-122.

Wes, P.D., and Bargmann, C.I. (2001). C. elegans odour discrimination requires asymmetric diversity in olfactory neurons. Nature 410, 698-701.

White, J.G., Southgate, E., Thomson, J.N., and Brenner, S. (1986). The structure of the nervous system of the nematode *Caenorhabditis elegans*. Phil Transact R Soc Lond B 314, 1-340.

Xia, X.B., and Mills, S.L. (2004). Gap junctional regulatory mechanisms in the AII amacrine cell of the rabbit retina. Vis Neurosci 21, 791-805.

CHAPTER 3.

From genes to circuits and behaviors: neuropeptides expand the coding potential of the nervous system

Abstract

Neuropeptide signaling remodels the composition of a chemosensory circuit and shapes behavior in *Caenorhabditis elegans.* We reported that the ASEL (ASE left) salt sensory neuron uses a proprotein convertase, BLI-4, to cleave the insulin-like peptide INS-6. INS-6 peptides are released from the ASEL neuron in response to high, but not low, salt stimuli. Fast INS-6 signaling functionally transforms the AWC olfactory sensory neuron into an interneuron in the neural circuit for high salt. This new circuit configuration potentiates behavioral attraction to high salt. Here, in the context of genes, circuits and behaviors, we discuss the diverse modes of neuropeptide processing and signaling, which expand the coding potential of the nervous system. First, neuropeptide processing and release genes prepare insulin peptides to signal in the nervous system. Second, this neuropeptide signaling diversifies the communication of neural circuits and introduces circuit-level flexibility. Finally, the resulting multisensory neurons and circuits drive finely tuned behavioral choices.

Introduction

Neuropeptides, including insulins, have numerous roles in modulating neural circuits and regulating the execution of diverse behaviors (Chalasani et al., 2010; Chen et al., 2013; Harris et al., 2010; Savigner et al., 2009). In the nervous system, insulin signaling regulates synapse development, the signal to noise ratio of olfactory sensory neuron activity, gustatory and olfactory learning behaviors (Chen et al., 2013; Hung et al., 2013; Marks et al., 2009; Savigner et al., 2009; Tomioka et al., 2006) and many other circuit functions. Recently, we reported a novel sensory context-dependent and insulin neuropeptide-mediated remodeling of a chemosensory neural circuit in *Caenorhabditis elegans* (Leinwand and Chalasani, 2013). We defined an unexpected mechanism for the processing and the release of insulin-like peptides, which change the composition of the neural circuit driving behavior in response to changes in salt. Upon high salt stimulation, the insulin-like peptide INS-6, which is processed by the proprotein convertase BLI-4, is released from the ASEL salt sensory neuron (**Figure 3.1c**) (Leinwand and Chalasani, 2013). The release of mature INS-6 peptides depends on the *C. elegans* homolog of calcium-dependent secretion activator, UNC-31, which is a key regulator of neuropeptide-containing dense core vesicle secretion (**Figure 3.1c**) (Hammarlund et al., 2008; Speese et al., 2007). INS-6 binds the DAF-2 insulin receptors on the AWC olfactory sensory neuron, activating this cell (**Figure 3.1c**) (Leinwand and Chalasani, 2013). Exciting the AWC neuron in this manner recruits AWC and its target interneurons to the high salt circuit and specifically potentiates attraction behavior towards high salt (Leinwand and Chalasani, 2013).

In this commentary, we divide our discussion about the significance and context of our novel findings into three sections focusing on genes, circuits and behaviors. At the level of genes, we discuss our findings about novel roles for several genes in the processing and release of insulins in the nervous system and speculate about the generality of these molecular mechanisms. At the level of circuits, we describe how neuropeptide signaling adds a dynamic new language of communication to the nervous system, and we highlight the intriguing spatial and temporal constraints that expand the neurotransmitter vocabulary. Finally, at the level of behaviors, we discuss how individual neurons may act in flexible neural circuits to direct behavior towards multiple stimulus modalities across species, in *C. elegans, D. melanogaster* and *M. musculus*.

Genes: a novel molecular mechanism for processing and releasing insulin peptides

Our work identified unexpected requirements for peptide processing and release genes in the nervous system. Neuropeptides are processed post-translationally in multiple steps. Proneuropeptides are cleaved by a proprotein convertase and then further modified by a variety of other enzymes (Li and Kim, 2008). A family of kex2/subtilisin-like proprotein convertases, which cleave these proneuropeptides, is conserved across eukaryotes (Steiner, 1998). Four convertase family members have been identified in *C. elegans*: *egl-3, bli-4, kpc-1 and aex-5* (Thacker and Rose, 2000). Prior to our study, it was hypothesized that these enzymes might cleave the 40 pro-insulin-like peptides in *C. elegans* to produce mature insulins; however, no genetic, proteomic or physiology experiments supported this theory (Husson et al., 2006; Li and Kim, 2008). Our research demonstrates that the insulin-like peptide INS-6 is produced through a BLI-4 proprotein

convertase-dependent cleavage step in the ASEL sensory neurons (**Figure 3.1**) (Leinwand and Chalasani, 2013). In ASEL neurons, we confirmed that BLI-4 recognizes an RXRR motif in INS-6 (**Figure 3.1**). This is the first description of a role for BLI-4 in the nervous system. We speculate that BLI-4 also cleaves other neuropeptides. Given that the BLI-4 cleavage site is highly conserved (RXRR or RXKR) (Thacker and Rose, 2000), a molecular genetic approach would be ideal for determining the identity of the other peptides that are also processed by this convertase.

The genes involved in releasing mature insulins in the nervous system were predicted to be similar to those involved in the release of other neuropeptides; however, this had not been confirmed experimentally. UNC-31, the homolog of calcium-dependent secretion activator, is a key regulator of dense core vesicle priming, docking and secretion (Hammarlund et al., 2008; Speese et al., 2007). Our results suggest that INS-6 peptides (along with other insulin-like peptides) are released from dense core vesicles in an UNC-31-dependent manner (**Figure 3.1**) (Leinwand and Chalasani, 2013). Interestingly, this insulin release from ASEL neurons activates AWC neurons only when the animals experience sufficiently large changes in salt, ≥20 mM NaCl (**Figure 3.1**). These large changes in salt cause significantly larger magnitude and longer duration calcium transients in the ASEL neurons than smaller changes in salt (10 mM NaCl) (Leinwand and Chalasani, 2013). Together, these findings suggest that insulin-containing dense core vesicles are only released when sufficiently high levels of calcium mobilization are achieved in the presynaptic neuron (**Figure 3.1c**). In contrast, we hypothesize that the lower levels of calcium in ASEL neurons resulting from low salt stimulation are only enough to release small, clear synaptic vesicles containing small

neurotransmitters such as glutamate. These results suggest that dense core vesicle release occurs only when high, global levels of calcium have been reached after strong stimulation, thereby supporting a theory that has long been proposed (Salio et al., 2006; Verhage et al., 1991) and extending it to also include insulin-containing vesicles. Additionally, our results provide the first illustration of circuit level and behavioral consequences of the different calcium levels triggered by varying sensory stimulation (**Figure 3.1**). Nevertheless, it cannot be ruled out that very low levels of dense core vesicle release do occur with lower intensity salt stimulation. In this scenario, the few peptides from these vesicles are simply insufficient to bind a high level of receptors on the postsynaptic AWC neuron or cause a detectable increase in the AWC calcium signal.

Furthermore, the requirement for global calcium to produce dense core vesicle release can be bypassed. TOM-1, the *C. elegans* homolog of Tomosyn, acts upstream of UNC-31 to inhibit neurotransmission (Gracheva et al., 2007) (**Figure 3.1b**). If this brake on neurotransmission is removed, then dense core vesicles can be released, even in the absence of high, global calcium. We found that TOM-1 RNAi knockdown specifically in ASEL neurons is sufficient to trigger low levels of dense core vesicle release in response to low (10 mM) salt stimulation (Leinwand and Chalasani, 2013) (**Figure 3.1b**). This manipulation activates the postsynaptic AWC neurons. Importantly, this result indicates that insulin peptides are present in a readily releasable pool. High calcium levels or upstream signaling simply function as the switches that permit exocytosis of the insulin-containing dense core vesicles from this readily releasable pool.

We speculate that other invertebrate species as well as mammals use homologs of the *C. elegans* insulin processing and release genes that we described. For example,

insulin, insulin-like growth factors (IGF-1 and IGF-II) and the related relaxin ligands in other species also require post-translational processing (Pierce et al., 2001), which could be performed by proprotein convertases of the BLI-4 family. There is evidence that pro-IGF-II is processed by a proprotein convertase, PC4, whose catalytic domain shares significant homology with *C. elegans* BLI-4 (Qiu et al., 2005; Thacker and Rose, 2000). This processing generates mature IGF-II that functions in the development of the human placenta (Qiu et al., 2005). If IGF-II processing is abnormally reduced, then serious developmental disorders result (Qiu et al., 2005). Taken together, the conservation of the peptide processing machinery indicates that processing events play crucial roles in generating mature insulins capable of signaling in animals and people.

Circuits: a neuropeptide language diversifies neural circuit communication

Insulins and other neuropeptides function as neuromodulators, co-transmitters and independent transmitters (Nassel, 2009). The diverse functions of neuropeptides acting at different spatial and temporal scales are still being appreciated. However, it is clear that peptide signaling adds an additional nuanced language for encoding dynamic experiences and driving complex behaviors (Bargmann, 2012). Whether a particular peptide signals locally and rapidly (< 1 second) to relay information in a neural circuit or globally and over longer developmental time periods cannot be predicted simply by the peptide identity (Hung et al., 2013; Leinwand and Chalasani, 2013).

Neuropeptide processing, release and downstream signaling mechanisms are likely to play a role in determining the bioactivity of peptides (**Figure 3.2**). A recent study showed that INS-6 peptides released from ASI sensory neurons play a crucial role

in shaping synapses at the neuromuscular junction (Hung et al., 2013) (**Figure 3.2**). Furthermore, this study showed that a different proprotein convertase, EGL-3, processes INS-6 in ASI neurons (Hung et al., 2013) (**Figure 3.2**). Taken together with our findings, these results indicate that the same ligand can act on two different timescales: in less than one second to recruit AWC neurons into the salt circuit when released from ASE neurons (Leinwand and Chalasani, 2013) and over multiple hours to shape neuromuscular synapses during development when released from ASI neurons (Hung et al., 2013) (**Figure 3.2**). We suggest three possible mechanisms that could explain these interesting dual roles for INS-6 peptides.

First, we speculate that properties of the neurons that release INS-6 ligands regulate the functions of these neuropeptides. It is possible that ASE and ASI neurons have differing release probabilities for INS-6 leading to these two functions. For example, in the adult, ASE neurons likely release INS-6 *acutely*. Upon high salt stimulation, ASE-released INS-6 immediately modifies the composition of the salt neural circuit by recruiting AWC neurons (Leinwand and Chalasani, 2013). These INS-6 peptides act as fast, locally acting transmitters, much like classical small molecule and amino acid neurotransmitters. In contrast, ASI neurons of young, larval stage animals may release INS-6 *tonically* to influence the development of neuromuscular junctions. The high level of INS-6 peptides released from ASI could influence neuromuscular synapses over multiple hours (Hung et al., 2013).

A second possibility for the dual functions of INS-6 is that there is specificity in peptide processing mechanisms. Since EGL-3 and BLI-4 proprotein convertases cleave the same site in the INS-6 proneuropeptide, it is unlikely mature peptides with different

sequences are released from ASI and ASE neurons (Hung et al., 2013; Leinwand and Chalasani, 2013). However, it is possible that the proprotein convertases associate with specific downstream processing components leading to differences in how INS-6 is modified in these two neurons. For example, EGL-3-processed INS-6 could be amidated, while BLI-4-processed INS-6 may not be modified in this same manner. Previous results have shown that amidated peptides are more stable and can therefore exert their influence over longer timescales (Li and Kim, 2008). This prediction of differential processing of the mature INS-6 from ASI and ASE neurons can be easily tested. We suggest that a mass spectrometry based approach is ideal for probing the status (amidation, acetylation, etc.) of the mature INS-6 peptides that are specifically released from the ASI or ASE neurons, respectively.

A third possibility is that the distance to and nature of the receiving cells enable INS-6 to have these dual functions. In one instance, ASE and AWC neurons are in close proximity to each other and share direct synapses (White et al., 1986). INS-6 signaling between these two neurons is rapid and serves to modify the target neuron (AWC). In a second instance, ASI-released INS-6 peptides have to travel many cell diameters in order to influence distant motor neurons and their synapses on the body wall muscle (Hung et al., 2013) (**Figure 3.2**). Moreover, the developing muscles targets retain the ability to sense INS-6 over many hours. Additionally, the downstream signaling pathways in the receiving cells may play a crucial role in transducing INS-6 signals over different timescales. Neuropeptide degradation may also contribute to the scale of peptide actions. NEP-1, a *C. elegans* proteolytic enzyme of the neprilysin family, could degrade neuropeptides before they reach their targets (Turner et al., 2001). Varying degradation

rates across developmental stages or preferential degradation of unstable peptides (which lack amidation) could differentially restrict peptide actions. These mechanisms could enable related peptides to have divergent effects on near and distant targets.

We suggest that properties of the releasing and the receiving neurons constrain the actions of all neuropeptides. Peptides could function either as local and fast acting or long-range and slower signals. Peptides with these different temporal and spatial ranges may also be processed in different ways. We speculate that similar mechanisms exist to regulate the bioactivity of neuropeptides in other species. Taken together, neuropeptides may signal across many temporal and spatial scales to introduce plasticity into neural circuits. These wide-ranging signaling mechanisms reveal an additional layer of complexity in the neuronal communication for coordinating developmental processes, processing sensory information and driving flexible behaviors.

Behaviors: multisensory neurons and circuits drive finely tuned behavioral choices

Across species, multimodal neurons exist, which are activated by changes in smell, taste, temperature and other sensory experiences. These multisensory neurons are uniquely positioned to signal that global environmental conditions are improving or worsening and to direct behavior. In *C. elegans*, a subset of sensory neurons responds directly to multiple modalities (Biron et al., 2008). Neurotransmission recruits other *C. elegans* neurons to circuits that encode several senses (Leinwand and Chalasani, 2013). AWC neurons were first identified as olfactory sensory neurons (Bargmann et al., 1993). However, recent work has shown that AWC neurons are also active under particular salt, temperature and sex pheromone conditions (Biron et al., 2008; Kuhara et al., 2008;

Leinwand and Chalasani, 2013; White et al., 2007) (**Figure 3.3a**). Excited AWC neurons may release glutamate and neuropeptides, exclusively or in combination, to recruit particular downstream effector circuits, thereby shaping behavioral outputs (Leinwand and Chalasani, 2013; Ohnishi et al., 2011; White et al., 2007) (**Figure 3.3a**).

Insulin-mediated recruitment of the AWC neurons into the high salt circuit is critical for strongly exciting downstream AIA interneurons (Leinwand and Chalasani, 2013). AWC uses neuropeptides, not glutamate, to signal high salt to AIA interneurons (Leinwand and Chalasani, 2013). In the future, it will be interesting to determine the identity of these AWC-released, UNC-31-dependent neuropeptides. Perhaps these neuropeptides from AWC also activate or inhibit other interneurons. For instance, AWC neuropeptides may recruit the AVA neurons to the high salt circuit, even though these neurons are not targets of the ASEL neurons and may not participate in the low salt circuit (White et al., 1986). Together, the interneurons and motor neurons downstream of the AWC neurons potentiate chemotaxis behavior towards high concentrations of salt (Leinwand and Chalasani, 2013). This circuit configuration may expand the upper end of the dynamic range of salt-guided behaviors. This could promote additional salt consumption and improved ion homeostasis for animal survival. Moreover, flexible, AWC circuits may integrate information about salt conditions with all other AWC-detected sensory modalities to regulate attraction behaviors (**Figure 3.3a**).

AWC neurons may express the receptors necessary for directly sensing temperature and sex pheromones (Biron et al., 2008; White et al., 2007). AWC neurons release glutamate to activate downstream interneurons and promote migration to warmer temperatures (Ohnishi et al., 2011). In neural circuits for temperature, AWC neurons may

integrate temperature information with all of the other environmental conditions that they detect (**Figure 3.3a**). AWC neurons could then fine-tune a behavioral program that was initiated by the broadly tuned primary thermosensory neurons, AFD (**Figure 3.3a**) (Biron et al., 2008). The same principle may apply to AWC's role in sex pheromone detection and male mating (White et al., 2007). AWC may contribute a global view of the sensory environment to shape male mating behavior, which was initiated by other sensory and male specific neurons (White et al., 2007). Together, these results demonstrate a general organizing principle: individual multisensory neurons can participate in overlapping circuits that drive behaviors directed toward multiple sensory modalities.

Multisensory neurons and circuits have been found in many species with significantly larger and more complex nervous systems than *C. elegans* (Dalton et al., 2000; Ghazanfar and Schroeder, 2006; Keene et al., 2004). However, to maximize the coding potential of their compact nervous system, *C. elegans* sensory neurons themselves may actually perform the integration and other computations that are typically reserved for higher order neurons of flies (*D. melanogaster*) and mammals. For instance, information from peripheral olfactory sensory neurons and gustatory neurons may be integrated in flies by the dorsal paired medial (DPM) neurons in the central nervous system, for appropriate behavior in some memory tasks (**Figure 3.3b**) (Keene et al., 2004). The neuropeptide AMN, a homolog of the mammalian pituitary adenylate cyclase-activating peptide, is required acutely for this multisensory behavior (**Figure 3.3b**) (Keene et al., 2004). Another study showed that insulin and short neuropeptide F signaling modulates flies' olfactory sensitivity and food-search behavior based on global satiety signals (Root et al., 2011). Neuropeptides have also been shown to be important

for various integrative behaviors in mammals (Dolen et al., 2013). For example, oxytocin peptides from the hypothalamus alter release probability in the nucleus accumbens and have effects on multisensory social behaviors and their reward value (Dolen et al., 2013). In summary, animals of all species integrate diverse sensory cues with state-dependent information to drive motor patterns that will improve the animal's quality of life. As the above examples show, neuropeptide signaling plays an important role in shaping the multisensory neural circuits and their motor outputs.

Conclusions

Animals have neural circuits that enable them to process and respond appropriately to dynamic, multisensory features of their environments. At the level of genes, circuits and behaviors, we have highlighted mechanisms that expand the coding potential of the nervous system. These principles of flexibility and neuropeptide regulation, which were uncovered in *C. elegans,* are likely to be conserved in other species. Therefore, they present a major challenge to researchers embarking on large-scale brain activity mapping projects like the BRAIN initiative. Here, we summarize the key points:

(1) Genes: Insulin neuropeptides are processed by a proprotein convertase, BLI-4. Mature insulins are released from dense core vesicles in an UNC-31-dependent manner, upon strong stimulation and a large rise in calcium.

(2) Circuits: Neuropeptides have spatial and temporal constraints on their bioactivity, which may result from their processing, release and downstream signaling. The identity of an insulin neuropeptide is insufficient to predict its function. Moreover, the vast

diversity of neuropeptide signaling mechanisms adds a dynamic, new language to the nervous system.

(3) Behaviors: *C. elegans* sensory neurons integrate multisensory cues to drive motor outputs that are appropriate for the global environment. Higher order neurons in *D. melanogaster* and mammals integrate multiple sensory stimuli with physiological needs to coordinate behavior. Neuropeptide signaling also fine-tunes behavior by introducing flexibility to the multisensory neurons and circuits.

Acknowledgments

This chapter is a reprint of the material as it appears in Leinwand, S.G. and Chalasani, S.H. (2014). From genes to circuits and behaviors: neuropeptides expand the coding potential of the nervous system. Worm, 3 and is included with permission from all authors. The dissertation author was the primary author of this paper.

Additionally, we acknowledge the members of the Chalasani laboratory for advice and insights. This work was funded by grants from The Searle Scholars Program, March of Dimes, Whitehall and Rita Allen Foundations, and the NIH R01MH096881-01A1 (S.H.C). S.G.L. was funded by a graduate research fellowship from the NSF.

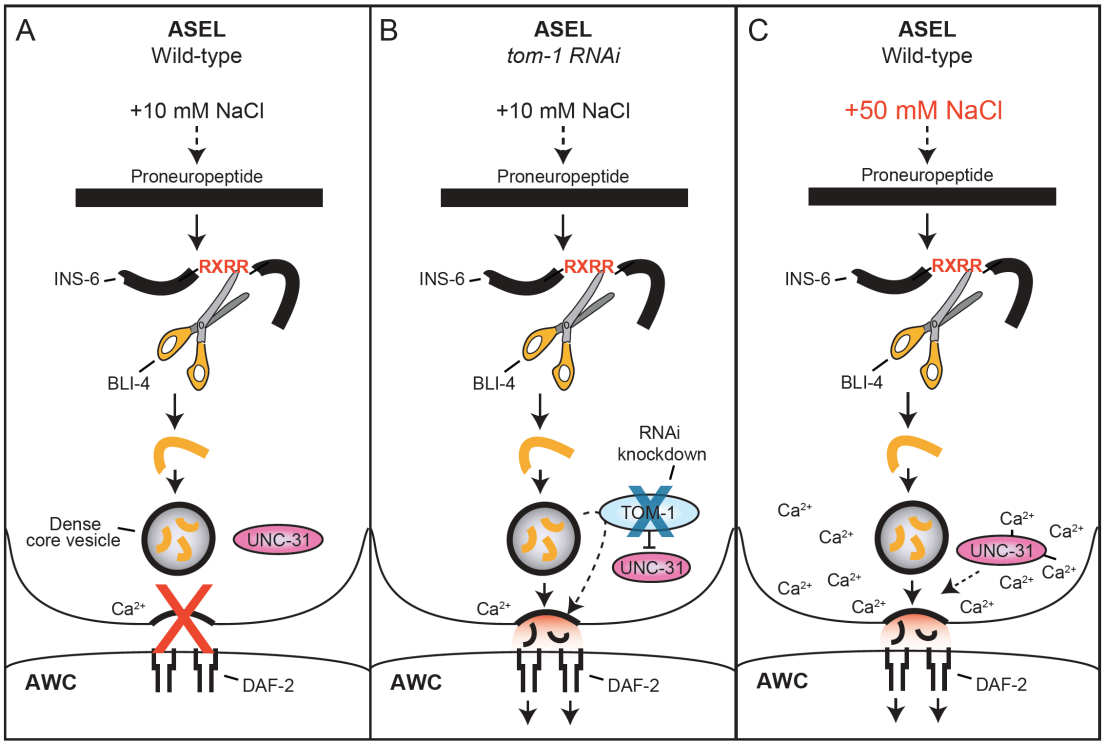

Figure 3.1: Genes: insulin neuropeptide processing and release machinery. (a-c) Proneuropeptides are processed to generate mature neuropeptides. The proprotein convertase BLI-4 recognizes and cleaves the pro-insulin-like peptide INS-6 at an RXRR motif to generate mature INS-6, in the ASEL sensory neuron (Leinwand and Chalasani, 2013). (a) Low +10 mM NaCl stimulation is insufficient to release INS-6 containing dense core vesicles in wild-type animals (Leinwand and Chalasani, 2013). (b) In ASEL neuron-specific *tom-1* RNAi transgenic animals, an inhibitor of dense core vesicle release is removed. +10 mM NaCl stimulation in these transgenics results in the release of INS-6 containing dense core vesicles from the readily releasable pool, even in the absence of a large increase in calcium. INS-6 signals through the DAF-2 insulin receptor on AWC neurons (Leinwand and Chalasani, 2013). (c) In wild-type animals, high +50 mM NaCl stimulation causes a large increase in calcium levels, which leads to UNC-31-dependent release of INS-6 containing dense core vesicles (Leinwand and Chalasani, 2013).

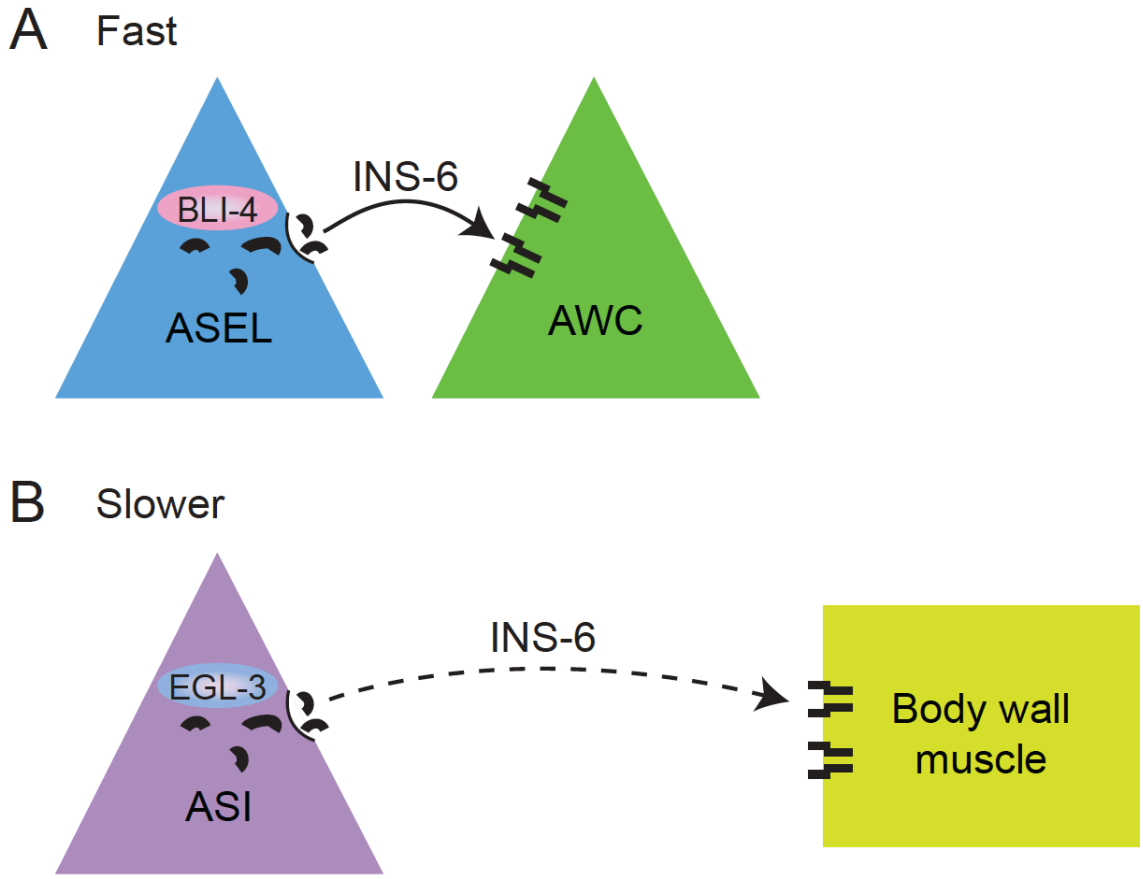

Figure 3.2: Circuits: neuropeptide processing, release and downstream signaling may influence the bioactivity of insulin peptides in neural circuits. (a) INS-6 peptides are processed by the proprotein convertase BLI-4 in ASEL sensory neurons (Leinwand and Chalasani, 2013). INS-6 released from ASEL acts as a fast neurotransmitter, signaling to nearby AWC neurons in less than a second (Leinwand and Chalasani, 2013). (b) INS-6 peptides are processed by the proprotein convertase EGL-3 in ASI sensory neurons (Hung et al., 2013). Insulins from ASI function as slow, long-range signals to distant body wall muscles (Hung et al., 2013).

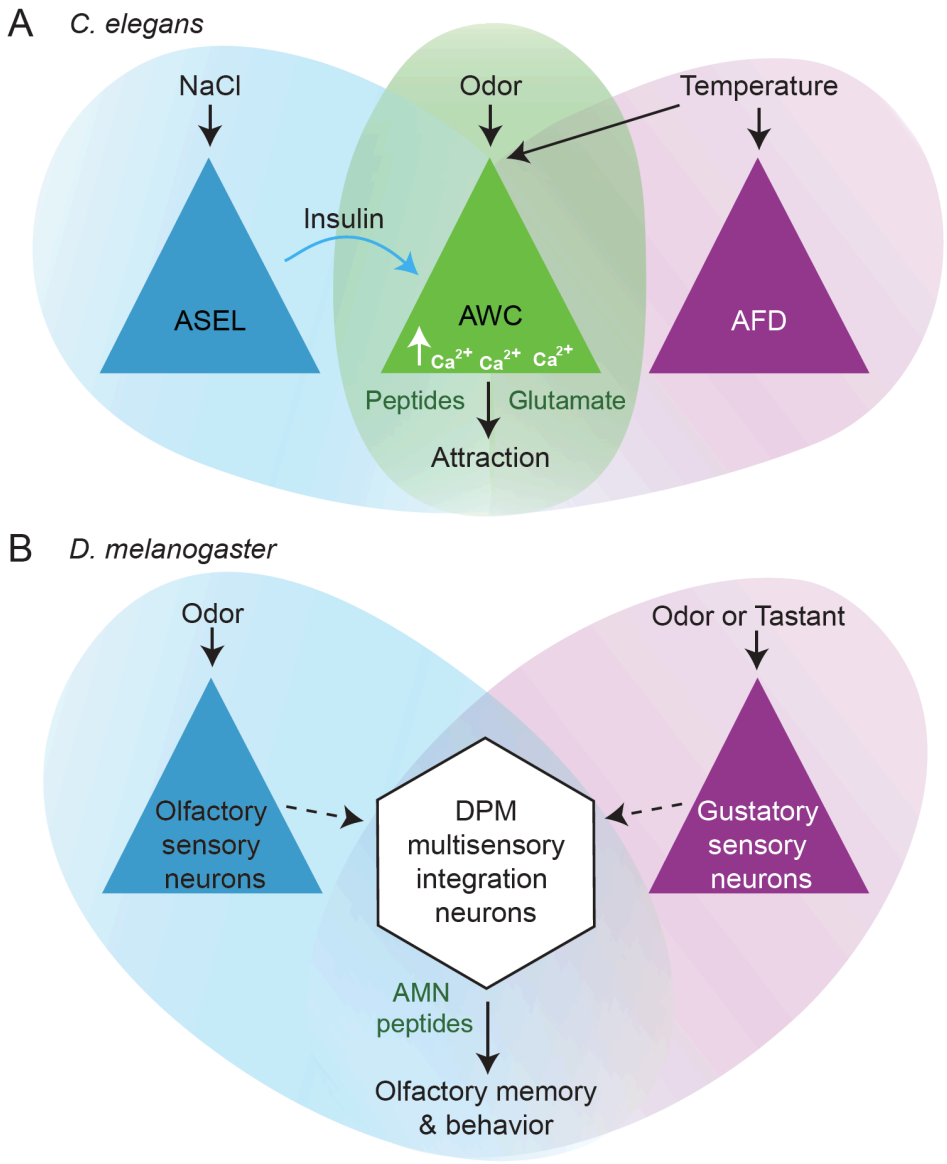

Figure 3.3: Behaviors: multisensory neurons integrate environmental cues to drive appropriate behaviors. (a) *C. elegans* AWC neurons are multisensory. AWC neurons sense and integrate information about odor together with salt information sent by the ASEL salt sensory neurons and temperature information that is also detected by the AFD thermosensory neurons (Bargmann, 2012; Biron et al., 2008; Leinwand and Chalasani, 2013). AWC neurons then release neuropeptides and/or glutamate to downstream circuitry to drive behavioral attraction towards multiple sensory modalities (Chalasani et al., 2010; Leinwand and Chalasani, 2013; Ohnishi et al., 2011). (b) *D. melanogaster* olfactory and gustatory sensory neurons detect odorants and tastants in the environment and relay the sensory information to the dorsal paired medial (DPM) neurons, which function as multisensory integrators (Keene et al., 2004). DPM neurons release AMN peptides to shape olfactory memory and behavior (Keene et al., 2004).

References

Bargmann, C.I. (2012). Beyond the connectome: how neuromodulators shape neural circuits. Bioessays 34, 458-465.

Bargmann, C.I., Hartwieg, E., and Horvitz, H.R. (1993). Odorant-selective genes and neurons mediate olfaction in C. elegans. Cell 74, 515-527.

Biron, D., Wasserman, S., Thomas, J.H., Samuel, A.D., and Sengupta, P. (2008). An olfactory neuron responds stochastically to temperature and modulates Caenorhabditis elegans thermotactic behavior. Proc Natl Acad Sci U S A 105, 11002-11007.

Chalasani, S.H., Kato, S., Albrecht, D.R., Nakagawa, T., Abbott, L.F., and Bargmann, C.I. (2010). Neuropeptide feedback modifies odor-evoked dynamics in Caenorhabditis elegans olfactory neurons. Nat Neurosci 13, 615-621.

Chen, Z., Hendricks, M., Cornils, A., Maier, W., Alcedo, J., and Zhang, Y. (2013). Two insulin-like peptides antagonistically regulate aversive olfactory learning in C. elegans. Neuron 77, 572-585.

Dalton, P., Doolittle, N., Nagata, H., and Breslin, P.A. (2000). The merging of the senses: integration of subthreshold taste and smell. Nat Neurosci 3, 431-432.

Dolen, G., Darvishzadeh, A., Huang, K.W., and Malenka, R.C. (2013). Social reward requires coordinated activity of nucleus accumbens oxytocin and serotonin. Nature 501, 179-184.

Ghazanfar, A., and Schroeder, C. (2006). Is neocortex essentially multisensory? Trends in cognitive sciences 10, 278-285.

Gracheva, E.O., Burdina, A.O., Touroutine, D., Berthelot-Grosjean, M., Parekh, H., and Richmond, J.E. (2007). Tomosyn negatively regulates CAPS-dependent peptide release at Caenorhabditis elegans synapses. J Neurosci 27, 10176-10184.

Hammarlund, M., Watanabe, S., Schuske, K., and Jorgensen, E.M. (2008). CAPS and syntaxin dock dense core vesicles to the plasma membrane in neurons. J Cell Biol 180, 483-491.

Harris, G., Mills, H., Wragg, R., Hapiak, V., Castelletto, M., Korchnak, A., and Komuniecki, R.W. (2010). The monoaminergic modulation of sensory-mediated aversive responses in Caenorhabditis elegans requires glutamatergic/peptidergic cotransmission. J Neurosci 30, 7889-7899.

Hung, W.L., Hwang, C., Gao, S., Liao, E.H., Chitturi, J., Wang, Y., Li, H., Stigloher, C., Bessereau, J.L., and Zhen, M. (2013). Attenuation of insulin signalling contributes to FSN-1-mediated regulation of synapse development. Embo J 32, 1745-1760.

Husson, S.J., Clynen, E., Baggerman, G., Janssen, T., and Schoofs, L. (2006). Defective processing of neuropeptide precursors in Caenorhabditis elegans lacking proprotein convertase 2 (KPC-2/EGL-3): mutant analysis by mass spectrometry. J Neurochem 98, 1999-2012.

Keene, A.C., Stratmann, M., Keller, A., Perrat, P.N., Vosshall, L.B., and Waddell, S. (2004). Diverse odor-conditioned memories require uniquely timed dorsal paired medial neuron output. Neuron 44, 521-533.

Kuhara, A., Okumura, M., Kimata, T., Tanizawa, Y., Takano, R., Kimura, K.D., Inada, H., Matsumoto, K., and Mori, I. (2008). Temperature sensing by an olfactory neuron in a circuit controlling behavior of C. elegans. Science 320, 803-807.

Leinwand, S.G., and Chalasani, S.H. (2013). Neuropeptide signaling remodels chemosensory circuit composition in Caenorhabditis elegans. Nat Neurosci 16, 1461-1467.

Li, C., and Kim, K. (2008). Neuropeptides. WormBook, 1-36.

Marks, D.R., Tucker, K., Cavallin, M.A., Mast, T.G., and Fadool, D.A. (2009). Awake intranasal insulin delivery modifies protein complexes and alters memory, anxiety, and olfactory behaviors. J Neurosci 29, 6734-6751.

Nassel, D.R. (2009). Neuropeptide signaling near and far: how localized and timed is the action of neuropeptides in brain circuits? Invert Neurosci 9, 57-75.

Ohnishi, N., Kuhara, A., Nakamura, F., Okochi, Y., and Mori, I. (2011). Bidirectional regulation of thermotaxis by glutamate transmissions in Caenorhabditis elegans. Embo J 30, 1376-1388.

Pierce, S.B., Costa, M., Wisotzkey, R., Devadhar, S., Homburger, S.A., Buchman, A.R., Ferguson, K.C., Heller, J., Platt, D.M., Pasquinelli, A.A.*, et al.* (2001). Regulation of DAF-2 receptor signaling by human insulin and ins-1, a member of the unusually large and diverse C. elegans insulin gene family. Genes Dev 15, 672-686.

Qiu, Q., Basak, A., Mbikay, M., Tsang, B.K., and Gruslin, A. (2005). Role of pro-IGF-II processing by proprotein convertase 4 in human placental development. Proc Natl Acad Sci U S A 102, 11047-11052.

Root, C.M., Ko, K.I., Jafari, A., and Wang, J.W. (2011). Presynaptic facilitation by neuropeptide signaling mediates odor-driven food search. Cell 145, 133-144.

Salio, C., Lossi, L., Ferrini, F., and Merighi, A. (2006). Neuropeptides as synaptic transmitters. Cell Tissue Res 326, 583-598.

Savigner, A., Duchamp-Viret, P., Grosmaitre, X., Chaput, M., Garcia, S., Ma, M., and Palouzier-Paulignan, B. (2009). Modulation of spontaneous and odorant-evoked activity

of rat olfactory sensory neurons by two anorectic peptides, insulin and leptin. J Neurophysiol 101, 2898-2906.

Speese, S., Petrie, M., Schuske, K., Ailion, M., Ann, K., Iwasaki, K., Jorgensen, E.M., and Martin, T.F. (2007). UNC-31 (CAPS) is required for dense-core vesicle but not synaptic vesicle exocytosis in Caenorhabditis elegans. J Neurosci 27, 6150-6162.

Steiner, D.F. (1998). The proprotein convertases. Curr Opin Chem Biol 2, 31-39.

Thacker, C., and Rose, A.M. (2000). A look at the Caenorhabditis elegans Kex2/Subtilisin-like proprotein convertase family. Bioessays 22, 545-553.

Tomioka, M., Adachi, T., Suzuki, H., Kunitomo, H., Schafer, W., and Iino, Y. (2006). The insulin/PI 3-kinase pathway regulates salt chemotaxis learning in Caenorhabditis elegans. Neuron 51, 613-625.

Turner, A.J., Isaac, R.E., and Coates, D. (2001). The neprilysin (NEP) family of zinc metalloendopeptidases: genomics and function. Bioessays 23, 261-269.

Verhage, M., McMahon, H.T., Ghijsen, W.E., Boomsma, F., Scholten, G., Wiegant, V.M., and Nicholls, D.G. (1991). Differential release of amino acids, neuropeptides, and catecholamines from isolated nerve terminals. Neuron 6, 517-524.

White, J.G., Southgate, E., Thomson, J.N., and Brenner, S. (1986). The structure of the nervous system of the nematode Caenorhabditis elegans. Philos Trans R Soc Lond B Biol Sci 314, 1-340.

White, J.Q., Nicholas, T.J., Gritton, J., Truong, L., Davidson, E.R., and Jorgensen, E.M. (2007). The sensory circuitry for sexual attraction in C. elegans males. Curr Biol 17, 1847-1857.

CHAPTER 4.

Neural mechanisms regulating aging-associated behavioral decline in *Caenorhabditis elegans*

Abstract

In humans and most animals, aging is associated with the deterioration of vital sensory abilities including olfaction. However, it is unclear how aging impairs the underlying neural circuits, leading to sensory behavioural declines. We identify an aging-associated decline in *C. elegans* behavior to the volatile chemoattractant benzaldehyde and map a novel underlying sensory circuit motif. Two primary sensory neuron pairs, AWC and AWA, directly detect benzaldehyde and release insulin peptides and acetylcholine to activate two secondary neuron pairs, ASE and AWB, and drive behavioral plasticity. Interestingly, odor-evoked activity in the secondary, but not primary, neurons degrades with age. Experimental manipulations to increase neurotransmitter release from primary neurons rescue these aging-associated neuronal deficits. Furthermore, the odor responsiveness of aged animals correlates with their lifespan. Together, these results show how odors are encoded by primary and secondary neurons and suggest reduced neurotransmission as a novel mechanism driving aging-associated sensory neural activity and behavioral declines.

Introduction

Aging animals endure a progressive decline in physiology, including systems-level deterioration in muscular (Walston, 2012), immune (Castelo-Branco and Soveral, 2014), and neuronal functions (Gutchess, 2014; Hummel et al., 2007). In the nervous system, these changes involve extensive interactions between genetic networks and signaling pathways (Yin et al., 2013). Therefore, successful modelling of neuronal aging requires an *in vivo* system that allows for extensive analysis of multiple genetic pathways and their functional outputs throughout the animal's lifespan. The nematode *C. elegans* is a genetically tractable, short lifespan model, which has been used extensively to identify conserved, organismal-level longevity pathways, such as insulin and mitochondrial signaling (Wolff and Dillin, 2006). Its well-studied nervous system with just 302 neurons (White et al., 1986b) has also been used to probe neuronal aging, identifying changes in associative memory at early stages of aging (Kauffman et al., 2010) and later changes in neuronal morphology (Toth et al., 2012) and motor neuron functions (Liu et al., 2013). However, little has been done to investigate functional changes in neuronal circuits during aging – an essential link between genes, individual cells and aging-associated behavioral decline.

The aging of sensory neural circuits is of particular interest because of the damaging effects on nutrition, quality of life and overall safety and survival across species (Doty and Kamath, 2014). In young adults, sensory circuits process environmental cues to drive robust appetitive and aversive behaviors, which are essential for finding food and avoiding toxins (Bargmann, 2006). In mice and flies, distinctive, sparse spatial patterns of neural activity form a population code for olfactory information

(Oka et al., 2006; Wang et al., 2003). In contrast, previous studies have shown that *C. elegans* uses single sensory neuron pairs to drive locomotion towards or away from particular odor stimuli (Bargmann, 2006). For example, single cell ablation experiments showed that the bilaterally asymmetric pair of AWC sensory neurons are necessary for attraction to benzaldehyde odor, while the AWA sensory neuron pairs are required for diacetyl odor attraction (Bargmann, 2006; Bargmann and Horvitz, 1991). The cell bodies of the AWC and AWA neurons along with those of ten other neuron pairs are located in the amphid ganglia (**Figure 4.1a**) (White et al., 1986a). All 24 of these neurons send their dendrites to the nose where they detect environmental changes and relay that information through their axons to the downstream circuitry (White et al., 1986b). We hypothesized that multiple amphid neurons could encode odor information and performed the first comprehensive analysis of odor-evoked neural activity in all amphid ganglia neurons. We identified a novel circuit motif consisting of primary and secondary olfactory neurons that encode odors and drive behavioral plasticity. Furthermore, we found that a selective vulnerability of neurotransmitter release pathways to the deleterious effects of aging underlies a specific decay of secondary olfactory neuron activity and aging-associated behavioral decline.

Results

A Distributed Olfactory Neural Circuit Drives Aging-regulated Olfactory Behavior

C. elegans sensory neurons detect and drive locomotion towards point sources of food odors (Bargmann, 2006). We used this chemotaxis behavior to probe the neural circuit mechanisms underlying aging-associated behavioral decline (**Figure 4.1b**). We

found that young adults were strongly attracted to benzaldehyde odor, while older animals (day 4-6) showed a significant impairment (**Figure 4.1c**). (For the remainder, we analyzed young (day 1) adults and animals at a post-reproductive, early stage of aging (day 5), which we refer to as "aged" adults). Importantly, this behavioral deficit is unlikely to be caused by changes in locomotory ability since the speed of chemotaxing aged animals did not differ from that of young adults (**Figure 4.1d**). Next, we used functional calcium imaging to characterize the sensory circuit that detects benzaldehyde and underlies this new model of aging-associated behavioral decline. Consistent with previous studies, we observed a large calcium transient indicating increased AWC activity upon removal of benzaldehyde (**Figure 4.1e,f**) (Chalasani et al., 2007). Unexpectedly, we found additional benzaldehyde responsive neurons: the diacetyl sensing AWA neurons (Bargmann et al., 1993) were activated by the addition of benzaldehyde, while ASE and AWB neurons [that were previously shown to sense salts (Bargmann and Horvitz, 1991) and volatile repellents (Bargmann, 2006; Troemel et al., 1997), respectively] also responded to the removal of this stimulus in young adults (**Figure 4.1e,f**). While the two AWC and ASE neurons can be genetically and functionally separated (Suzuki et al., 2008; Wes and Bargmann, 2001), each one in the pair showed similar responses to benzaldehyde stimuli; therefore, we chose to focus our subsequent analysis on the AWC^{ON} and ASEL (left) neurons (**Figures 4.1e** and **4.2b,c**). Moreover, none of the other amphid neurons responded to this benzaldehyde stimulus (**Figures 4.1a,e,f** and **4.2**). Our data suggests that four pairs of sensory neurons (AWC, AWA, ASE and AWB) signal the presence of benzaldehyde, with distributed patterns of activity in subsets of these neurons defining active neural circuits for different

concentrations of volatile attractants (**Figures 4.1f** and **4.2**). (Throughout, unless low or high benzaldehyde is specifically noted, a medium concentration of benzaldehyde was used.) Furthermore, by genetically ablating individual neurons (Beverly et al., 2011; Yoshida et al., 2012) and blocking synaptic transmission [with tetanus toxin (Schiavo et al., 1992)], we found that signaling from all four of these benzaldehyde-responsive sensory neurons is required for normal chemotaxis in young adults (**Figure 4.1g**). Together, these results show that the specialized responses of narrowly tuned single neurons are insufficient to encode odor; rather, a population code of activity across several neurons is essential to drive olfactory behaviors, much like in other species (Oka et al., 2006; Wang et al., 2003).

Primary and Secondary Olfactory Neurons Encode Benzaldehyde Odor

Previously, we defined two classes of sensory neurons: primary neurons, which directly detect stimuli and secondary neurons, which respond to neurotransmission from primary neurons (Leinwand and Chalasani, 2013). To classify the benzaldehyde-responsive neurons, we examined genetic mutants that primarily block the release of small, clear synaptic vesicles [Munc13 or *unc-13* in *C. elegans* (Richmond et al., 1999)] or neuropeptide-containing dense core vesicles [CAPS, calcium-dependent activator protein for secretion, or *unc-31* in *C. elegans* (Speese et al., 2007)]. We found that AWA and AWC neurons retained their odor responsiveness in the absence of neurotransmission, suggesting that these neurons directly detect benzaldehyde and are primary olfactory sensory neurons (**Figures 4.3a,b** and **4.4a**). In contrast, odor-evoked ASE activity required neuropeptide signaling (**Figures 4.3c** and **4.4b,c**). Restoring

neuropeptide release function specifically to AWC neurons rescued ASEL activity in *unc-31* mutants, suggesting that AWC neurons release peptides to activate ASEL neurons (**Figure 4.3c**). Furthermore, AWB responses were blocked in *unc-13* mutants, suggesting that these neurons are recruited to this olfactory circuit by classical neurotransmitter(s) (**Figure 4.3d** and **4.4d**). Blocking synaptic transmission [with tetanus toxin (Schiavo et al., 1992)] and our laser neuron ablations (Bargmann and Avery, 1995) suggest that the AWA primary olfactory neurons signal to AWB neurons (**Figures 4.3d** and **4.4e**). Collectively, these data show a novel sensory circuit configuration in which the four neurons are not equal: the olfactory circuit for benzaldehyde odor is composed of two pairs of primary sensory neurons (AWC and AWA) that release neuropeptides and classical neurotransmitters to activate two pairs of secondary neurons (ASE and AWB), respectively.

Insulin Peptidergic and Cholinergic Transmission from Primary Olfactory Sensory Neurons Activates Secondary Olfactory Neurons

We then mapped the neuropeptide and neurotransmitter pathways transferring information from primary to secondary neurons. The *C. elegans* genome includes at least 122 neuropeptide genes and pathways to generate several classical neurotransmitters including glutamate, GABA and acetylcholine (Hobert, 2013). To identify the cognate neuropeptide(s) activating ASE neurons, we used ASE activity as readout to screen a number of neuropeptide gene mutants. We found that the insulin-like peptide *ins-1* (Pierce et al., 2001) was required for benzaldehyde-evoked ASEL responses (**Figure 4.5a**). Moreover, restoring INS-1 function specifically to AWC neurons rescued mutant

ASEL activity deficits, suggesting that AWC neurons release INS-1 peptides to activate ASEL neurons in the circuit (**Figure 4.5a**). We then investigated the receptor and downstream signaling components in ASEL neurons that transduce the AWC-released INS-1 signal. We found that odor-evoked ASEL activity required the canonical insulin receptor [*daf-2* in *C. elegans* (Pierce et al., 2001)] and PI3-Kinase [*age-1* in *C. elegans* (Morris et al., 1996)] signaling in ASEL neurons (**Figure 4.5b,c**). Furthermore, we found that the insulin receptor mutant (*daf-2*) had a stronger reduction in ASEL activity compared to the response in the insulin ligand mutant (*ins-1*) (**Figure 4.5a,b**). These results suggest that AWC neurons may co-release additional insulin peptide(s) along with INS-1 to bind the insulin receptor on ASEL neurons. Together, these results indicate that AWC-released insulin peptides signal via the insulin receptor and PI3-Kinase to rapidly activate ASE secondary neurons (within 5 seconds) and encode benzaldehyde stimulus.

We also mapped the classical neurotransmitter pathway recruiting AWB neurons into the circuit. We found that mutations in the vesicular acetylcholine transporter, *unc-17*, which packs acetylcholine into synaptic vesicles (Alfonso et al., 1994), reduced AWB odor responses (**Figure 4.5d**). Restoring cholinergic function specifically in AWA primary neurons was sufficient to activate the AWB secondary neurons (**Figure 4.5d**). This AWA-released acetylcholine likely binds to one or more of the nearly 70 *C. elegans* cholinergic receptors (Hobert, 2013). Importantly, we also confirmed that AWC and AWA primary olfactory neuron dynamics were normal in all genetic mutants analyzed (**Figure 4.6**). These experiments support the conclusion that changes in mutant secondary neuron activity are downstream of sensory transduction in the primary neurons and related to transmitter release from primary neurons. Together, these data show that

benzaldehyde stimulus is encoded by two primary sensory neurons, which use insulin peptidergic and cholinergic neurotransmission to activate two secondary neurons (**Figure 4.5e**). Thus, multiple neuropeptide and neurotransmitter pathways are integrated to shape odor encoding and behavior.

Attractive Odor-evoked Activity of Secondary Neurons Specifically Decays with Aging

We hypothesized that changes in neuronal activity in this circuit underlie the aging-associated decline in benzaldehyde attraction (**Figure 4.1c**). To test this, we analyzed the responses of the primary (AWA and AWC) and secondary (ASE and AWB) neurons to benzaldehyde in both young (day 1) and aged (day 5) animals. Overall, aging did not affect the reliability, duration or magnitude of odor-evoked activity in AWC^{ON} and AWA primary neurons (**Figures 4.7a,b,e** and **4.8a**). In contrast, odor-evoked ASEL and AWB secondary neuron activity was highly variable with aging, with many neurons failing to show any responses to odor, revealing a possible mechanism for behavioral decline (**Figures 4.7c-e**). Interestingly, the calcium transients of odor-responsive aged ASEL and AWB neurons were indistinguishable from responses in younger animals (**Figures 4.7c,d**). These results suggest that ASEL and AWB neurons follow an "all-or-none" rule in their benzaldehyde responses. Consistent with these results, we found that the weak chemotaxis performance of aged animals towards benzaldehyde only required the primary AWC and AWA neurons, and not the unreliable secondary ASE and AWB neurons (**Figure 4.7f**). Conversely, we found that strong stimulation with a higher benzaldehyde concentration, which is similarly repulsive in young and aged animals and

encoded by a distinct but overlapping subset of neurons, could overcome the aging associated activity declines, suggesting that the effects of aging are dose-dependent (**Figures 4.2b** and **4.8b-e**).

To test whether aging-associated decline was specific to benzaldehyde, we also analyzed responses to a different volatile attractant, isoamyl alcohol. We observed a similar aging-associated decline in neuronal activity and behavior to isoamyl alcohol (**Figure 4.9a-e**). These results suggest that declines in neuronal activity might be generally associated with appetitive behavioral deficits in older animals. To further examine this, we tested whether performance in the chemotaxis assay is correlated with the odor responsiveness of the ASE and AWB secondary neurons (**Figure 4.10a**). We found that aged animals that failed to chemotax towards benzaldehyde were significantly more likely to have odor non-responsive ASE and AWB neurons than aged animals that successfully found the odor source (**Figure 4.10b-d**). Taken together, these data reveal a distributed neural circuit that detects attractive odors and suggest that benzaldehyde behavioral declines arise from unreliable activity of aged secondary ASE and AWB neurons in this circuit.

Next, we investigated whether aging impairs all or only selective functions of ASE and AWB neurons. To test this, we analyzed responses to salt (sodium chloride) and a repulsive odorant (2-nonanone), which are directly transduced by ASE (Bargmann, 2006; Suzuki et al., 2008) and AWB neurons (Troemel et al., 1997), respectively. We found that neuronal activity and behavior in response to these stimuli remained reliable and robust in aged animals (**Figures 4.7g,h** and **4.11a-d**). These data indicate that functionality of both ASE and AWB neurons in aged animals is sensory context

dependent. Specifically, their primary responses to salt (ASE) and 2-nonanone (AWB) are preserved, while their function as secondary neurons in encoding attractive benzaldehyde stimuli is impaired during aging.

Increased Primary Neuron Release Rescues Aging-associated Secondary Neuronal Activity and Behavioral Decay

Collectively, our results show that the secondary olfactory neurons (ASE and AWB) have inconsistent attractive odor-evoked activity in aged animals. Therefore, a breakdown in the peptidergic and cholinergic neurotransmission that recruits these secondary neurons could underlie the aging-associated deficits in activity and behavior. In order to identify the mechanisms for aging-induced neural declines, we manipulated the primary to secondary neurotransmission pathway in four different ways. (1) First, we hypothesized that aging down-regulates the levels of postsynaptic receptors. This would reduce signaling in aged ASE neurons. We tested this hypothesis by overexpressing the DAF-2 insulin receptor (Pierce et al., 2001) specifically in ASE neurons (**Figure 4.12a**, left panel). We found no change in the reliability of these animals' odor-evoked ASE activity (**Figures 4.12b** and **4.13b**). This suggests that receptor expression is not limiting in these aged animals.

Next, we considered three mechanisms that could reduce the transmitter release from primary neurons and leading to unreliable secondary neurons in aged animals. (2) The primary sensory neurons may synthesize less neuropeptide or neurotransmitter as the animal ages, causing a breakdown in signaling to recruit secondary neurons. To test this, we over-expressed the neuropeptide INS-1 (Pierce et al., 2001) in the primary AWC

neurons (**Figure 4.12a**, middle panel). This manipulation succeeded in improving the reliability of odor-evoked activity in aged ASEL neurons, suggesting that increased neuropeptide production, and consequently release, can rescue aging-associated deficits (**Figure 4.12b** and **4.13a,b,g**). (3) We hypothesized that insufficient neurotransmitters are packed into vesicles in aged animals. To test this hypothesis, we over-expressed the vesicular acetylcholine transporter, UNC-17, specifically in AWA neurons; a manipulation that was previously shown to increase the quantity of acetylcholine packed into and released from synaptic vesicles (**Figure 4.12a**, right panel) (Song et al., 1997). This manipulation also significantly increased the reliability of aged AWB odor responses (**Figure 4.12c** and **4.13c,d**) and significantly improved chemotaxis in aged animals (**Figure 4.12d**), further supporting the idea that increased neurotransmitter release rescues aged neuronal functions. (4) Finally, aged animals might have vesicle priming, docking or fusion defects, which reduce the number of vesicles exocytosed, leading to unreliable secondary neurons. We generated an AWC-specific knockdown of a syntaxin-interacting protein that normally acts as a brake on all neurotransmission [Tomosyn or *tom-1* in *C. elegans* (Gracheva et al., 2007; Leinwand and Chalasani, 2013)] to increase neuropeptide and neurotransmitter release from AWC neurons (**Figure 4.12a**, middle panel). This increased release from AWC neurons generated more reliable ASEL odor activity and improved chemotaxis in aged animals (**Figures 4.12b,d** and **4.13a,b**). Additionally, to increase acetylcholine release, we used a pharmacological agent, arecoline, which is a cholinergic agonist known to act presynaptically to stimulate synaptic vesicle fusion (Liu et al., 2013) (**Figure 4.12a**, right panel). Acute arecoline treatment in aged animals significantly increased the probability of AWB odor responses

(**Figure 4.12c** and **4.13c,d**). Importantly, none of these manipulations had significant effects on young (day 1) animals' ASEL and AWB neuronal activity (**Figure 4.13a-g**). Thus, the results from all of our manipulations converge to show that increasing neurotransmitter release from primary olfactory neurons improves neuronal functions in aged animals. This identifies neurotransmission as particularly sensitive to aging's damaging effects. In particular, we suggest that neurotransmitter production, packing or release decays with age and restoring these functions, even acutely, can alleviate aging-induced deficits.

Olfactory Behavior of Aged Animals is Correlated with Lifespan

Finally, we investigated the consequences of individual variation in aged olfactory abilities at the whole animal level by testing whether the olfactory abilities we analyzed could be correlated with longevity. We performed chemotaxis assays and separated the animals into two populations that did or did not navigate up an attractive benzaldehyde gradient (**Figure 4.12e**). We then assayed the lifespan of these two populations of animals. Notably, we observed a significant extension (average of 16.2% in three separate trials, $p<0.001$, Mantel-Cox test) in the lifespan of animals that successfully chemotaxed to the odor as aged adults, compared to animals that failed to do so (**Figure 4.12f** and **Table 4.1**). However, we found no difference in the lifespan of animals that were sorted on the basis of their chemotaxis performance as young adults (**Figure 4.12g** and **Table 4.1**). These results suggest that the olfactory prowess of aged animals is indicative of whole animal physiology and health. These data also provide further support for a conserved principle wherein inter-individual variation in aged

animal phenotypes contributes to heterogeneous lifespans (Pincus and Slack, 2010; Vijg, 2014).

Discussion

Our results define a new neural circuit mechanism for encoding sensory information to drive behavior and demonstrate age-related functional declines in this circuit. These data provide the first indication that *C. elegans* employ a similar olfactory population coding strategy as in flies and mice, suggesting that this is essential for behavioral plasticity (Oka et al., 2006; Wang et al., 2003). Moreover, we suggest that primary olfactory neurons directly detect odors and use neurotransmission to recruit additional secondary neurons. However, activity in the secondary neurons declines with aging, leading to behavioral deficits.

We propose that the combination of primary and secondary neurons may be a common motif in sensory neural circuits. We have previously shown that the *C. elegans* salt neural circuit is composed of a primary salt sensory neuron, which releases different insulin neuropeptides to recruit a secondary sensory neuron into the circuit in particular sensory contexts (Leinwand and Chalasani, 2013). This combined primary and secondary neuron population coding strategy is likely to increase the signal-to-noise ratios, thus preventing failures to encode sensory information. This may enhance the ability of young adults to successfully find food, perhaps to enhance reproductive success, while the aging-associated declines occur in post-reproductive animals that may have reduced nutritional demands. Furthermore, the insulin peptidergic and cholinergic signaling from primary to secondary olfactory neurons could add salience to volatile food signals in a

complex, multisensory environment. Previous studies have also shown that insulin (Lacroix et al., 2008) and cholinergic receptors (Ogura et al., 2011) are expressed in mammalian olfactory processing centers. Collectively, these results suggest a conserved role for these signaling pathways in encoding odors. Detailed analyses of the architecture of sensory circuits, including the neurotransmission between sensory neurons, in other species are needed to determine whether the circuit motif described here is broadly conserved.

We find that the activity of neurons functioning as secondary, but not primary, neurons decays with age. These results suggest that sensory context rather than neuronal identity is a key determinant of the reliability of sensory-evoked activity in aged animals. Specifically, we speculate that the early aging-associated impairments are driven by reduced neurotransmitter release from primary neurons, a mechanism likely applicable across species. These results are consistent with reports of reduced synapse number in the aged mammalian olfactory bulb, which should disrupt olfactory circuits (Richard et al., 2010). We speculate that these differences in synaptic transmission explain some of the inter-individual variability in aging phenotypes (Pinto et al., 2014; Vijg, 2014). Subsequently, these circuit-level changes could produce hyposmia or anosmia, which may be among the earliest predictors of lifespan and mortality across species (Liu et al., 2013; Pinto et al., 2014; Toth et al., 2012). More generally, we suggest that alterations in transmitter release, which disrupt neuronal communication throughout the brain (Dickstein et al., 2007) are likely to underlie age-related cognitive and behavioral decline.

Methods

C. elegans strains were grown and maintained under standard conditions (Brenner, 1974). A complete listing of all strains used in this study and their genotypes is located in Table 4.2.

Molecular biology and transgenesis

cDNA corresponding to the entire coding sequences of *unc-31, daf-2*, *age-1 and tom-1* and the *ins-1* genomic region were amplified by PCR and expressed under cell-selective promoters. *unc-17* cDNA was synthesized (GenScript) and expressed under a cell-selective promoter. Neuron-selective RNAi transgenes were created as previously described by co-injection of equal concentrations of sense and antisense oriented gene fragments driven by cell-specific promoters (Esposito et al., 2007). Cell-specific expression was achieved using the following promoters: *ceh-36deletion* or *odr-3* for both AWC, *str-2* for AWC^{ON}, *srsx-3* for AWC^{OFF}, *gpa-4* for AWA and ASI, *gpa-4deletion* for AWA, *gcy-7* for ASEL, *gcy-5* for ASER, *str-1* for AWB, *sre-1* for ADL, *srh-142* for ADF, *gcy-8* for AFD, *ops-1* for ASG, *sra-6* for ASH, *trx-1* for ASJ and *sra-9* for ASK. For all experiments, a splice leader (SL2) fused to a *mCherry* or *gfp* transgene was used to confirm cell-specific expression of the gene of interest.

Germline transformations were performed by microinjection of plasmids (Mello and Fire, 1995) at concentrations between 25 and 200 ng/µl with 10 ng/µl of *unc-122::rfp*, *unc-122::gfp* or *elt-2::gfp* as co-injection markers. For rescue and overexpression experiments, DNA was injected into mutant or wild-type *C. elegans* carrying GCaMP arrays.

Calcium imaging

Transgenic worms expressing GCaMP calcium indicators under a cell-selective promoter were trapped in a custom designed PDMS microfluidic device and exposed to odor stimuli (Chalasani et al., 2007; Chronis et al., 2007). For aging experiments, a new PDMS device with larger channels was designed to trap and stimulate day 5 adult worms (Chokshi et al., 2010). Older, day 6 adult worms exhibit much larger variation in whole animal size than day 5 adults and could not be trapped consistently without introducing bias into the experiment. Fluorescence from the neuronal cell body was captured using a Zeiss inverted compound microscope for 3 minutes. We first captured 10s of baseline activity in chemotaxis assay buffer (5mM K_3PO_4 (pH 6), 1mM $CaCl_2$, 1mM $MgSO_4$, and 50mM NaCl), then 2 minutes of exposure to an odor (or salt) dissolved in chemotaxis buffer stimulus, and lastly 50s of buffer only. Benzaldehyde refers to a 1:20,000 dilution in chemotaxis assay buffer, except where low benzaldehyde (1:1,000,000) or high benzaldehyde (1:1000) is specifically mentioned. Additionally, a 1:10,000 dilution of isoamyl alcohol, 1:1000 dilution of 2-nonanone and 50mM sodium chloride were used as indicated. For arecoline experiments, worms were pre-treated with 0.15mM arecoline in chemotaxis buffer for approximately 20 minutes and immediately imaged in the presence of the drug. Laser ablations of the paired AWC, AWA, ASE or ASH sensory neurons, along with control mock ablations, were performed as previously described (Bargmann and Avery, 1995) in transgenic animals expressing GCaMP in the AWB neurons. A single neuron was imaged in each animal, and each animal was imaged only once.

We used Metamorph and an EMCCD camera (Photometrics) to capture images at a rate of 10 frames per second. The average fluorescence in a 8s window (t=1-9s) was set

as F_0. A Matlab script was used to analyze the average fluorescence for the cell body region of interest and to plot the percent change in fluorescence for the region of interest relative to F_0, as previously described (Chalasani et al., 2007). For all figures, average and standard error at each time point were generated and plotted in Matlab. For statistical analysis, the average fluorescence and standard error were calculated for each animal over a short period corresponding to the duration of a response. Specifically, to analyze on responses to the addition of stimulus, the average fluorescence and standard error were calculated in the 10s period following the addition of odor (or salt) (t=10-20s). For AWA neurons, the response duration was very brief; therefore, a 4s time period was used instead (t=10-14s) so that small, fast responses could be appropriately quantified. To analyze off responses to the removal of stimulus, F_0 was set to the time just prior to odor removal (t=121-129s) and then the average fluorescence and standard error were calculated in the period following the removal of odor (t=130-140s for all cells except ASE, and t=130-145 for the slower, longer duration ASE responses). To determine whether there was an odor-evoked increase or suppression of the calcium signal (see **Figure 4.1f**), the average fluorescence in these time windows in buffer only trials was compared (by a two-tailed unpaired t-test) to the average fluorescence in odor stimulation trials, for each neuron. Two-tailed unpaired *t*-tests were used to compare the responses of different genotypes, and the Bonferroni correction was used to adjust for multiple comparisons. For all aging experiments, the percent of odor responsive neurons was calculated by determining the proportion of cells displaying an average fluorescence (DF/F) greater than 10 percent. 10 percent DF/F was used as the cut-off for odor responsiveness because, for any sensory neuron imaged, buffer changes only elicited

such a response in fewer than 5% of trials, making it a conservative measure of odor responsiveness. For aging experiments, a two-tailed Chi-Square test was used to compare the percent of odor responsive neurons in different conditions. Wild-type controls, mutants, and transgenic or drug treated strains for each figure were imaged in alternation, in the same session.

Chemotaxis assays

Odor chemotaxis assays were performed as previously described (Ward, 1973). For aging assays, worms were synchronized by hatch offs in which 8 young adult worms were given 150 min to lay eggs on a large plate before being picked off. These eggs were grown at 20 degrees until the appropriate day of adulthood. Chemotaxis assays were performed on 2% agar plates (10cm diameter) containing 5mM potassium phosphate (pH 6), 1mM $CaCl_2$ and 1mM $MgSO_4$. Animals were washed once in M9 and three times in chemotaxis buffer (5mM K_3PO_4 (pH 6), 1mM $CaCl_2$ and 1mM $MgSO_4$). Odor concentration gradients were established by spotting diluted benzaldehyde or isoamyl alcohol (1:2000, in ethanol) near the edge of the plate, with a control 1µl of ethanol spotted at the opposite end of the plate. Where noted, 1µl of neat benzaldehyde was used for high concentration point source assays. For 2-nonanone experiments, a 1:2 dilution of 2-nonanone in ethanol was used. For salt chemotaxis experiments, salt gradients were established by placing a control or a high salt (500mM NaCl) agar plug on the assay plate and allowing 16-20 hours for the salt to diffuse and form a gradient (Leinwand and Chalasani, 2013). 1µl of sodium azide was added to the odor (or salt) and the control spots to anesthetize animals reaching the end points. Washed worms were placed on the

plate and allowed to move freely for one hour. The chemotaxis index was computed as the number of worms in the region near the odor (or salt) minus the worms in the region near the control divided by the total number of worms that moved beyond the origin. Nine or more assays were performed on at least three different days. Two-tailed unpaired *t*-tests were used to compare the responses of different genotypes or ages, and the Bonferroni correction was used to adjust for multiple comparisons.

Correlated chemotaxis and imaging experiments

Transgenic worms bearing GCaMP arrays, synchronized by a hatch off as described above, were grown until day 5 of adulthood at 20 degrees. Animals were tested in a (1:2000) benzaldehyde odor chemotaxis assay as above, with two modifications. First, no sodium azide was used to paralyze the animals. Second, animals were given only 30 min to move freely on the chemotaxis plate. The chemotaxis assay plate was then cut into three regions corresponding to the benzaldehyde odor side, the middle, and the ethanol control region immediately after 30 min and worms were washed off each section separately and allowed to recover on OP50 bacteria plates for at least 90 min. Worms from the odor and the control sections of the chemotaxis assay were imaged in alternation as described above.

Lifespan assays

Worms, synchronized by a hatch off as described above, were grown until day 1 or 5 of adulthood at 20 degrees. Animals were tested in a (1:2000) benzaldehyde odor chemotaxis assay as above, but without sodium azide and with only 30 min for the

animals to move freely on the chemotaxis plate. The chemotaxis assay plate was then cut into a benzaldehyde odor, middle, and ethanol control region and worms were washed off each section separately. 100 adults from the odor region or the control region were transferred onto 10 small OP50 plates (10 adults per plate) and grown at 20 degrees. Survival was analyzed every other day and worms were scored alive or dead based on their response to a gentle head touch (or lack thereof) as previously described (Kenyon et al., 1993). Worms were censored if they bagged, exploded or desiccated on the side of the plate. The chemotaxis assay followed by lifespan analysis was repeated three times per condition, on separate days. The percent change in mean survival was calculated as the mean survival of animals from the odor side minus the mean survival of animals from the control side divided by the mean odor side survival. Statistical analysis of lifespan was performed by the Mantel-Cox Log-Rank test, using GraphPad Prism and OASIS (Yang et al., 2011).

Speed analysis

Chemotaxis assays to benzaldehyde were set up as described above, but with modifications to enable automated analysis of animal speed. 200mM Cu(II)SO_4-soaked filter paper was placed on a standard chemotaxis assay plate to contain the worms in a reduced chemotaxis arena (1.25 by 1.25 inch square). 1μl of benzaldehyde (diluted 1:2000 in ethanol) and a control 1μl of ethanol were spotted at opposite corners of the square arena, without any paralytic. After washing, only 5 worms were placed on the chemotaxis plate; this number minimized collisions and enabled more accurate tracking. The movement of the animals was tracked over 60 min using a Pixelink camera and

speed was analyzed with custom Matlab code to track the centroid of the animal (Ramot et al., 2008). The results from eleven chemotaxis plates were averaged for each age. NS indicates $P > 0.05$, two-tailed t-test.

Aged worm measurements

Day 5 and day 6 adult worms from hatch offs performed on three separate days were immobilized with tetramisole and imaged on 2% agarose pads. Images were captured on a Zeiss Observer D1 microscope using a 10X objective with DIC. The perimeters of 55 worms were measured using MetaMorph software.

Acknowledgments

This chapter is a reprint of the material as it appears in Leinwand, S.G., Yang, C.J., Bazopoulou, D., Srinivasan, J., Chronis, N., and Chalasani, S.H. (2015). Neural mechanisms regulating aging-associated behavioral decline in *Caenorhabditis elegans* (in preparation) and is included with permission from all authors. The dissertation author was the primary author of this paper.

Additionally, the following centers and people deserve thanks for their contribution to this work: *Caenorhabditis* Genetics Center, the National Brain Research Project (Japan), C. Bargmann, P. Sengupta, Y. Iino, I. Maruyama, D. Kim, P. Sternberg and A. Zaslaver for worm strains. I also acknowledge M. Ailion for *unc-31* cDNA, P. Sengupta for neuron specific promoters and L. Stowers, C. Stevens, J. Wang, Y. Jin, M. Hansen, L. Hale, K. Quach and C. Yeh for helpful discussions and comments on the manuscript. And, I am grateful to A. Tong, Z. Liu and other members of the Chalasani

laboratory for their help and advice. Grants from the Rita Allen Foundation, the W.M. Keck Foundation, the NIH (R01MH096881-03) (S.H.C.) and a National Science Foundation Graduate Research Fellowship and Achievement Rewards for College Scientists Scholarship (S.G.L.) funded this work.

Figure 4.1: Population coding in a distributed olfactory circuit drives aging-regulated olfactory behavior. (a) Image of a young adult *C. elegans* and schematic depicting the twelve pairs of sensory neurons in the anterior amphid ganglia whose dendrites project to the nose of the animal to detect sensory stimuli. (b) Chemotaxis assay schematic depicting *C. elegans* attraction to the odor benzaldehyde (BZ). (c) Chemotaxis performance of wild-type worms from young adulthood (day 1) through early stage aging (day 6) towards a point source of benzaldehyde. (d) Speed of wild-type young (day 1) and aged (day 5) adult animals chemotaxing towards a point source of benzaldehyde odor. Numbers on bars indicate number of assay plates and error bars indicate s.e.m. NS, $p > 0.05$, two-tailed *t*-test. (e) Average GCaMP fluorescence change in young adult (day 1), wild-type sensory neurons in response to benzaldehyde stimulation. Shaded box indicates two minute benzaldehyde odor stimulation beginning at t=10s. The light color shading around curves indicates s.e.m. and numbers in parentheses indicate number of neurons imaged. (f) Summary chart of the calcium responses of all amphid sensory neurons to various concentrations of benzaldehyde odor. This chart shows the composition of the *C. elegans* olfactory neural circuit and depicts a sensory neuron population code for odor concentration. The calcium signal in particular neurons (as indicated) is suppressed by the addition of odor (see methods section). (g) Young adult (day 1) benzaldehyde chemotaxis performance of wild-type, AWC or AWB or ASH neuron-specific genetic ablation, AWA neuron-specific tetanus toxin expression worms or *che-1* mutants missing ASE neurons (Uchida et al., 2003). (c,g) Numbers on bars indicate number of assay plates and error bars indicate s.e.m. $*p < 0.05$, two-tailed *t*-test with Bonferroni correction, compared to young adults or wild-type. (c-e,g) A medium concentration of benzaldehyde odor is used for all behavior and imaging experiments, except as noted in Figure 4.1f.

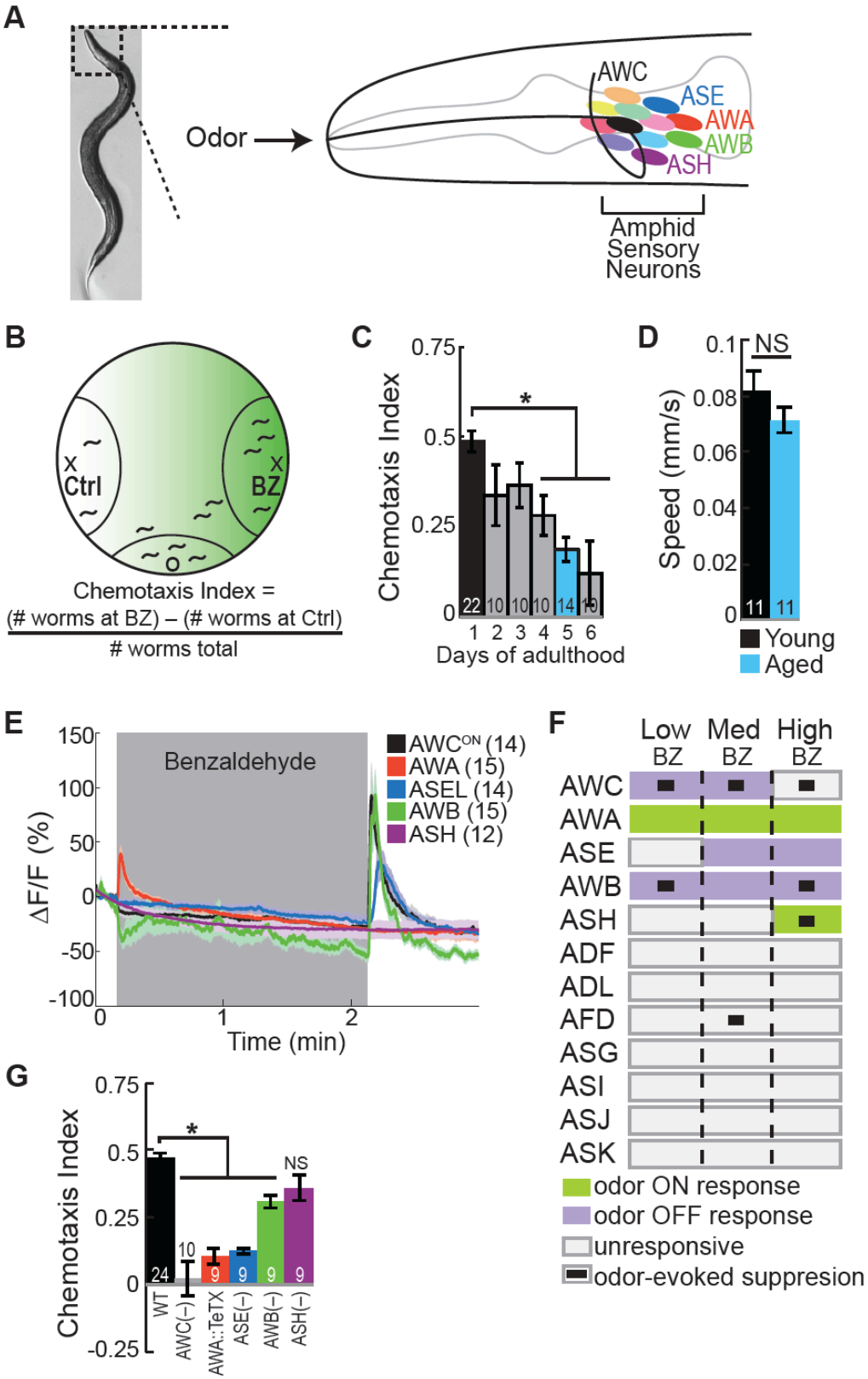
A
Odor
AWC
ASE
AWA
AWB
ASH
Amphid
Sensory
Neurons
B
Ctrl
BZ
Chemotaxis Index =
(# worms at BZ) – (# worms at Ctrl)
worms total
C
Chemotaxis Index
Days of adulthood
D
Speed (mm/s)
NS
Young
Aged
E
Benzaldehyde
AWC^ON (14)
AWA (15)
ASEL (14)
AWB (15)
ASH (12)
ΔF/F (%)
Time (min)
F
Low BZ
Med BZ
High BZ
AWC
AWA
ASE
AWB
ASH
ADF
ADL
AFD
ASG
ASI
ASJ
ASK
odor ON response
odor OFF response
unresponsive
odor-evoked suppresion
G
Chemotaxis Index
WT
AWC(–)
AWA::TeTX
ASE(–)
AWB(–)
ASH(–)
NS

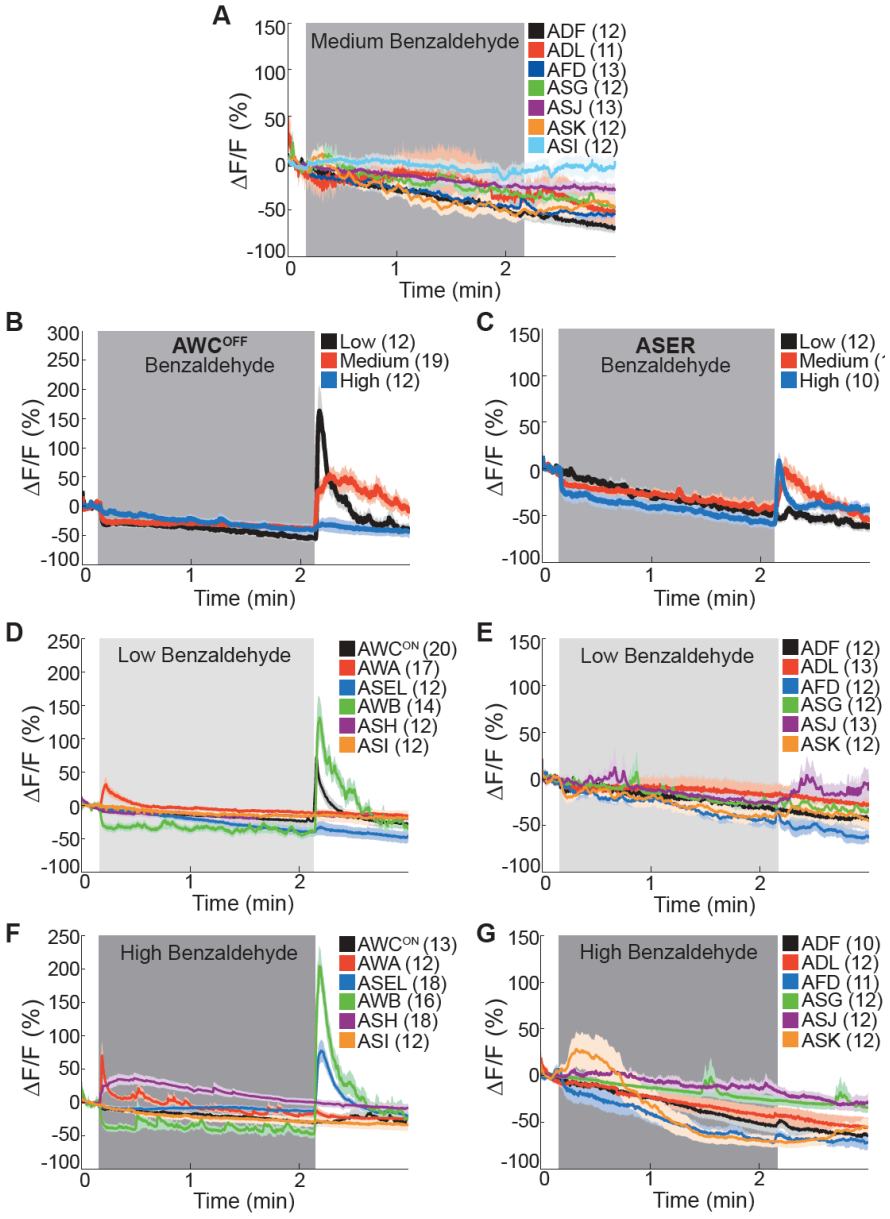

Figure 4.2: Olfactory population coding in young adult *C. elegans*. (a) Average calcium responses of young adult, wild-type amphid sensory neurons to medium benzaldehyde. (b,c) Average GCaMP fluorescence change in young adult, wild-type (b) AWC^{OFF} or (c) ASE right (ASER) sensory neurons in response to low, medium or high concentration benzaldehyde stimulus. (d-g) Average calcium responses of wild-type amphid sensory neurons to (d,e) low and (f,g) high concentration benzaldehyde stimulus. (a-g) Shaded box represents two minute benzaldehyde stimulation beginning at t=10s. Light shading around curves indicates s.e.m. and numbers in parentheses indicate number of neurons imaged.

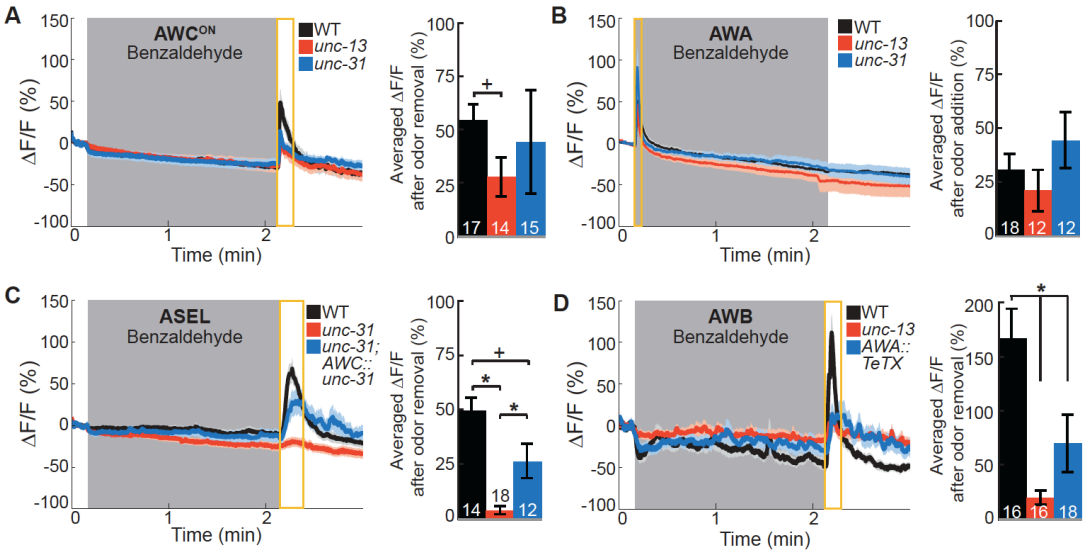

Figure 4.3: Primary and secondary olfactory neurons directly and indirectly detect benzaldehyde odor, respectively. (a,b) Average young adult (a) AWC^{ON} and (b) AWA neuron calcium responses to benzaldehyde in wild-type, *unc-13* mutants with impaired synaptic vesicle release, and *unc-31* mutants with impaired dense core vesicle release. (c) ASEL responses to benzaldehyde in *unc-31* mutants and *unc-31;* AWC-specific *unc-31* rescue. (d) AWB responses to benzaldehyde in *unc-13* mutants and animals with AWA-specific expression of tetanus toxin. (a-d) Shaded box indicates two-minute benzaldehyde odor stimulation. Yellow box indicates the time period after stimulus change for which the fluorescence change was averaged in the bar graphs. The light color shading around curves and bar graph error bars indicate s.e.m. Numbers on bars indicate number of neurons imaged. *$p < 0.05$ or +$p < 0.1$, two-tailed *t*-test with Bonferroni correction, compared to wild-type or mutant as indicated.

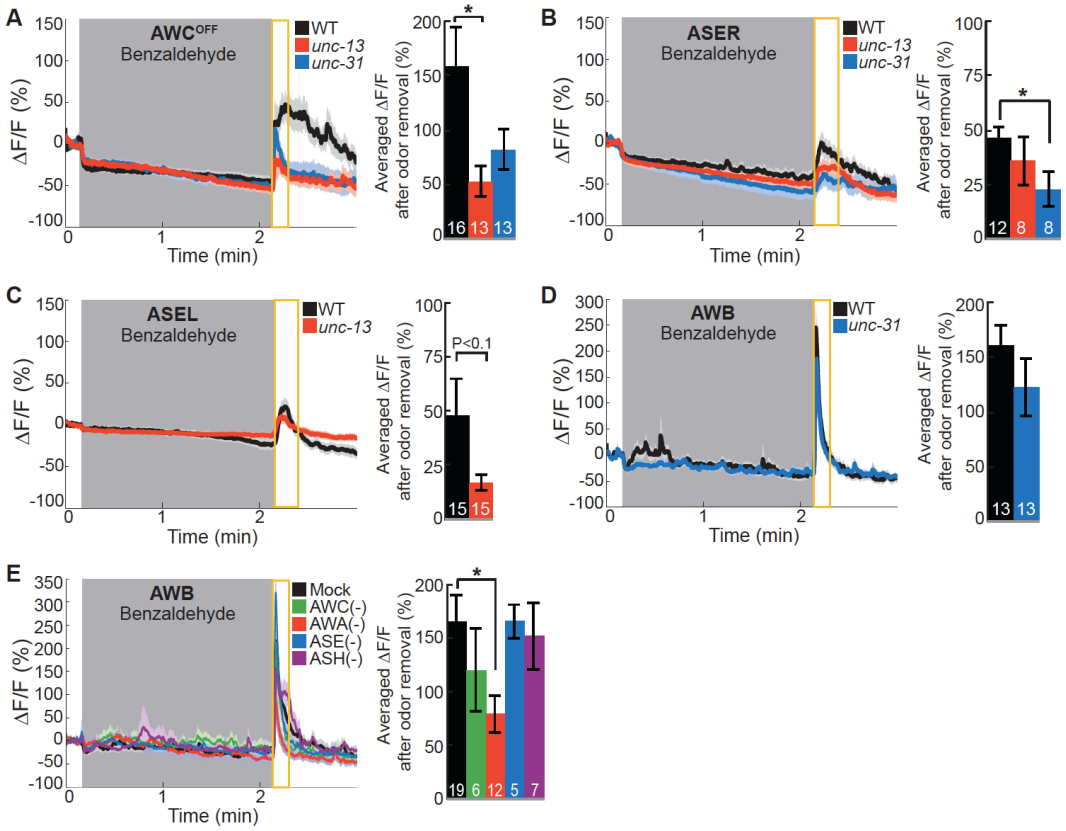

Figure 4.4: Primary and secondary olfactory neurons respond to benzaldehyde. (a-d) Average calcium responses of young adult (a) AWC^{OFF}, (b) ASER, (c) ASEL and (d) AWB neurons in wild-type, *unc-13* mutants with impaired synaptic vesicle release, and *unc-31* mutants with impaired dense core vesicle release to benzaldehyde stimulation. (e) Average young adult AWB neuron responses to benzaldehyde in control mock-ablated animals compared to animals with AWC, AWA, ASE or ASH sensory neurons laser ablated (at an early larval stage). (a-e) Shaded box indicates two-minute benzaldehyde odor stimulation beginning at t=10s. Yellow box indicates the time period after stimulus change for which the fluorescence change was averaged in the bar graphs. Numbers on bar graphs indicate number of neurons imaged. Light color shading around curves and bar graph error bars indicate s.e.m. *$p < 0.05$, two-tailed *t*-test with Bonferroni correction, compared to wild-type or mock ablated animals as indicated.

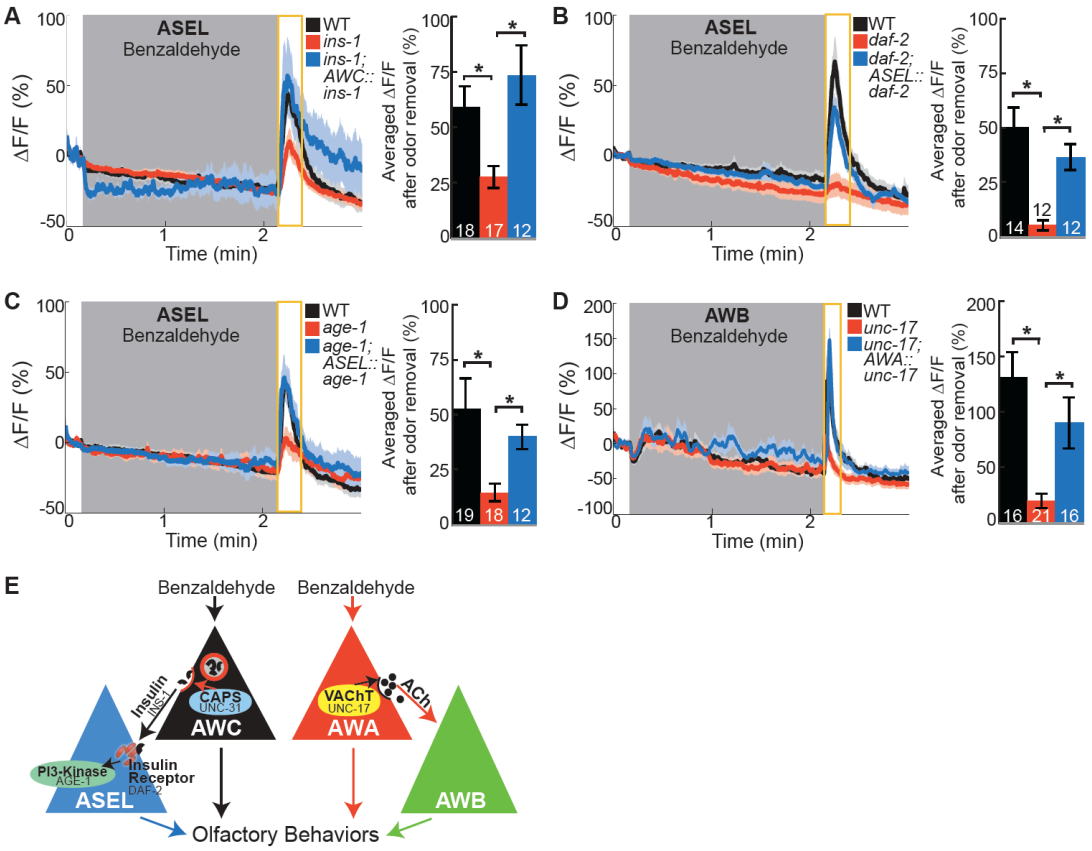

Figure 4.5: Insulin peptidergic and cholinergic transmission from two primary olfactory sensory neurons activates two secondary olfactory neurons. (a-c) Benzaldehyde-evoked activity in young adult ASEL neurons in (a) *ins-1* insulin-like peptide mutants and *ins-1*; AWC-specific *ins-1* rescue, (b) *daf-2* insulin receptor mutants and *daf-2*; ASEL-specific *daf-2* rescue, and (c) *age-1* PI3-Kinase mutants and *age-1*; ASEL-specific *age-1* rescue compared to wild-type. (d) AWB neuronal activity in response to benzaldehyde in young adult wild-type, *unc-17* vesicular acetylcholine transporter mutants and *unc-17;* AWA-specific *unc-17* rescue. (e) Proposed young adult benzaldehyde circuit model. (a-d) *p < 0.05, two-tailed *t*-test with Bonferroni correction, compared to wild-type or mutant as indicated.

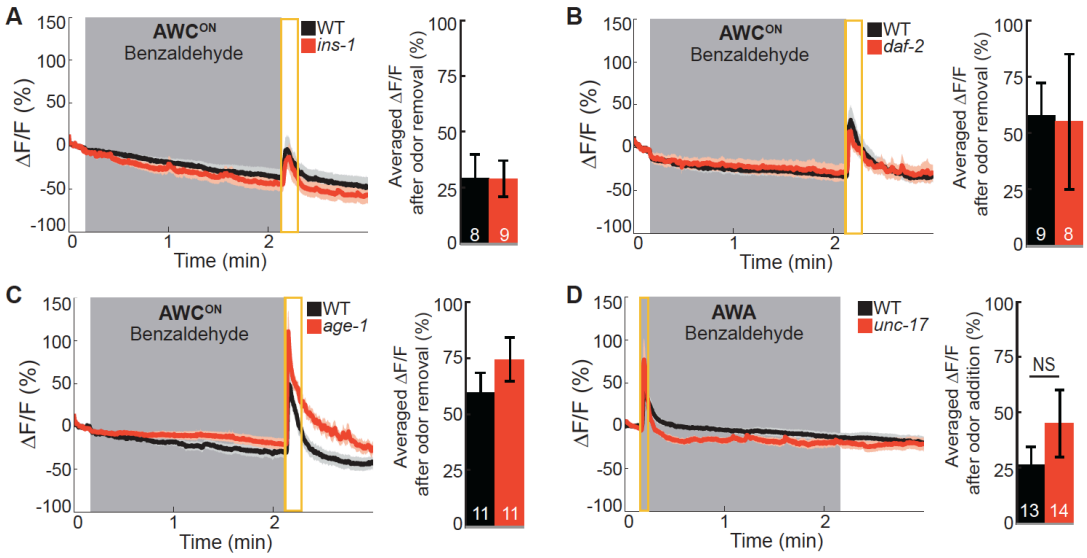

Figure 4.6: Odor-evoked calcium dynamics in genetic mutants. (a-c) Young adult AWC^{ON} neuron average responses to benzaldehyde stimulation in wild-type animals compared to (a) insulin-like peptide *ins-1* mutants, (b) *daf-2* insulin receptor mutants and (c) *age-1* PI3-Kinase mutants. (d) Average AWA neuron responses to benzaldehyde in wild-type and *unc-17* vesicular acetylcholine transporter mutants. (a-d) NS, $p > 0.05$, two-tailed *t*-test.

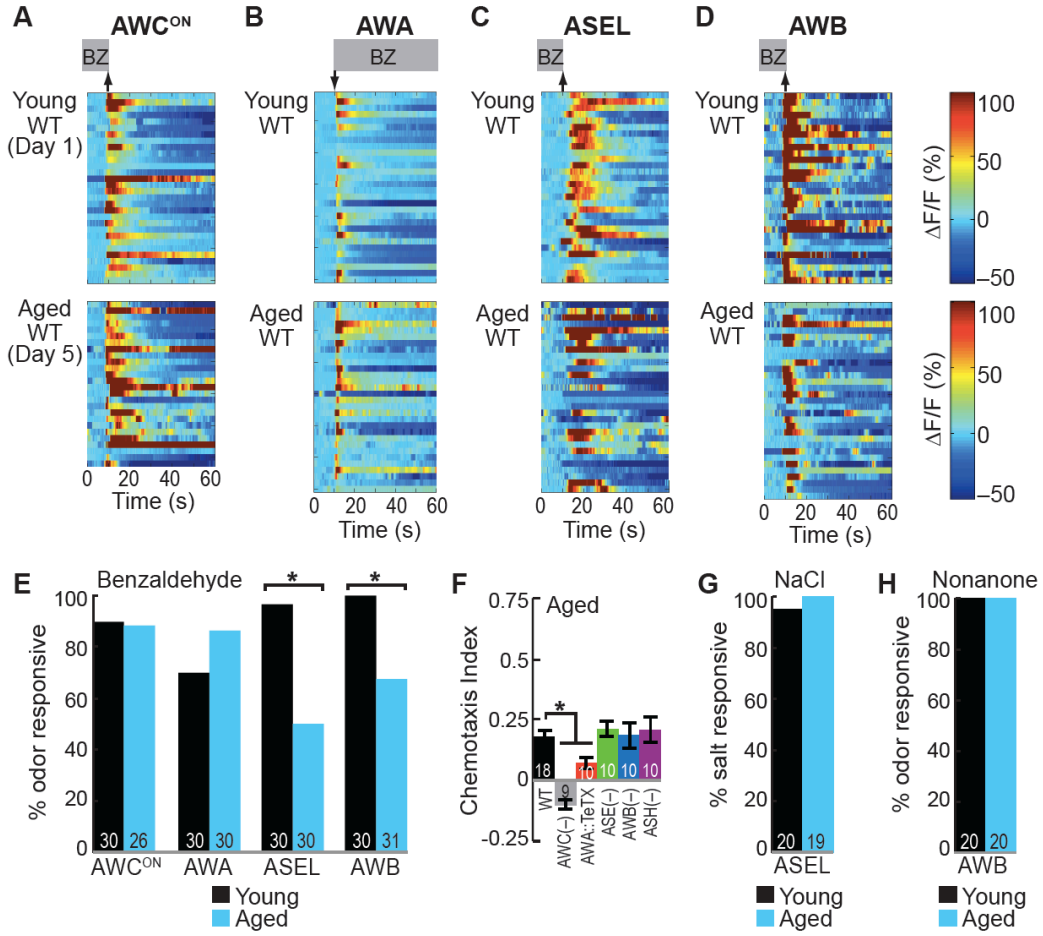

Figure 4.7: Attractive odor-evoked secondary neuron activity specifically degrades with age. (a-d) Heat maps of ratio change in fluorescence to total fluorescence for wild-type young adult (day 1) and aged adult (day 5) sensory neuron responses to the addition or removal (at t=10s) of benzaldehyde (BZ), as indicated by shaded box and arrow. One row represents activity from one neuron. (e) Quantification of the percent of odor responsive neurons shown in a-d. (f) Aged (day 5) adult benzaldehyde chemotaxis performance of wild-type, AWC or AWB or ASH neuron-specific genetic ablation, AWA neuron-specific tetanus toxin expression worms or *che-1* mutants missing ASE neurons. *p < 0.05, two-tailed *t*-test with Bonferroni correction, compared to wild-type. (g,h) The percent of wild-type young (day 1) and aged (day 5) adult (g) ASEL neurons responsive to sodium chloride and (h) AWB neurons responsive to 2-nonanone odor. (e,g,h) Odor or salt responsive defined as having a DF/F to stimulus greater than 10%. Numbers on bars indicate number of neurons imaged. *p < 0.05, two-tailed Chi Square test.

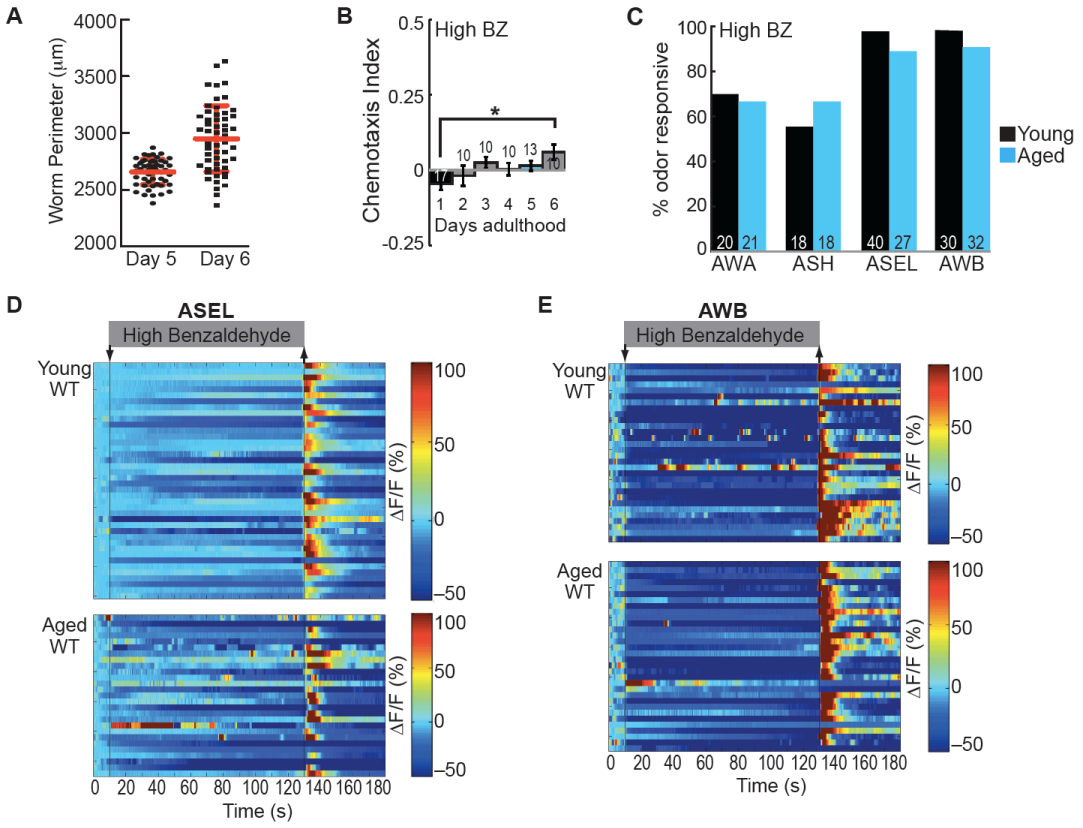

Figure 4.8: Dose-dependent odor-evoked calcium dynamics in young and aged adults. (a) Measurement of the perimeter of day 5 aged worms and the more variable day 6 aged worms (see Methods section). Thick red line shows mean and error bars represent standard deviation (Day 5: 2656.3µm +/- 112.07, Day 6: 2950.5µm +/- 291.21, n=55 animals for each age). (b) Chemotaxis performance of wild-type worms of different ages towards a point source of high concentration benzaldehyde. Numbers on bars represent number of assay plates and error bars indicate s.e.m. *$p < 0.05$, two-tailed *t*-test with Bonferroni correction, compared to young adults. (c) Quantification of the percent of high concentration benzaldehyde responsive neurons. Numbers on bars represent number of neurons imaged and odor responsive is defined as having a DF/F to odor greater than 10%. NS, $p > 0.05$, two-tailed Chi Square test. (d,e) Heat maps of ratio change in fluorescence to total fluorescence for wild-type young adult (day 1) and aged adult (day 5) (d) ASEL and (e) AWB sensory neuron responses to high concentration benzaldehyde stimulation. Two-minute odor stimulation indicated by shaded box and arrows. One row represents activity from one neuron.

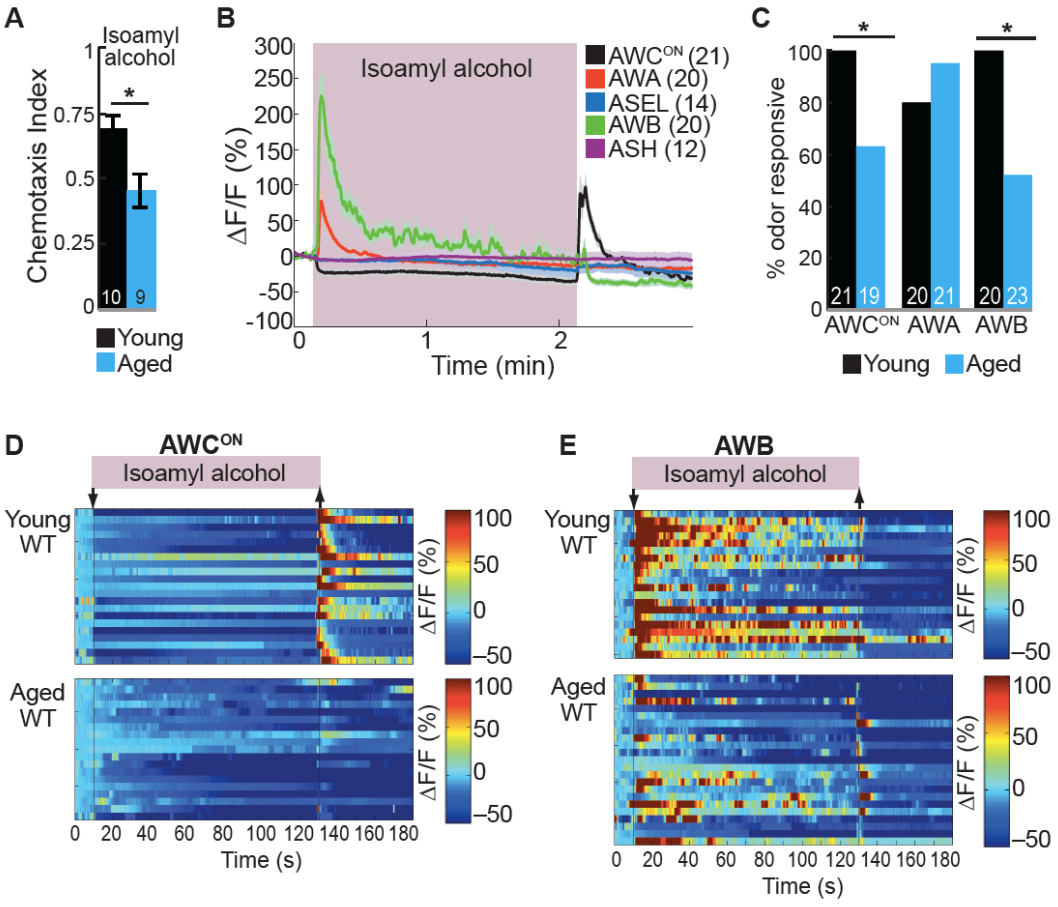

Figure 4.9: Aging-associated declines in behavior and neural activity evoked by the attractive odor isoamyl alcohol. (a) Chemotaxis performance of wild-type young (day 1) and aged (day 5) adults towards a point source of isoamyl alcohol odor. (b) Average GCaMP fluorescence change in young adult (day 1), wild-type sensory neurons in response to isoamyl alcohol odor stimulation. Shaded box indicates two minute odor stimulation beginning at t=10s. The light color shading around curves indicates s.e.m. and numbers in parentheses indicate number of neurons imaged. (c) Quantification of the percent of isoamyl alcohol odor responsive neurons in young and aged animals. (d,e) Heat maps of ratio change in fluorescence to total fluorescence for wild-type young adult (day 1) and aged adult (day 5) (d) AWC^{ON} and (e) AWB sensory neuron responses to isoamyl alcohol stimulation.

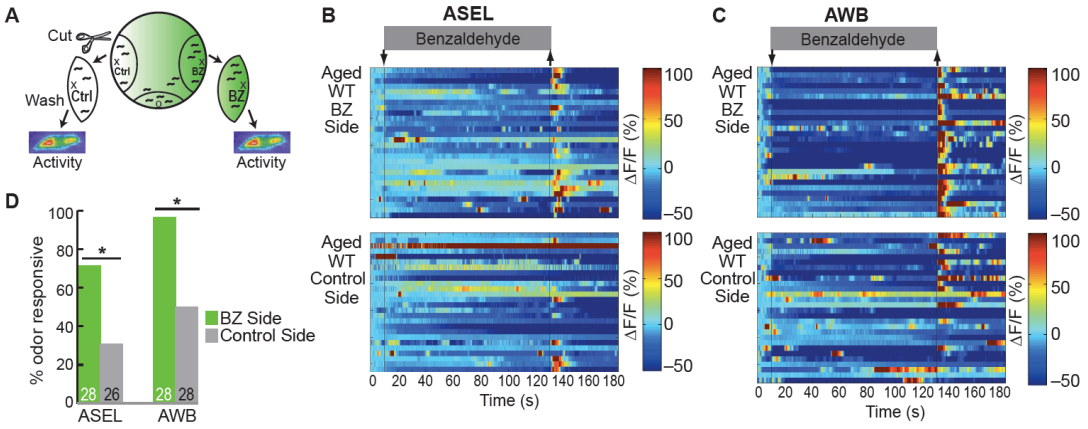

Figure 4.10: Olfactory behavior in aged animals is correlated with reliability of odor-evoked neuronal activity. (a) Schematic of animals from a chemotaxis assay washed and sorted into two populations, based on success or failure in navigating up the benzaldehyde odor gradient, for calcium imaging. (b,c) Heat maps of ratio change in fluorescence to total fluorescence for benzaldehyde-evoked activity in wild-type (day 5) aged (b) ASEL and (c) AWB neurons in animals that did or did not successfully chemotax towards the benzaldehyde point source. (d) Quantification of the percent of benzaldehyde responsive neurons shown in b and c.

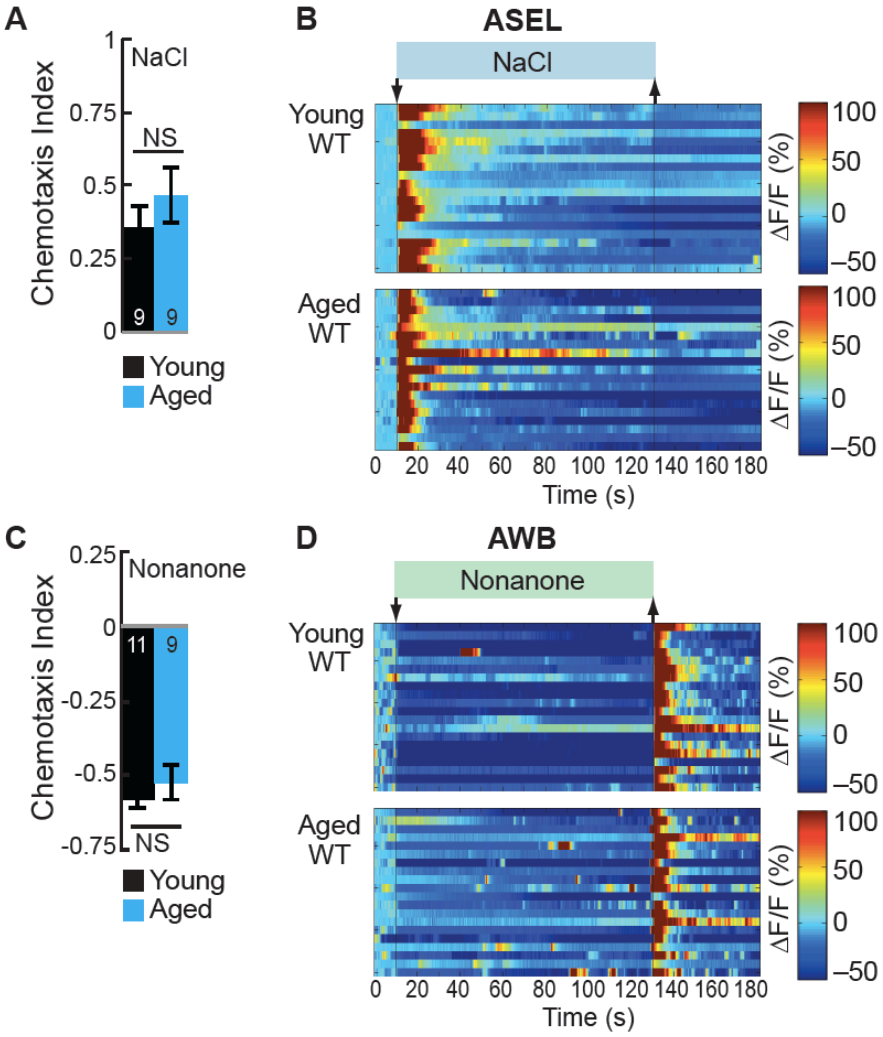

Figure 4.11: ASE and AWB primary responses to salt and 2-nonanone, respectively, remain reliable with aging. (a) Chemotaxis performance of wild-type young (day 1) and aged (day 5) adults towards a point source of 500mM NaCl. (b) Heat maps of ratio change in fluorescence to total fluorescence for wild-type young adult (day 1) and aged adult (day 5) ASEL neurons to +50mM NaCl stimulation. (c) Chemotaxis performance of wild-type young (day 1) and aged (day 5) adults towards a point source of repulsive 2-nonanone odor. (d) Heat maps of ratio change in fluorescence to total fluorescence for wild-type young and aged adult AWB neurons to 2-nonanone odor stimulation. NS $p > 0.05$, two-tailed *t*-test.

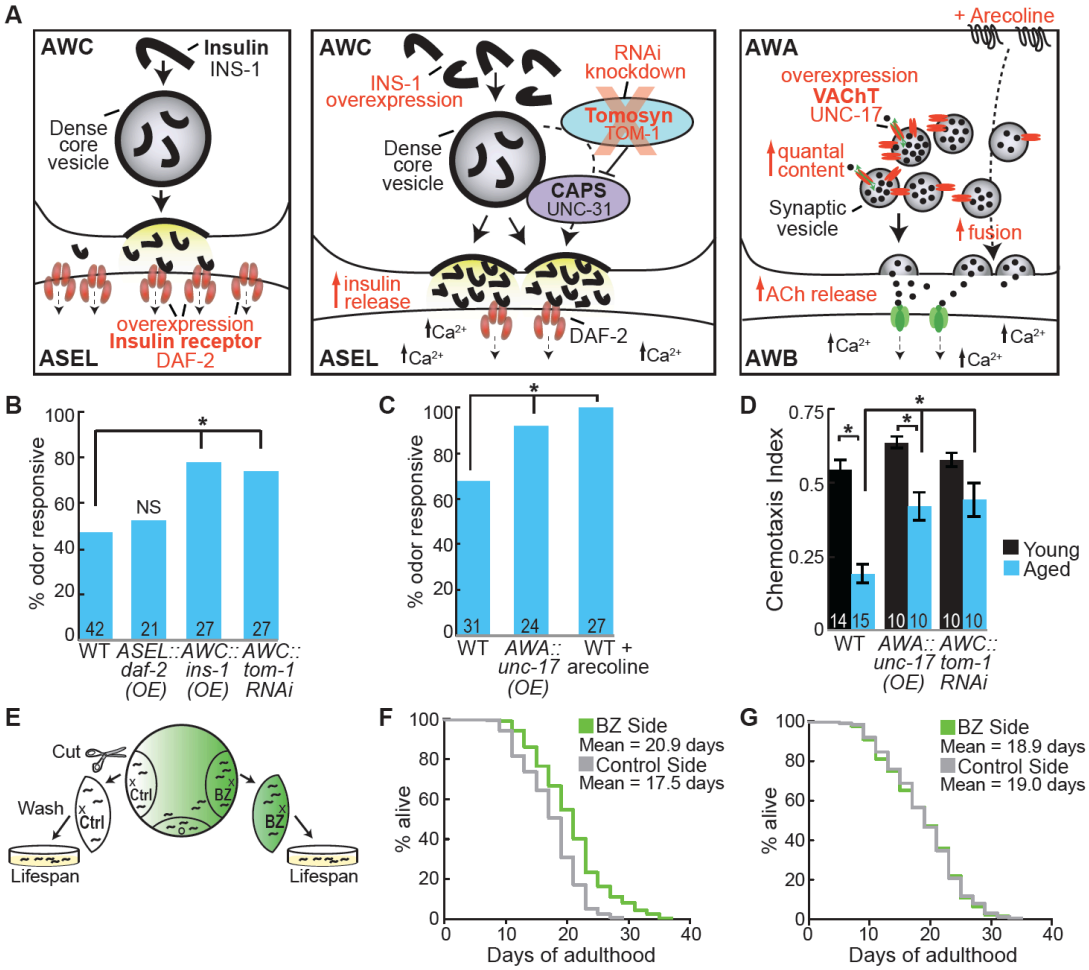

Figure 4.12: Increased release from primary neurons rescues aging-associated neuronal activity and behavioral deficits, which are correlated with longevity. (a) Schematic representation of genetic and pharmacologic manipulations to overcome aging-associated decay of neurotransmission. (b) Percent benzaldehyde responsive aged ASEL neurons in wild-type, ASEL-specific *daf-2* overexpression, AWC-specific *ins-1* overexpression and AWC-specific *tom-1* RNAi. (c) Percent benzaldehyde responsive aged AWB neurons in wild-type, AWA-specific *unc-17* overexpression and animals treated acutely with the cholinergic agonist arecoline. (d) Benzaldehyde chemotaxis in young and aged wild-type, AWC-specific *tom-1* RNAi and AWA-specific *unc-17* overexpression animals. (b-d) *p < 0.05, with statistics as described above. (e) Schematic of animals from a chemotaxis assay washed and sorted into two populations based on successful or failed navigation up the benzaldehyde (BZ) odor gradient, for lifespan analysis. (f) Animals that chemotaxed to the benzaldehyde odor side of the chemotaxis plate as aged adults (day 5) have a 16.2% average extension in their lifespan compared to animals from the opposite, control side ($p < 0.01$ by Mantel-Cox test, see Table 4.1 for quantification). (g) Animals sorted by their young adult chemotaxis do not have significantly different lifespans. (f,g) Mean survival is reported in days of adulthood.

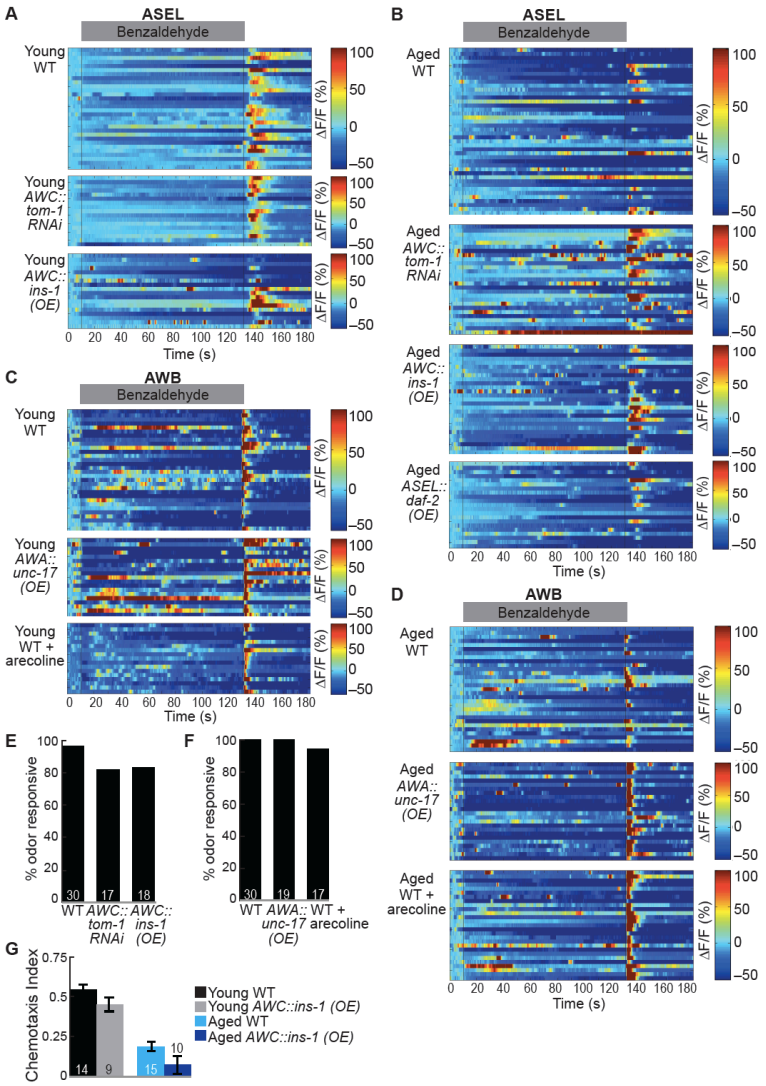

Figure 4.13: Increased release from primary neurons rescues aging-associated neuronal activity and behavioral deficits. (a,b) Heat maps of ratio change in fluorescence to total fluorescence for ASEL neuron responses to benzaldehyde in wild-type animals and in transgenic animals with AWC-specific *tom-1* RNAi, AWC-specific *ins-1* overexpression and ASEL-specific *daf-2* overexpression in (a) young adults (day 1) and (b) aged adults (day 5). (c,d) Heat maps of ratio change in fluorescence to total fluorescence for AWB neuron responses to benzaldehyde in wild-type animals, transgenic animals with AWA-specific *unc-17* overexpression and wild-type animals that received acute treatment with the cholinergic agonist arecoline in (c) young adults (day 1) and (d) aged adults (day 5). (e,f) Quantification of the percent of odor responsive young adult (e) ASEL neurons shown in A and (f) AWB neurons shown in C. NS, $p > 0.05$, two-tailed Chi Square test. (g) Chemotaxis behavior in young and aged wild-type and AWC-specific *ins-1* overexpression animals, showing a trend towards dampened behavioral responses to benzaldehyde point sources in these transgenic animals. Numbers on bars indicate number of assay plates and error bars indicate s.e.m. NS, $p > 0.05$, two-tailed *t*-test.

Table 4.1: Animal lifespan after benzaldehyde chemotaxis. Wild-type (N2) worms were separated into a population that successfully reached the benzaldehyde (BZ) odor side of the chemotaxis plate and a population that failed to do so (Ctrl Side) as young or aged adults and then their survival was analyzed. Data from three separate trials are shown. *p < 0.05 by the Mantel-Cox test. Percent change in mean survival is the mean survival of animals from the odor side minus the mean survival of animals from the control side divided by the mean survival of the odor side.

Lifespan Post-Day 5 Adult Benzaldehyde Chemotaxis

Trial	Condition	# deaths/ animals	Mean survival (days)	S.E.M survival (days)	Median survival (days)	Mantel-Cox Test P-value	% change in mean survival
A	N2 BZ Odor Side	83/100	20.0	0.7	19	*0.0018	+11.5%
	N2 Ctrl Side	92/100	17.7	0.5	17		
B	N2 BZ Odor Side	81/100	21.3	0.6	21	*8.4e-06	+15.0%
	N2 Ctrl Side	90/100	18.1	0.4	19		
C	N2 BZ Odor Side	85/100	21.3	0.7	21	*2.8e-06	+22.1%
	N2 Ctrl Side	86/100	16.6	0.5	17		
Avg	N2 BZ Odor Side	Mean Survival is 20.9 days of adulthood					+16.2%
	N2 Ctrl Side	Mean Survival is 17.5 days of adulthood					

Lifespan Post-Day 1 Adult Benzaldehyde Chemotaxis

Trial	Condition	# deaths/ animals	Mean survival (days)	S.E.M survival (days)	Median survival (days)	Mantel-Cox Test P-value	% change in mean survival
A	N2 BZ Odor Side	78/100	20.4	0.6	21	0.90, NS	-0.5%
	N2 Ctrl Side	78/100	20.5	0.7	21		
B	N2 BZ Odor Side	75/100	19.7	0.6	21	0.85, NS	0%
	N2 Ctrl Side	82/100	19.7	0.6	21		
C	N2 BZ Odor Side	81/100	16.6	0.7	15	0.87, NS	-1.2%
	N2 Ctrl Side	76/100	16.8	0.7	17		
Avg	N2 BZ Odor Side	Mean Survival is 18.9 days of adulthood					-0.6%
	N2 Ctrl Side	Mean Survival is 19.0 days of adulthood					

Table 4.2: Strain list. List of all *C. elegans* strains.

Strain	Genotype
Calcium imaging: wild-type GCaMP strains	
CX10536	*kyEx2595 [str-2::GCaMP2.2b, unc-122::gfp]*
PS6253	*pha-1(e2123) III; syEx1238 [srsx-3::GCaMP3, pha-1::pha-1]*
IV388	*ueEx7 [gcy-7::GCaMP3, unc-122::gfp]*
IV28	*ueEx10 [gcy-5::GCaMP3, unc-122::gfp]*
PY6554	*oyEx [gpa-4p::GCaMP2.2b, unc-122::dsRed]*
PY7336	*oyEx [str-1::GCaMP3, unc-122::dsRed]*
IV346	*kyEx2865 [sra-6::GCaMP3, unc-122::gfp]*
CX10981	*kyEx2866 [sra-9::GCaMP2.2b, unc-122::gfp]*
IV413	*ueEx254 [srh-142::GCaMP3, unc-122::gfp]*
CX12022	*kyEx3290 [sre-1:: GCaMP3, unc-122::dsRed]*
IV69	*oyEx [gcy-8::GCaMP3, unc-122::rfp]*
OF977	*ixEx196 [ops-1::GCaMP3, lin-44::rfp]*
ZD1184	*qdEx103 [trx-1::GCaMP5, unc-122::gfp]*
Calcium imaging: mutant, rescue and overexpression GCaMP strains	
IV15	*unc-13(e51) I; kyEx2595 [str-2::GCaMP2.2b, unc-122::gfp]*
IV23	*unc-31(e928) IV; kyEx2595 [str-2::GCaMP2.2b, unc-122::gfp]*
IV141	*unc-13(e51) I; pha-1 (e2123) III; syEx1238 [srsx-3::GCaMP3, pha-1::pha-1]*
IV44	*unc-31(e928) IV; pha-1 (e2123) III; syEx1238 [srsx-3::GCaMP3, pha-1::pha-1]*
IV244	*unc-13(e51) I; oyEx [gpa-4p::GCaMP2.2b, unc-122::dsRed]*
IV234	*unc-31(e928) IV; oyEx [gpa-4p::GCaMP2.2b, unc-122::dsRed]*
IV104	*unc-13(e51) I; ueEx7 [gcy-7::GCaMP3, unc-122::gfp]*
IV22	*unc-31(e928) IV; ueEx7 [gcy-7::GCaMP3, unc-122::gfp]*
IV54	*unc-31(e928) IV; ueEx7 [gcy-7::GCaMP3, unc-122::gfp]; kyEx875 [odr-3::unc-31, elt-2::gfp]*
IV68	*unc-13(e51) I; ueEx10 [gcy-5::GCaMP3, unc-122::gfp]*
IV32	*unc-31(e928) IV; ueEx10 [gcy-5::GCaMP3, unc-122::gfp]*
IV383	*unc-13(e51) I; oyEx [str-1::GCaMP3, unc-122::dsRed]*
IV381	*unc-31(e928) IV; oyEx [str-1::GCaMP3, unc-122::dsRed]*
IV193	*ins-1(nr2091) IV; ueEx7 [gcy-7::GCaMP3, unc-122::gfp]*
IV245	*ins-1(nr2091) IV; ueEx7 [gcy-7::GCaMP3, unc-122::gfp]; ueEx152 [odr-3::ins-1:sl2mCherry, unc-122::rfp]*
CX10926	*ins-1(nr2091) IV; kyEx2595 [str-2::GCaMP2.2b, unc-122::gfp]*

Table 4.2: Strain list, continued.

Strain	Genotype
IV172	*daf-2(e1370) III; ueEx7 [gcy-7::GCaMP3, unc-122::gfp]*
IV224	*daf-2(e1370) III; ueEx7 [gcy-7::GCaMP3, unc-122::gfp]; ueEx139 [gcy-7::daf-2:sl2mCherry, unc-122::rfp]*
IV175	*daf-2(e1370) III; kyEx2595 [str-2::GCaMP2.2b, unc-122::gfp]*
IV96	*age-1(hx546) II; ueEx7 [gcy-7::GCaMP3, unc-122::gfp]*
IV114	*age-1(hx546) II; ueEx7 [gcy-7::GCaMP3, unc-122::gfp]; ueEx54 [gcy-7::age-1:sl2mCherry, unc-122::rfp]*
IV98	*age-1(hx546) II; kyEx2595 [str-2::GCaMP2.2b, unc-122::gfp]*
IV401	*unc-17(e245) IV; oyEx [str-1::GCaMP3, unc-122::dsRed]*
IV487	*unc-17(e245) IV; oyEx [str-1::GCaMP3, unc-122::dsRed]; ueEx305 [gpa-4deletion::unc-17:sl2mCherry, unc-122::gfp]*
IV539	*unc-17(e245) IV; oyEx [gpa-4p::GCaMP2.2b, unc-122::dsRed]*
IV416	*oyEx [str-1::GCaMP3, unc-122::dsRed]; ueEx257 [gpa-4deletion::TeTX:sl2mCherry, unc-122::gfp]*
IV404	*ueEx7 [gcy-7::GCaMP3, unc-122::gfp]; ueEx247 [ceh-36deletion::tom-1 sense:sl2mCherry, ceh-36deletion::tom-1 antisense:sl2mCherry, unc-122::rfp]*
IV467	*ueEx7 [gcy-7::GCaMP3, unc-122::gfp]; ueEx292 [odr-3::ins-1:sl2mCherry, unc-122::rfp]*
IV511	*ueEx7 [gcy-7::GCaMP3, unc-122::gfp]; ueEx321 [gcy-7::daf-2:sl2mCherry, unc-122::rfp]*
IV497	*oyEx [str-1::GCaMP3, unc-122::dsRed]; ueEx310 [gpa-4deletion::unc-17:sl2mCherry, unc-122::gfp]*
Additional strains for behavior	
N2	Bristol strain
PY7502	*oyIs [ceh-36del::caspase-3(p12)::nz, ceh-36del::cz::caspase-3(p17), srtx-1::gfp, unc-122::dsRed]*
PR672	*che-1(p672) I*
JN1715	*peIs [str-1::mCasp-1, unc-122::mCherry]*
JN1713	*peIs [sra-6::mCasp-1, unc-122::mCherry]*

References

Alfonso, A., Grundahl, K., McManus, J.R., and Rand, J.B. (1994). Cloning and characterization of the choline aceytltransferase structural gene (cha-1) from C. elegans. J Neurosci 14, 2290-2300.

Bargmann, C.I. (2006). Chemosensation in C. elegans. WormBook, 1-29.

Bargmann, C.I., and Avery, L. (1995). Laser killing of cells in Caenorhabditis elegans. Methods Cell Biol 48, 225-250.

Bargmann, C.I., Hartwieg, E., and Horvitz, H.R. (1993). Odorant-selective genes and neurons mediate olfaction in C. elegans. Cell 74, 515-527.

Bargmann, C.I., and Horvitz, H.R. (1991). Chemosensory neurons with overlapping functions direct chemotaxis to multiple chemicals in C. elegans. Neuron 7, 729-742.

Beverly, M., Anbil, S., and Sengupta, P. (2011). Degeneracy and neuromodulation among thermosensory neurons contribute to robust thermosensory behaviors in Caenorhabditis elegans. J Neurosci 31, 11718-11727.

Brenner, S. (1974). The genetics of Caenorhabditis elegans. Genetics 77, 71-94.

Castelo-Branco, C., and Soveral, I. (2014). The immune system and aging: a review. Gynecological endocrinology : the official journal of the International Society of Gynecological Endocrinology 30, 16-22.

Chalasani, S.H., Chronis, N., Tsunozaki, M., Gray, J.M., Ramot, D., Goodman, M.B., and Bargmann, C.I. (2007). Dissecting a circuit for olfactory behaviour in Caenorhabditis elegans. Nature 450, 63-70.

Chokshi, T.V., Bazopoulou, D., and Chronis, N. (2010). An automated microfluidic platform for calcium imaging of chemosensory neurons in Caenorhabditis elegans. Lab Chip 10, 2758-2763.

Chronis, N., Zimmer, M., and Bargmann, C.I. (2007). Microfluidics for in vivo imaging of neuronal and behavioral activity in Caenorhabditis elegans. Nat Methods 4, 727-731.

Dickstein, D.L., Kabaso, D., Rocher, A.B., Luebke, J.I., Wearne, S.L., and Hof, P.R. (2007). Changes in the structural complexity of the aged brain. Aging Cell 6, 275-284.

Doty, R.L., and Kamath, V. (2014). The influences of age on olfaction: a review. Frontiers in psychology 5, 20.

Esposito, G., Di Schiavi, E., Bergamasco, C., and Bazzicalupo, P. (2007). Efficient and cell specific knock-down of gene function in targeted C. elegans neurons. Gene 395, 170-176.

Gracheva, E.O., Burdina, A.O., Touroutine, D., Berthelot-Grosjean, M., Parekh, H., and Richmond, J.E. (2007). Tomosyn negatively regulates both synaptic transmitter and neuropeptide release at the C. elegans neuromuscular junction. J Physiol 585, 705-709.

Gutchess, A. (2014). Plasticity of the aging brain: new directions in cognitive neuroscience. Science 346, 579-582.

Hobert, O. (2013). The neuronal genome of Caenorhabditis elegans. WormBook, 1-106.

Hummel, T., Kobal, G., Gudziol, H., and Mackay-Sim, A. (2007). Normative data for the "Sniffin' Sticks" including tests of odor identification, odor discrimination, and olfactory thresholds: an upgrade based on a group of more than 3,000 subjects. European archives of oto-rhino-laryngology : official journal of the European Federation of Oto-Rhino-Laryngological Societies 264, 237-243.

Kauffman, A.L., Ashraf, J.M., Corces-Zimmerman, M.R., Landis, J.N., and Murphy, C.T. (2010). Insulin signaling and dietary restriction differentially influence the decline of learning and memory with age. PLoS Biol 8, e1000372.

Kenyon, C., Chang, J., Gensch, E., Rudner, A., and Tabtiang, R. (1993). A C. elegans mutant that lives twice as long as wild type. Nature 366, 461-464.

Lacroix, M.C., Badonnel, K., Meunier, N., Tan, F., Schlegel-Le Poupon, C., Durieux, D., Monnerie, R., Baly, C., Congar, P., Salesse, R., and Caillol, M. (2008). Expression of insulin system in the olfactory epithelium: first approaches to its role and regulation. J Neuroendocrinol 20, 1176-1190.

Leinwand, S.G., and Chalasani, S.H. (2013). Neuropeptide signaling remodels chemosensory circuit composition in Caenorhabditis elegans. Nat Neurosci 16, 1461-1467.

Liu, J., Zhang, B., Lei, H., Feng, Z., Liu, J., Hsu, A.L., and Xu, X.Z. (2013). Functional aging in the nervous system contributes to age-dependent motor activity decline in C. elegans. Cell Metab 18, 392-402.

Mello, C., and Fire, A. (1995). DNA transformation. Methods Cell Biol 48, 451-482.

Morris, J.Z., Tissenbaum, H.A., and Ruvkun, G. (1996). A phosphatidylinositol-3-OH kinase family member regulating longevity and diapause in Caenorhabditis elegans. Nature 382, 536-539.

Ogura, T., Szebenyi, S.A., Krosnowski, K., Sathyanesan, A., Jackson, J., and Lin, W. (2011). Cholinergic microvillous cells in the mouse main olfactory epithelium and effect of acetylcholine on olfactory sensory neurons and supporting cells. J Neurophysiol 106, 1274-1287.

Oka, Y., Katada, S., Omura, M., Suwa, M., Yoshihara, Y., and Touhara, K. (2006). Odorant receptor map in the mouse olfactory bulb: in vivo sensitivity and specificity of receptor-defined glomeruli. Neuron 52, 857-869.

Pierce, S.B., Costa, M., Wisotzkey, R., Devadhar, S., Homburger, S.A., Buchman, A.R., Ferguson, K.C., Heller, J., Platt, D.M., Pasquinelli, A.A., *et al*. (2001). Regulation of DAF-2 receptor signaling by human insulin and ins-1, a member of the unusually large and diverse C. elegans insulin gene family. Genes Dev 15, 672-686.

Pincus, Z., and Slack, F.J. (2010). Developmental biomarkers of aging in Caenorhabditis elegans. Dev Dyn 239, 1306-1314.

Pinto, J.M., Wroblewski, K.E., Kern, D.W., Schumm, L.P., and McClintock, M.K. (2014). Olfactory dysfunction predicts 5-year mortality in older adults. PLoS One 9, e107541.

Ramot, D., Johnson, B.E., Berry, T.L., Jr., Carnell, L., and Goodman, M.B. (2008). The Parallel Worm Tracker: a platform for measuring average speed and drug-induced paralysis in nematodes. PLoS One 3, e2208.

Richard, M.B., Taylor, S.R., and Greer, C.A. (2010). Age-induced disruption of selective olfactory bulb synaptic circuits. Proc Natl Acad Sci U S A 107, 15613-15618.

Richmond, J.E., Davis, W.S., and Jorgensen, E.M. (1999). UNC-13 is required for synaptic vesicle fusion in C. elegans. Nat Neurosci 2, 959-964.

Schiavo, G., Benfenati, F., Poulain, B., Rossetto, O., Polverino de Laureto, P., DasGupta, B.R., and Montecucco, C. (1992). Tetanus and botulinum-B neurotoxins block neurotransmitter release by proteolytic cleavage of synaptobrevin. Nature 359, 832-835.

Song, H., Ming, G., Fon, E., Bellocchio, E., Edwards, R.H., and Poo, M. (1997). Expression of a putative vesicular acetylcholine transporter facilitates quantal transmitter packaging. Neuron 18, 815-826.

Speese, S., Petrie, M., Schuske, K., Ailion, M., Ann, K., Iwasaki, K., Jorgensen, E.M., and Martin, T.F. (2007). UNC-31 (CAPS) is required for dense-core vesicle but not synaptic vesicle exocytosis in Caenorhabditis elegans. J Neurosci 27, 6150-6162.

Suzuki, H., Thiele, T.R., Faumont, S., Ezcurra, M., Lockery, S.R., and Schafer, W.R. (2008). Functional asymmetry in Caenorhabditis elegans taste neurons and its computational role in chemotaxis. Nature 454, 114-117.

Toth, M.L., Melentijevic, I., Shah, L., Bhatia, A., Lu, K., Talwar, A., Naji, H., Ibanez-Ventoso, C., Ghose, P., Jevince, A., *et al*. (2012). Neurite sprouting and synapse deterioration in the aging Caenorhabditis elegans nervous system. J Neurosci 32, 8778-8790.

Troemel, E.R., Kimmel, B.E., and Bargmann, C.I. (1997). Reprogramming chemotaxis responses: sensory neurons define olfactory preferences in C. elegans. Cell 91, 161-169.

Uchida, O., Nakano, H., Koga, M., and Ohshima, Y. (2003). The C. elegans che-1 gene encodes a zinc finger transcription factor required for specification of the ASE chemosensory neurons. Development 130, 1215-1224.

Vijg, J. (2014). Aging genomes: a necessary evil in the logic of life. Bioessays 36, 282-292.

Walston, J.D. (2012). Sarcopenia in older adults. Current opinion in rheumatology 24, 623-627.

Wang, J.W., Wong, A.M., Flores, J., Vosshall, L.B., and Axel, R. (2003). Two-photon calcium imaging reveals an odor-evoked map of activity in the fly brain. Cell 112, 271-282.

Ward, S. (1973). Chemotaxis by the nematode Caenorhabditis elegans: identification of attractants and analysis of the response by use of mutants. Proc Natl Acad Sci U S A 70, 817-821.

Wes, P.D., and Bargmann, C.I. (2001). C. elegans odour discrimination requires asymmetric diversity in olfactory neurons. Nature 410, 698-701.

White, J.G., Southgate, E., Thomson, J.N., and Brenner, S. (1986a). The structure of the nervous system of the nematode Caenorhabditis elegans. Philos Trans R Soc Lond B Biol Sci 314, 1-340.

White, J.G., Southgate, E., Thomson, J.N., and Brenner, S. (1986b). The structure of the nervous system of the nematode *Caenorhabditis elegans*. Phil Transact R Soc Lond B 314, 1-340.

Wolff, S., and Dillin, A. (2006). The trifecta of aging in Caenorhabditis elegans. Exp Gerontol 41, 894-903.

Yang, J.S., Nam, H.J., Seo, M., Han, S.K., Choi, Y., Nam, H.G., Lee, S.J., and Kim, S. (2011). OASIS: online application for the survival analysis of lifespan assays performed in aging research. PLoS One 6, e23525.

Yin, F., Jiang, T., and Cadenas, E. (2013). Metabolic triad in brain aging: mitochondria, insulin/IGF-1 signalling and JNK signalling. Biochem Soc Trans 41, 101-105.

Yoshida, K., Hirotsu, T., Tagawa, T., Oda, S., Wakabayashi, T., Iino, Y., and Ishihara, T. (2012). Odour concentration-dependent olfactory preference change in C. elegans. Nature communications 3, 739.

CHAPTER 5.

Conclusions and future directions

In order to generate pro-survival behaviors, animals have to represent and interpret the multisensory features of their complex and changing environments. The preceding chapters demonstrate that previous models of sensory encoding in *C. elegans* were incomplete because sensory neural circuits are reconfigured by external and internal contexts. In response to specific sensory cues, *C. elegans* use peptidergic and classical neurotransmission to recruit additional sensory neurons, acting as secondary neurons, to chemosensory circuits. This circuit flexibility yields behavioral plasticity. Thus, sensory context and neuropeptide signaling act in tandem to shape the active neural circuits that drive behavior. However, these circuit mechanisms degrade with aging, resulting in sensory behavioral declines. In this chapter, I will further discuss the conclusions that can be drawn from this research and highlight several directions that merit additional study, which may provide new insights into some of the mysteries of nervous system function.

Models for sensory encoding

The research described in Chapters 2-4 requires that models of *C. elegans* sensory encoding be updated. Previous research in *C. elegans* suggested a labeled line model of sensory encoding in which single neurons were necessary and sufficient to drive

hardwired appetitive or aversive behaviors (Bargmann et al., 1993; Bargmann and Horvitz, 1991; Troemel et al., 1997). However, I find that sensory neural circuits are more complex. Multiple neurons are responsive to salt and odor. Individual cells such as the ASE and AWB neurons can even function in both attractive and repulsive circuits depending on the identity and concentration of a stimulus. This violates the labeled line model's one neuron-one behavior rule. In its place, my data supports a population coding strategy in which activity patterns across multiple (primary and secondary) neurons encode sensory stimuli in *C. elegans*. Furthermore, these flexible circuits drive different behaviors, rather than fixed pathways driving set motor outputs. This suggests that worms' sensory processing is more similar to insects' and mammals' than previously proposed, indicating that circuit principles uncovered in *C. elegans* may be widely applicable in the animal kingdom (Honegger et al., 2011; Oka et al., 2006; Stettler and Axel, 2009; Wang et al., 2003).

An interesting feature of this form of sensory coding is that it may support multisensory integration and the representation of valence. For example, ASE neurons contribute information about salt, odor and carbon dioxide (Bretscher et al., 2011; Suzuki et al., 2008). The AWC neurons similarly sense odor and salt, along with pheromone cues and temperature (Bargmann et al., 1993; Biron et al., 2008; Leinwand and Chalasani, 2013; White et al., 2007). These multimodal neurons are uniquely positioned to integrate information about the environment. These neurons may also signal the saliency or valence of the sensory stimuli detected to their downstream targets by releasing particular complements of neuropeptides or neurotransmitters. Specifically, signaling from primary to secondary neurons and other interneurons may strengthen the representation of a

particular sensory cue, for example a food-like odor, which could lead to robust food-search behavior, perhaps even when low levels of salt and other stimuli are detectable in other parts of the environment. In support of this hypothesis, research in this dissertation and published previously suggests that AWC neurons may release either glutamate or neuropeptides, which are interpreted differently by the downstream circuitry (Chalasani et al., 2010; Leinwand and Chalasani, 2013). In the odor circuit, AWC-released glutamate inhibits the activity of interneuron, AIA; however, in the salt circuit, AWC-released neuropeptides excite AIA interneurons (Chalasani et al., 2010; Leinwand and Chalasani, 2013). Perhaps this signaling results in a hierarchical representation of the relative importance of odor and salt cues in the environment to drive appropriate behaviors. How other neurons integrate sensory information and multiplex different neurotransmitters must be investigated more systematically.

I speculate that population codes composed of the distributed activity of (multi)sensory neurons represent information about global environmental conditions, rather than unitary features of the sensory environment. Two lines of future research are required to increase our understanding of this topic. First, it will be necessary to map the active connections from all the sensory neurons that jointly encode a given sensory stimulus to interneurons (and ultimately motor neurons) to determine how information is transformed to generate behavior. Blocking particular forms of neurotransmitter or neuropeptide release in a cell-specific manner and examining the effects on downstream activity may achieve this goal. This task may be aided by the use of new, fast selective plane illumination microscopy techniques for visualizing the activity and network dynamics in almost the entire nervous system (Prevedel et al., 2014; Schrodel et al.,

2013; Wu et al., 2011). Second, as our understanding of the encoding of unitary stimuli increases, neuronal (and behavioral) responses to mixed stimuli, which more accurately represent the complex environment that an animal would encounter, must be also studied. Several studies have begun to examine the encoding of odor mixtures, but the processing and integration of multimodal stimuli must also be investigated (Howard and Gottfried, 2014; McMeniman et al., 2014; Su et al., 2012).

Circuit flexibility

Another important conclusion that may be drawn from this research is that neural circuits are flexible, not fixed. Moreover, information can be selectively routed via many, alternative paths in neural networks. Chapters 2-4 of this dissertation suggest that sensory context is an essential determinant of the composition of behaviorally relevant sensory neural circuits. Neuropeptide signaling mediates this context-dependent reorganization of sensory neural circuits. Specifically, my research identified a circuit motif consisting of primary and secondary neurons, whose combined activity encodes the identity and concentration of a sensory stimulus. Primary neurons directly detect sensory cues in the environment. The ASE neurons are primary salt sensory neurons, while the AWC and AWA neurons are primary olfactory sensory neurons. These primary neurons release neuropeptides and neurotransmitters to recruit secondary neurons to the circuit. The secondary neurons are classically defined as sensory neurons, yet they function transiently as interneurons. The ASE primary salt neurons release INS-6 insulin-like peptides to activate and recruit the secondary AWC neurons specifically to the high salt circuit, but not to the low salt circuit (Chapter 2). In contrast, upon benzaldehyde odor

detection, the AWC neurons release INS-1 insulin-like peptides to recruit the ASE neurons to the olfactory circuit (Chapter 4). The AWA neurons similarly function as primary neurons; they release acetylcholine to activate secondary AWB neurons upon benzaldehyde stimulation (Chapter 4). (Additional experiments are required to identify the acetylcholine receptor(s) in AWB from the nearly 70 candidates (Hobert, 2013).) Behavioral experiments silencing or ablating individual neurons reveal that the combined activity of the primary and secondary neurons is essential for proper responses to olfactory stimuli and high salt. Therefore, sensory context (i.e. salt or odor) determines which neurons function as primary neurons, which function as secondary neurons and which neurotransmission pathways are required within flexible neural circuits.

Multiplexing different neuropeptides, cholinergic signaling and other classical, small molecule or amino acid neurotransmitters may offer a general mechanism to rapidly modulate the information content of overlapping neural circuits in diverse species. Effectively, this would increase the computational capacity of the nervous system. From worms to flies and mammals, neuromodulators like dopamine, serotonin, insulin, vasopressin, neuropeptide Y and their homologs are expressed throughout sensory processing brain regions, where they alter sensory neurons' signal to noise ratios, sync sensory neuron activity with feeding state, and integrate social cues with other sensory information (Bester-Meredith et al., 2015; Kuczewski et al., 2014; Leinwand and Chalasani, 2013; Marella et al., 2012; Root et al., 2011; Savigner et al., 2009). Furthermore, there is evidence that dopamine can regulate the flow of visual information through different cell types in mammalian retinal circuits (Xia and Mills, 2004). This regulation depends on the sensory context, in this instance light intensity (Xia and Mills,

2004). However, in most other cases, it is unknown if neuropeptides can alter neural circuit composition. The time courses and functional consequences of these peptidergic effects in other species await further investigation.

From circuits to complete connectomes?

Given that sensory context and neuropeptide signaling reshape active neural circuits, a single, fixed snapshot of an animal's connectome is vastly insufficient for inferring how the nervous system generates behavior. Moreover, sensory information can theoretically flow in a great many different directions because dense neural networks reciprocally connect primary sensory processing brain regions with most other brain regions (Felleman and Van Essen, 1991; Markov et al., 2014). Nevertheless, connectomics projects to date have largely aimed to trace all of the anatomical connections that exist in the brain at one fixed time point, with no means of investigating the effects of context or modulatory state (Alivisatos et al., 2012; Chiang et al., 2011; DeFelipe, 2010; Helmstaedter et al., 2013; Takemura et al., 2013; White et al., 1986). This approach may reveal the full set of possible connections; however, as we have learned from *C. elegans,* this cannot reveal the active circuit configurations that drive behavior. Consequently, this mapping just gets to the very tip of the iceberg, i.e. a long list of untested hypotheses about the anatomy-function link. Instead, a different and far more difficult approach is needed, in which detailed mapping is performed of the active neurons and routes of information flow in many different contexts and modulatory states. Only with such data about the functional, active neural circuits can neuroscientists draw meaningful conclusions about brain function.

The results described in this dissertation suggest that future studies must examine the architecture of sensory circuits and test whether all sensory cells function as primary neurons in all contexts in other species. Tetanus toxin and other genetic or pharmacologic reagents may be used to determine the effects of blocking neurotransmission on the neuronal (and ideally also the behavioral) responses to diverse sensory stimuli. The combined activity of primary and secondary neurons may be broadly useful for reducing failures of sensory encoding. In particular, the primary-secondary neuron circuit motif could also increase the signal-to-noise ratio to distinguish different strength stimuli, perhaps to improve animals' food-seeking success and nutrition. Therefore, I suggest that this circuit organization is not simply an adaptation for *C. elegans* to cope with its small nervous system; instead, it is likely advantageous to have circuits with similar, flexible configurations in larger and more complex brains. Taken together, these findings suggest that wiring diagrams cannot be read like maps to understand behavior until a complete understanding of the effects of context and neuromodulatory states is achieved.

Mechanisms for aging-associated behavioral decline

My research suggests that aging further alters the dynamics of the neural circuits that drive chemosensory behaviors. The *C. elegans* chemotaxis model of aging-associated sensory behavioral decline (Chapter 4) offers a system in which the molecular, cellular and circuit-basis of aging may be probed with fine resolution. Using this model, my experiments suggest that neurotransmission in the olfactory circuit is selectively vulnerable to the deleterious effects of aging, underlying aging-associated (secondary neuron) activity and behavioral impairments. Furthermore, I find a fascinating correlation

between olfactory ability and lifespan; aged animals with preserved olfactory abilities live significantly longer than those with weaker olfactory abilities. Also, experimental manipulations to increase neurotransmission in the olfactory circuit (which rescue aged animals' olfactory behavior) extend lifespan. These results suggest that neuronal functions and behavior at an early stage of aging may predict health and longevity. Together, this data offers an exciting new mechanism for age-related behavioral decline, which could have broad implications for a neurotransmission basis of sensory system aging in diverse species.

My studies suggest that several different genetic and pharmacology approaches to increasing presynaptic neurotransmitter release overcome aging-associated sensory deficits. "Upstream" manipulations to increase the production of neuropeptides and the packing of transmitters into vesicles rescue aged neural activity and behavior. On the other hand, directly manipulating the "downstream" regulation of the SNARE complex and machinery for vesicle fusion and exocytosis is also effective in improving aged neuronal functions. This leaves open the question of what is the root cause of the aging-associated olfactory circuit impairments? Analysis of transmitter release pathway protein expression in the primary olfactory neurons at different ages may provide mechanistic insights. Quantification of synaptic and dense core vesicles (by electron microscopy) or real-time vesicular release (by a synaptic vesicle associated pH-sensitive fluorophore) in young and aged animals may also reveal how aging degrades neurotransmission (Richmond et al., 1999; Samuel et al., 2003). Additionally, experiments at the individual animal level are needed to determine the precise mechanisms and implications of the considerable inter-individual variation observed in aged animal phenotypes in my studies

and elsewhere (Golden et al., 2008; Hsu et al., 2009; Pincus and Slack, 2010). Together, these studies will enhance our understanding of animal aging.

More generally, my research also reveals that studying an early stage of aging can reveal new health and physiology principles. Previously, studies of aging focused almost exclusively on lifespan extension (Bansal et al., 2015). However, lifespan is not perfectly correlated with health metrics, and many signaling pathways that mediate lifespan extension simply extend a frail state of life (Bansal et al., 2015). This is highly problematic for human therapeutics since it would only increase the time that people spend feeling sick, leading to unsustainable increases in individuals' lifetime healthcare costs. In contrast, my olfactory function research suggests that information learned by studying circuits and behavior at an early stage of aging, just after the end of the reproductive period, might be used to improve not just the length of life, but also quality of life. Specifically, the proper intervention delivered at an early stage of aging may rejuvenate neuronal functions (ex. acute arecoline pharmacology or other, specific methods of increasing neurotransmission). This could benefit elderly people whose impaired sensory abilities threaten their nutrition, enjoyment of life and overall safety.

Taken together, the work described here provides new insights into neural circuit function and behavior. Sensory context, neuropeptide signaling and aging all have fascinating roles modulating neural circuit dynamics. As we continue to make progress in understanding how environmental signals are processed at different ages, it is evident that we will be rewarded with a greater understanding of how the nervous system generates behavior that is appropriate for animals' internal and external states.

References

Alivisatos, A.P., Chun, M., Church, G.M., Greenspan, R.J., Roukes, M.L., and Yuste, R. (2012). The brain activity map project and the challenge of functional connectomics. Neuron 74, 970-974.

Bansal, A., Zhu, L.J., Yen, K., and Tissenbaum, H.A. (2015). Uncoupling lifespan and healthspan in Caenorhabditis elegans longevity mutants. Proc Natl Acad Sci U S A 112, E277-286.

Bargmann, C.I., Hartwieg, E., and Horvitz, H.R. (1993). Odorant-selective genes and neurons mediate olfaction in C. elegans. Cell 74, 515-527.

Bargmann, C.I., and Horvitz, H.R. (1991). Chemosensory neurons with overlapping functions direct chemotaxis to multiple chemicals in C. elegans. Neuron 7, 729-742.

Bester-Meredith, J.K., Fancher, A.P., and Mammarella, G.E. (2015). Vasopressin Proves Es-sense-tial: Vasopressin and the Modulation of Sensory Processing in Mammals. Frontiers in endocrinology 6, 5.

Biron, D., Wasserman, S., Thomas, J.H., Samuel, A.D., and Sengupta, P. (2008). An olfactory neuron responds stochastically to temperature and modulates Caenorhabditis elegans thermotactic behavior. Proc Natl Acad Sci U S A 105, 11002-11007.

Bretscher, A.J., Kodama-Namba, E., Busch, K.E., Murphy, R.J., Soltesz, Z., Laurent, P., and de Bono, M. (2011). Temperature, oxygen, and salt-sensing neurons in C. elegans are carbon dioxide sensors that control avoidance behavior. Neuron 69, 1099-1113.

Chalasani, S.H., Kato, S., Albrecht, D.R., Nakagawa, T., Abbott, L.F., and Bargmann, C.I. (2010). Neuropeptide feedback modifies odor-evoked dynamics in Caenorhabditis elegans olfactory neurons. Nat Neurosci 13, 615-621.

Chiang, A.S., Lin, C.Y., Chuang, C.C., Chang, H.M., Hsieh, C.H., Yeh, C.W., Shih, C.T., Wu, J.J., Wang, G.T., Chen, Y.C., *et al*. (2011). Three-dimensional reconstruction of brain-wide wiring networks in Drosophila at single-cell resolution. Curr Biol 21, 1-11.

DeFelipe, J. (2010). From the connectome to the synaptome: an epic love story. Science 330, 1198-1201.

Felleman, D.J., and Van Essen, D.C. (1991). Distributed hierarchical processing in the primate cerebral cortex. Cereb Cortex 1, 1-47.

Golden, T.R., Hubbard, A., Dando, C., Herren, M.A., and Melov, S. (2008). Age-related behaviors have distinct transcriptional profiles in Caenorhabditis elegans. Aging Cell 7, 850-865.

Helmstaedter, M., Briggman, K.L., Turaga, S.C., Jain, V., Seung, H.S., and Denk, W. (2013). Connectomic reconstruction of the inner plexiform layer in the mouse retina. Nature 500, 168-174.

Hobert, O. (2013). The neuronal genome of Caenorhabditis elegans. WormBook, 1-106.

Honegger, K.S., Campbell, R.A., and Turner, G.C. (2011). Cellular-resolution population imaging reveals robust sparse coding in the Drosophila mushroom body. J Neurosci 31, 11772-11785.

Howard, J.D., and Gottfried, J.A. (2014). Configural and elemental coding of natural odor mixture components in the human brain. Neuron 84, 857-869.

Hsu, A.L., Feng, Z., Hsieh, M.Y., and Xu, X.Z. (2009). Identification by machine vision of the rate of motor activity decline as a lifespan predictor in C. elegans. Neurobiol Aging 30, 1498-1503.

Kuczewski, N., Fourcaud-Trocme, N., Savigner, A., Thevenet, M., Aime, P., Garcia, S., Duchamp-Viret, P., and Palouzier-Paulignan, B. (2014). Insulin modulates network activity in olfactory bulb slices: impact on odour processing. J Physiol 592, 2751-2769.

Leinwand, S.G., and Chalasani, S.H. (2013). Neuropeptide signaling remodels chemosensory circuit composition in Caenorhabditis elegans. Nat Neurosci 16, 1461-1467.

Marella, S., Mann, K., and Scott, K. (2012). Dopaminergic modulation of sucrose acceptance behavior in Drosophila. Neuron 73, 941-950.

Markov, N.T., Ercsey-Ravasz, M.M., Ribeiro Gomes, A.R., Lamy, C., Magrou, L., Vezoli, J., Misery, P., Falchier, A., Quilodran, R., Gariel, M.A.*, et al*. (2014). A weighted and directed interareal connectivity matrix for macaque cerebral cortex. Cereb Cortex 24, 17-36.

McMeniman, C.J., Corfas, R.A., Matthews, B.J., Ritchie, S.A., and Vosshall, L.B. (2014). Multimodal integration of carbon dioxide and other sensory cues drives mosquito attraction to humans. Cell 156, 1060-1071.

Oka, Y., Katada, S., Omura, M., Suwa, M., Yoshihara, Y., and Touhara, K. (2006). Odorant receptor map in the mouse olfactory bulb: in vivo sensitivity and specificity of receptor-defined glomeruli. Neuron 52, 857-869.

Pincus, Z., and Slack, F.J. (2010). Developmental biomarkers of aging in Caenorhabditis elegans. Dev Dyn 239, 1306-1314.

Prevedel, R., Yoon, Y.G., Hoffmann, M., Pak, N., Wetzstein, G., Kato, S., Schrodel, T., Raskar, R., Zimmer, M., Boyden, E.S., and Vaziri, A. (2014). Simultaneous whole-

animal 3D imaging of neuronal activity using light-field microscopy. Nat Methods 11, 727-730.

Richmond, J.E., Davis, W.S., and Jorgensen, E.M. (1999). UNC-13 is required for synaptic vesicle fusion in C. elegans. Nat Neurosci 2, 959-964.

Root, C.M., Ko, K.I., Jafari, A., and Wang, J.W. (2011). Presynaptic facilitation by neuropeptide signaling mediates odor-driven food search. Cell 145, 133-144.

Samuel, A.D., Silva, R.A., and Murthy, V.N. (2003). Synaptic activity of the AFD neuron in Caenorhabditis elegans correlates with thermotactic memory. J Neurosci 23, 373-376.

Savigner, A., Duchamp-Viret, P., Grosmaitre, X., Chaput, M., Garcia, S., Ma, M., and Palouzier-Paulignan, B. (2009). Modulation of spontaneous and odorant-evoked activity of rat olfactory sensory neurons by two anorectic peptides, insulin and leptin. J Neurophysiol 101, 2898-2906.

Schrodel, T., Prevedel, R., Aumayr, K., Zimmer, M., and Vaziri, A. (2013). Brain-wide 3D imaging of neuronal activity in Caenorhabditis elegans with sculpted light. Nat Methods 10, 1013-1020.

Stettler, D.D., and Axel, R. (2009). Representations of odor in the piriform cortex. Neuron 63, 854-864.

Su, C.Y., Menuz, K., Reisert, J., and Carlson, J.R. (2012). Non-synaptic inhibition between grouped neurons in an olfactory circuit. Nature 492, 66-71.

Suzuki, H., Thiele, T.R., Faumont, S., Ezcurra, M., Lockery, S.R., and Schafer, W.R. (2008). Functional asymmetry in Caenorhabditis elegans taste neurons and its computational role in chemotaxis. Nature 454, 114-117.

Takemura, S.Y., Bharioke, A., Lu, Z., Nern, A., Vitaladevuni, S., Rivlin, P.K., Katz, W.T., Olbris, D.J., Plaza, S.M., Winston, P., *et al*. (2013). A visual motion detection circuit suggested by Drosophila connectomics. Nature 500, 175-181.

Troemel, E.R., Kimmel, B.E., and Bargmann, C.I. (1997). Reprogramming chemotaxis responses: sensory neurons define olfactory preferences in C. elegans. Cell 91, 161-169.

Wang, J.W., Wong, A.M., Flores, J., Vosshall, L.B., and Axel, R. (2003). Two-photon calcium imaging reveals an odor-evoked map of activity in the fly brain. Cell 112, 271-282.

White, J.G., Southgate, E., Thomson, J.N., and Brenner, S. (1986). The structure of the nervous system of the nematode Caenorhabditis elegans. Philos Trans R Soc Lond B Biol Sci 314, 1-340.

White, J.Q., Nicholas, T.J., Gritton, J., Truong, L., Davidson, E.R., and Jorgensen, E.M. (2007). The sensory circuitry for sexual attraction in C. elegans males. Curr Biol 17, 1847-1857.

Wu, Y., Ghitani, A., Christensen, R., Santella, A., Du, Z., Rondeau, G., Bao, Z., Colon-Ramos, D., and Shroff, H. (2011). Inverted selective plane illumination microscopy (iSPIM) enables coupled cell identity lineaging and neurodevelopmental imaging in Caenorhabditis elegans. Proc Natl Acad Sci U S A 108, 17708-17713.

Xia, X.B., and Mills, S.L. (2004). Gap junctional regulatory mechanisms in the AII amacrine cell of the rabbit retina. Vis Neurosci 21, 791-805.

APPENDIX.

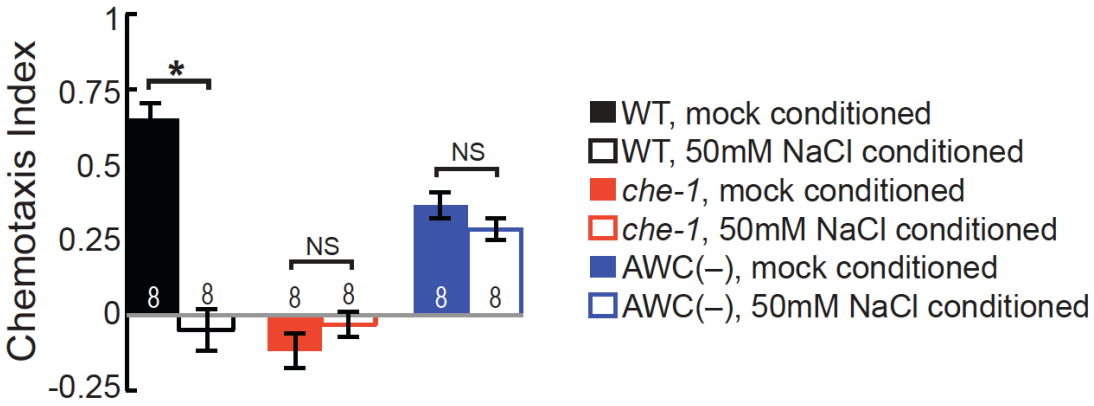

Figure A.1: Salt chemotaxis learning behavior requires the AWC neurons. Wild-type animals pre-conditioned by incubation in 50mM NaCl (in liquid for 1 hour) are no longer attracted to a 500mM point source of salt, compared to mock conditioned wild-type animals. *che-1* mutants lacking ASE sensory neurons display similar chance-like behavior after both mock and salt conditioning. Animals with AWC neurons genetically ablated are weakly attracted to a 500mM point source of salt when mock conditioned; however, pre-conditioned with 50mM NaCl does not significantly alter their subsequent chemotaxis behavior, suggesting that AWC neurons may be critical for high salt experience-dependent learning. Chemotaxis behavior was scored after 30 mins of free movement on the chemotaxis assay plate. Numbers on bars indicate number of assay plates. Error bars indicate s.e.m. *Significantly different from mock conditioned, as indicated ($P < 0.05$, two-tailed *t*-test).

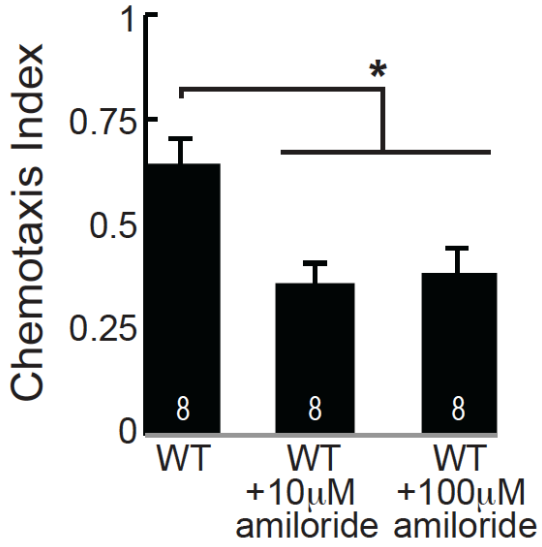

Figure A.2: Salt chemotaxis behavior is reduced by amiloride pharmacology. Preliminary data suggests that wild-type *C. elegans* chemotaxis to a 500mM NaCl gradient is reduced by a 1 hour pre-treatment (in a tube, dissolved in chemotaxis assay buffer) with the drug amiloride hydrochloride hydrate. Amiloride has previously been shown to inhibit the epithelial sodium channels (ENaC) that are involved in mammalian salt transduction. (Follow-up experiments are required to determine whether animal mobility is altered by the drug treatment, to investigate different point source concentrations of salt in the chemotaxis assay and to establish a dose-response curve.) Numbers on bars indicate number of assay plates. Error bars indicate s.e.m. *Significantly different from untreated wild-type, as indicated ($P < 0.05$, two-tailed *t*-test).

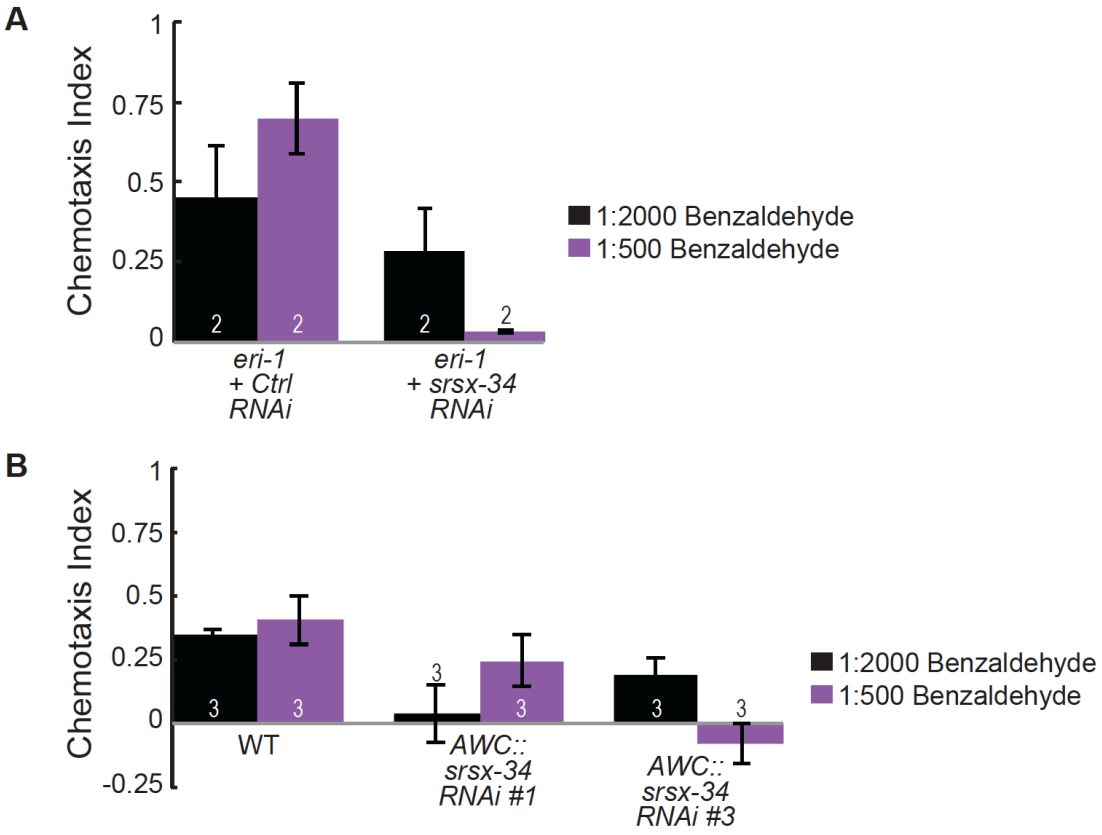

Figure A.3: *srsx-34* is a candidate benzaldehyde receptor. (a) Feeding RNAi to knockdown the predicted G-protein coupled receptor *srsx-34* in the *eri-1* sensitized background reduced chemotaxis to two intermediate benzaldehyde concentrations, compared to control (L4440) RNAi treated animals. (b) Two independent strains with AWC neuron-specific *srsx-34* knockdown show reduced benzaldehyde chemotaxis compared to wild-type animals. (a,b) Numbers on bars indicate number of assay plates. Error bars indicate s.e.m.

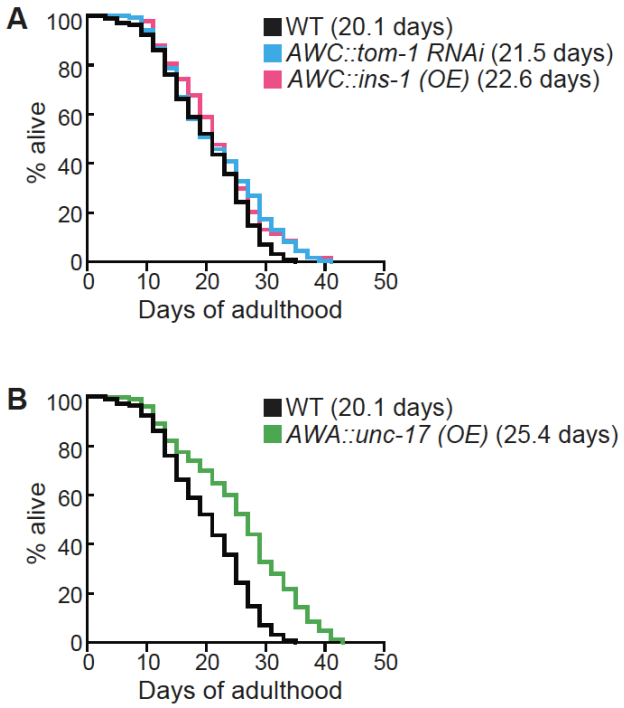

Figure A.4: Lifespan of neurotransmission release pathway transgenic animals. (a) Survival of wild-type, AWC neuron-specific tomosyn (*tom-1)* RNAi knockdown, and AWC neuron-specific insulin-like peptide (*ins-1)* overexpression transgenic animals. These AWC neuron-specific neurotransmitter release manipulations to not significantly alter lifespan, though there may be a trend towards a small extension in lifespan. (*AWC::tom-1 RNAi*: +7.3% extension compared to wild-type, NS, $p>0.05$; and *AWC::ins-1 (OE)*: +13.6% extension compared to wild-type, NS, $p>0.05$; in two or three independent replicates.) (b) Survival of wild-type animals and AWA neuron-specific vesicular acetylcholine transporter (*unc-17)* overexpression. Increased cholinergic transmission from the AWA neurons significantly extends lifespan (average of + 26.6% extension in lifespan in three independent replicates, *$p<0.0001$, Mantel-Cox Test). (a,b) Numbers in parentheses indicates mean survival (in days of adulthood).